e. Textile Composite Engineering

16

Microwaves Solution for Improving Woven Fabric

Drago Katovic
University of Zagreb
Faculty of Textile Technology
Croatia

1. Introduction

According to well known physical definition, electromagnetic waves are oscillating electric and magnetic fields traveling together through space. In the electromagnetic radiation spectrum, shown in figure 1, microwaves (300 MHz – 300 GHz) lie between radio wave (RF) and infrared (IR) frequencies, with relatively large wavelength (1m-1mm) (Metaxas & Meredith)

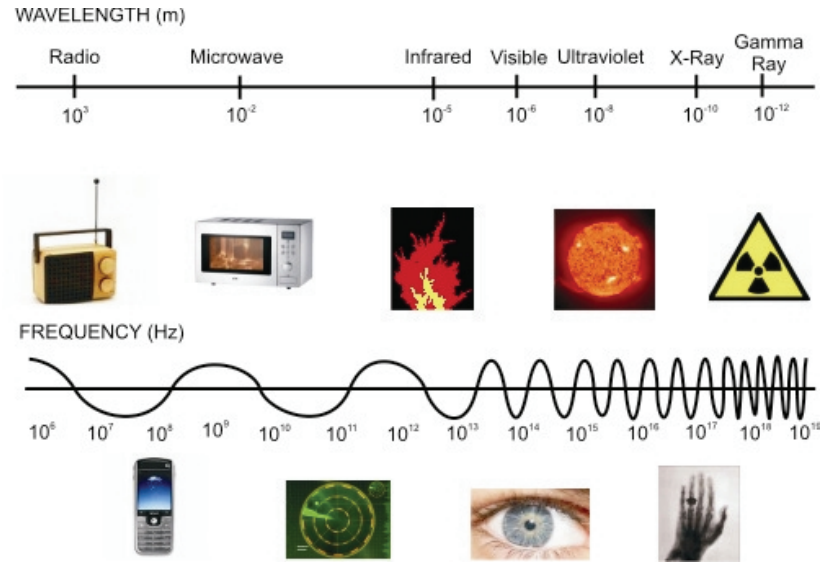

Fig. 1. Electromagnetic spectrum

Electromagnetic wave is formed by the electrical charge in the conductor that produces an electrical field in the spreading direction. The electrical field produces the magnetic filed. The so-formed magnetic field reproduces the electrical field in the space. The electrical field is perpendicular to the magnetic field, and both are perpendicular to the direction of the spreading wave.

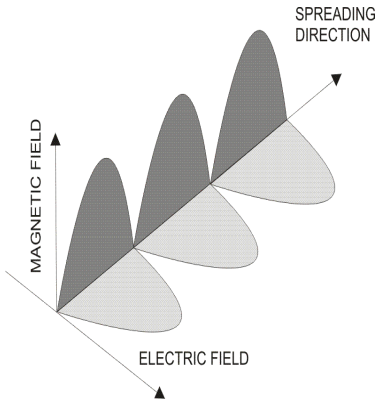

Fig. 2. Direction spread of electromagnetic wave

The energy of microwave photons is very low (0,125 kJ/mol) relative to the typical energies for chemical bonds (335-84 kJ/mol); thus microwave will not directly affect the molecular structure. They cannot change the electronic structure around atoms or among them, but they can interact with the electronic differences between atoms. However, chemical reactions can accelerate due to selective absorption of microwave energy by polar molecules, while non-polar molecules are inert to the microwave (MW) radiation (Varma 2001).

Different materials can be divided according to their response on microwave radiation:

- The materials that reflect MW radiation (stayed cold)
- The materials that are transparent to MW radiation (non-heated)
- The materials that absorb MW energy (being heated).

However, chemical reactions can be accelerated due to selective absorption of electromagnetic energy by polar molecules, while non-polar molecules are inert to the electromagnetic radiation. Besides influencing dipole water molecules, an alternating electromagnetic field also acts on partially polar molecules of textiles such as polyurethane (PU), polyacrylonitrile (PAN), or polyamide (PA)

A microwave electromagnetic field oscillating at 2.45 GHz, which is preferred frequency for heating applications, the charge changes polarity nearly 5 billion times per second. Microwave radiation is specially tuned to the natural frequency of water molecules to maximize the interactions.

Some important applications of microwaves come from their interaction with various types of material. The interaction of microwaves with dielectric materials causes a net polarization of the substance. There are several different mechanisms of polarization: electronic polarization, ionic, molecular (dipole) polarization and interfacial (space-charge) polarization. The overall net polarization creates a dipole moment. Dipole rotation is an interaction, in which polar molecules or species try to align themselves with the rapidly changing electric field of applied radiation. The motion of the molecule as it tries to orient to the field results in a transfer of energy. The second way to transfer energy is ionic conduction that occurs if there are free ions or ionic species present in the substance being heated.

The main difference between conventional heating with hot air and microwave heating is the heating mechanism. While conventional techniques heat a surface, the microwaves heat the whole volume of the treated object. During the conventional heating, the heat is

generated outside the treated product and conveyed by conduction or convection. Hence, the surface is heated at first and afterwards the heat flows toward the inside, which always remains colder than the surface. The required internal temperature can be reached only by sufficient increase of the surface temperature of the material above the temperature needed for particular treatment.

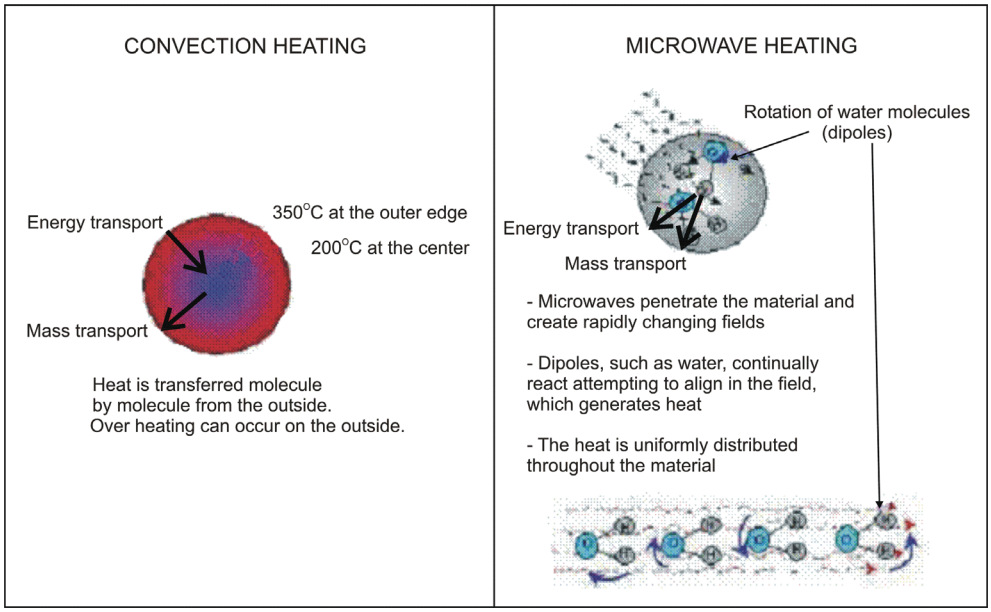

Fig. 3. Energy transfer comparison

On the contrary, in electromagnetic treatment, the heat is generated in a distributed manner inside of the material, allowing more uniform and faster heating. According to the literature (Metaxas & Meredith 1983) the energy consumption is 60-70 % lower in a case of electromagnetic treatment. For dielectric heating the generated power density per volume is calculated by

$$p = \omega \cdot \varepsilon_r^{''} \cdot \varepsilon_0 \cdot E^2 \tag{1}$$

where ω is the angular frequency, ε_r'' is the imaginary part of the complex relative permittivity, ε_0 is the permittivity of free space and E the electric field strength. The imaginary part of the complex relative permittivity is a measure for the ability of dielectric material to convert radio frequency electromagnetic field energy into heat.

What are the advantages microwave? Because volumetric heating is not dependent on heat transfer by conduction or convection, it is possible to use microwave heating for applications where conventional heat transfer is inadequate. One example is in heterogeneous fluids where the identical heating of solids and liquids is required to minimize over-processing. Another is for obtaining very low final moisture levels for product without over-drying. Other advantages include: Microwaves generate higher power densities, enabling increased production speeds and decreased production costs.

Microwave systems are more compact, requiring a smaller equipment space or footprint. Microwave energy is precisely controllable and can be turned on and off instantly, eliminating the need for warm-up and cool-down. Lack of high temperature heating surfaces reduces product fouling in cylindrical microwave heaters. This increases production run times and reduces both cleaning times and chemical costs. Microwaves are a non-contact drying technology. One example is the application of IMS planar dryers in the textile industry, which reduce material finish marring, decrease drying stresses, and improve product quality. Microwave energy is selectively absorbed by areas of greater moisture. This results in more uniform temperature and moisture profiles, improved yields and enhanced product performance. The use of industrial microwave systems avoids combustible gaseous by-products, eliminating the need for environmental permits and improving working conditions.

What are the disadvantages? Historically, the primary technological drawback to using microwave energy for industrial processing has been the inability to create uniform energy distribution. If uniform energy distribution is not present, wet regions of the target material are underexposed, and other regions are overexposed. This is analogous to the hot spots and cold spots generated in your microwave oven at home when heating or defrosting food like a potato or frozen chicken. Severe overexposure of non-uniform energy distribution may provide excessive focus of heat build up resulting in burnt material or a fire hazard. The uniformity of distribution designed into IMS microwave equipment overcomes this problem. Another disadvantage is the depth of penetration achievable using microwave energy. This is a function of microwave frequency, dielectric properties of the material being heated and its temperature. As a general rule, the higher the frequency, the lower the depth of penetration. 2,450 MHz versus 915 MHz? 915 MHz generators can provide up to 100 KW from a single magnetron. Although the cost is similar, the largest commercial 2,450 MHz units available use 30 KW magnetrons. 915 MHz generators lose about 15% efficiency in producing electromagnetic energy from electric power. However, the conversion of that energy into useful heating or drying is often greater than 95% so that the total system efficiency usually exceeds 80%. This compares with 55 to 70% total system efficiency obtainable from 2,450 MHz generators. The depth of penetration of microwave energy at 915 MHz is about three times as great as that at 2,450 MHz. With their higher total system efficiencies, 915 MHz heaters and dryers tend to have lower running costs than comparable 2,450 MHz units. One 100 KW 915 MHz generator will be about 50% cheaper than seven 15 KW 2,450 MHz units. The low power 2,450 MHz magnetrons developed from the proliferation of domestic microwave ovens are inexpensive and readily available. This makes them ideal for low flow capacity R & D applications. The size of magnetrons and wave-guides for a 2,450 MHz system is considerably smaller than those used in 915 MHz units. This makes them suitable for small-scale installations. 2,450 MHz is efficient where fast product expansion is required, such as dry frying of starch-based foods.

Today they are widely accepted and spread to mobile phones, television, wireless computer networks and some special applications such as rocket engines.

2. Microwave in textile finishing

The term "microwaves" was used for the first time in 1932nd, and its first usage was during the Second World War in radio communication and radar technology. The activity of electromagnetic field of high frequency was discovered accidentally during a radar-related

research project, while testing a new vacuum tube, called a magnetron. After more then 50 years of investigation and development, the microwave heating technology is nowadays widely used in number of fields. Studies in the last decade suggest that microwave energy may have a unique ability to influence chemical processes. These include chemical and materials syntheses as well as separations (Tompsett et al. 2006). Until now, MW have been used for food preparation, chemical sludge, medical waste, organic synthesis (Cablewski et al. 1994), analytics and curing (Saito et al. 2004) of hi-tech polymers (Zubizarreta L at all). There are a number of papers dealing with synthesis of organic compounds using microwave (Varma R. 2001). Numerous chemical reaction of textile materials are discussed and presented; e.g. (Barantsev et al. 2007) substitution, additions esterfication (Satge et al (2000), transesterfications, acetylization, amidation and decarboxylation (Hou & Wang 2008). One of the advantages of using microwave radiation is its influence on the reaction kinetics. Kaynak investigated the influence of polymerization time and dopant concentraction on the absorption of microwave radiation in conducting polypyrrole coated textiles (Kaynak et al. 2009). Chang investigated microwave heating for butyrylation of wood with aim of reducing the reaction time (Chang & Chang 2003).

The effect of the sintering temperature on the structural characteristies of nanosized zirconium dioxide particles treated by microwave radiation the during process was investigated by small-angle X-ray scattering and the BET method. It was shown that the specific surface area, particle size, polydispersvity index, and surface and mass fractal dimensionality of zirconium dioxide depend on heat treatment conditions (Strizhak et al).

Microwave moisture measurement is capable of measuring the moisture application behind the padder in continuous dyeing processes and of evaluating the measured values for the padder control. They can also used to determine the residual moisture content behind the stenter exit. A defined microwave emission is thereby beamed onto the damp fabric. The proportion of microwaves, not absorbed because of its density, is measured and relates to the humidity by calibration (Rouette 2002).

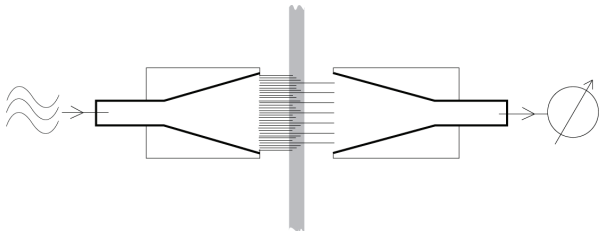

Fig. 4. Principle of moisture measurement using microwaves

The first idea of microwave application for textile finishing processes originated in 1970-es when cellulose fabrics were treated with Durable Press (DP) finishing agents and cured in microwave oven (Englert & Berriman 1974). Until now, microwave irradiation for textile finishing has been used (anonymous 1996) for the combined de-sizing, scouring and bleaching processes, dyeing (Nando & Patel 2002), printing (Neral et al. 2007), and drying processes, as well as for eradication of insects from wool textiles (Regan 1982). Microwave sterilization has many advantages in comparison with conventional methods. It is able to raise the temperature of a material in a short time and selectively heat the material. This results in the reduction of usage and the rapid completion of sterilization Bacillus subtilis (ATCC 9372) and Bacillus stearothermophilus (ATCC 7953) (Wang et al. 2005)

Although these first results microwave irradiation for textile finishing, were promising, the idea was abandoned until 1955, when Miller patented his Pre-set process without awareness of the earlier patent. Both cases involved garment microwave treatment, but they were abandoned because of efforts to control the process failed.

2.1 State of the art

The influence of three different drying methods, convection, contact and as a novelty – microwave one, on physical-mechanical parameters of yarn sizing was investigated by Katovic et al. The research was performed on 4 different types of 100% cotton yarn which had been sized on newly constructed laboratory sizing device. In this way the following parameters: sizing velocity, temperature of the sizing agent, tension and inlet moisture of the warp, outlet moisture of the warp, after drying and drying intensity were continuously controlled and regulated. The application of microwave drying method for wrap sizing showed to be good or even better in some cases, compared to the other drying methods (Katovic et al., 2008).

For microwave vacuum drying (Therdthai & Zhou 2009), three microwave intensities were applied with pressure controlled at 13.33 kPa. For hot air drying, two drying temperatures were examined. The microwave vacuum drying could reduce drying time by 85-90% compared with the hot air drying. In addition, colors change during drying was investigated. From scanning electron micrographs, the microwave vacuum dried mint leaves had a more porous and uniform structure than the hot air ones.

Microwave heating has been proved to be more rapid, uniform and efficient, and easy penetrate to particle inside. To investigate the effect of microwave irradiation on the physical property and morphological structure of cotton cellulose, cellulose fabric was treated with microwave irradiation at different condition. The morphological structures and thermal stabilities of the untreated and treated cellulose were investigated with differential structures and thermal stabilities of were investigated with differential scanning calorimetry and X-ray diffraction. The thermal stability of the treated cellulose was changed. The crystallinity and preferred orientation of the treated cotton cellulose increased (Hou et al. 2008).

The release of formaldehyde from plywood has been greatly reduced by treatment with microwave radiation. Microwave released formaldehyde from plywood samples more effectively compared to samples subjected to thermal energy from external heating. This suggests that microwaves directly activate free formaldehyde molecules, which have a polarity that is susceptible to microwaves. (Saito, Y. et al, 2004).

The influence of microwaves on the efficiency of polycarboxilic acid esterification was studied by FT-IR spectroscopy. Polycarboxilic acid is used as non-formaldehyde durable press finishing agents and maximum effects can be obtained with 1,2,3,4 butantetracaroxylic acid (BTCA) and citric acid (CA). Instead of the usual curing process performed at very high temperatures microwaves were used. Fabric resilience improved while the whiteness was not significantly lowered (Katovic & Bischof Vukusic, 2002).

The esterification involved in Durable Press (DP) finishing is one among several chemical reactions that can be improved by microwave radiation. Cotton material is usually esterified with modified 1, 3 dimethylol 4, 5 dihydroxyethylene urea (DMDHEU). In this study, a novel microwave planar device was used for simultaneous drying and curing processes. The experimental results showed that microwave-assisted textile finishing yields better results than conventional curing at tender frame. Noticeable improvements were obtained in

wrinkle recovery resistance and tensile strength reduction. In addition, the influence of microwaves on formaldehyde release was investigated in order to decrease formaldehyde emission from textile material. Several different experimental methods were used in order to identify a mechanism of formaldehyde release (Katovic et al. 2002, 2005). An alternative approach to formaldehyde-releasing conventional N-methylol compounds is based on the use of non-formaldehyde durable press polycarboxlic acid (PCA) finishing agents. Another alternative approach, investigated, is using microwave energy to impart durable crease resistance to dyed cotton fabric. The bi-functional reactive dyes are used in the study, and the isocratic HPLC method is employed to quantify the PCA reacted with the cellulosic material for two different curing procedures. Shade change evaluation reveals that microwave curing has a greater influence on the dE values than conventional curing. In all other aspects, primarily wrinkle recovery and deformation resistance, microwave curing offers much better results (Katovic et al 2000) and (Bischof Vukusic et al, 2000).

A new microwave curing system was used to affect cross-linking of cotton fabric with non-formaldehyde finishes, namely, glyoxal, glutaraldehyde and BTCA along with water soluble chitosan in order to impart ease care and antibacterial properties to the fabrics (Fouda et al., 2009).

The esterification involved in Durable Press (DP) finishing is one among several chemical reactions that can be improved by microwave radiation. Cotton material is usually esterified with modified 1,3 dimethylol 4,5 dihydroxyethylene urea (DMDHEU). The experimental results obtained on a novel microwave planar device used for simultaneous drying and curing processes showed that MW-assisted textile finishing yields better results than conventional curing at stenter frame, especially for wrinkle recovery resistance and tensile strength reduction (Katovic et al., 2005).

Esterification of cellulose with fatty acids is relatively more recent than acylation of cellulose. The fatty acid esters of cellulose are potentially biodegradable plastics. Most of the undertaken studies using conventional heating resulted in long reaction times. Rapid homogeneous esterification of cellulose with long chain acyl chloride induced by microwave irradiation was studied by Satge et al. The use of microwave resulted in dramatic drop in reaction time: 1 min irradiation was sufficient, compared with 30 min to 2 days, when conventional heating is used. In this work, a systematic study of the effect of degree of substitution as the main parameter for estimating biodegradability was performed (Satge et al., 2002).

Temperature changes in conducting polypyrrole/para-toluene-2-sulfuric acid coated nylon textiles due to microwave absorption in the 8-9 GHz frequency ranges were obtained by a thermography station during simulataneous irradiation of the samples. The temperature values are compared and related to the amounts of reflection, transmission and absorption obtained with a non-contact free space transmission technique, indicating a relationship between microwave absorption and temperature increase. Non-conductive samples showed no temperature increase upon irradiation irrespective of frequency range. The maximum temperature difference around 4° C in the conducting fabrics relative to ambient temperature was observed in samples having 48 %absorption and 26.5 ± 4%reflection. Samples polymerized for 60 or 120 min with a dopand concentraction of 0.018 mol/l or polymerized for 180 min with a dopant concentraction of 0.009 mol/l yielded optimum absorption levels. As the surface resistivity decreased and the reflection levels increased, the temperature increase upon irradiation reduced (Kaynak et al., 2009).

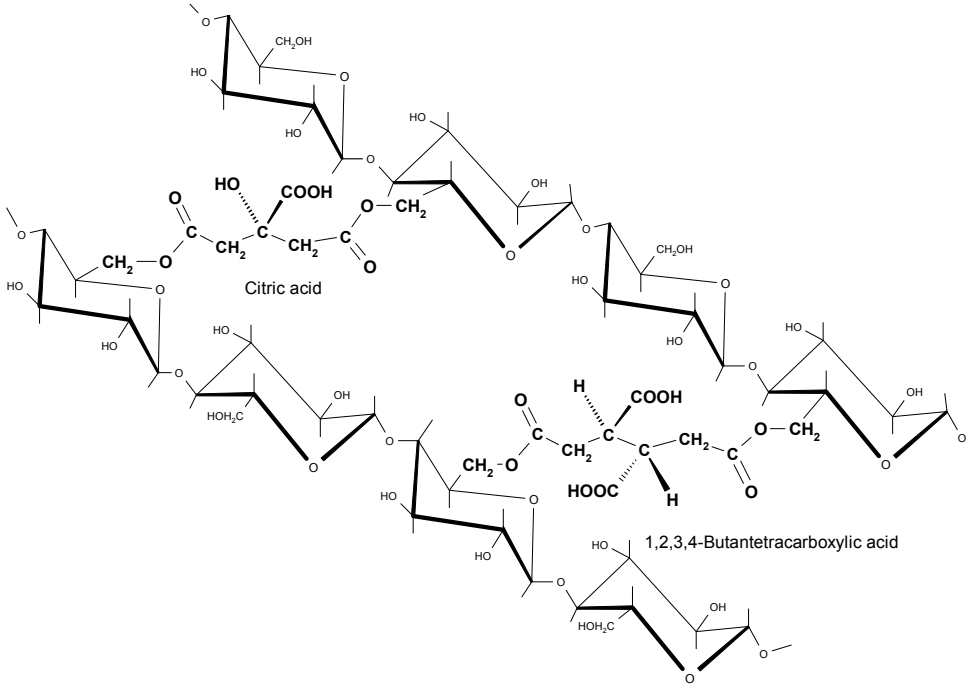

Fig. 5. Cross-linking via ester linkages of CA and BTCA with cellulosic chains

The important possibility of conducting sol-gel synthesis of oxide systems on the surface of para-aramid fibres under the effect of microwave radiation was demonstrated. Selection and control of the basic process parameters (duration and intensity of exposure to electromagnetic radiation, concentration of salts and carbamide) allow regulation of the effectiveness of interaction of reaction system with the microwave fields and eliminating degradation of the polymer (Barantsev et a., 2007).

Results of water- and oil-repellency obtained on planar MW apparatus have been compared with the ones obtained using conventional curing treatment. Simultaneous drying and curing processes have been conducted with MW at planar microwave device for the first time. Microwave technology offers better effects than conventional curing at stenter frame. Only in the case of durability to washing, cotton material treated with microwaves has shown a decrease. Lower effects, primarily caused by de-orientation of fluorocarbon chains, have been improved with thermal re-activation performed after washing and dry cleaning. Greatest advantages of the microwave device constructed are lower production costs and the elimination of separate drying procedure. In this way, conventional treatment, which might cause uneven effects, is eliminated (Bischof Vukusic et al., 2004). The influence of microwave pre-treatment on the UV protective properties of white polyester woven fabrics was investigated. The fabric samples for shade structures of various construction characteristics have been air dried and dried using laboratory microwave device. The impact of microwave pre-treatment has been verified after microwave untreated and treated samples examination and micro-structural changes of the fabrics treated influenced by intra- and inter- structural PES multifilament yarn changes attributed to specific character of the

treatment applied. It was found that changes mentioned, confirmed with obtained results of fabric mass per unit area, fabric thickness, yarns diameter, percent cover, volume porosity and air permeability, have a strong influence on UVA and UVB transmission trough the fabrics. Synergistic influence on the UV protection effect obtained by unconventional pre-treatment and agents based on organic UV absorbers has also been evaluated (Tomljenovic & Katovic 2008).

The efficiency of microwave fixation of prints of the reactive dye applied to a cotton fabric using the digital print technology has been investigated. The results of the fixation of prints with saturated steam and hot air were compared with the characteristics of the microwave-fixed prints. The effects of time and microwave power on change in characteristics of impregnated textile substrates were teed. Based on the results obtained it may be concluded that the characteristic of microwave-fixed prints comparable with the characteristics of digital prints are of reactive dyes fixed by classic methods (Neral et al. 2007).

This paper deals with calibration and standardization of microwave oven, selection of energy level, configuration and placement of fabric swatch in the oven and fixation time to get optimum results viz., shade closest to that obtainable by the cold pad-batch method. Both vinyl sulphone as well asheterobifunctional dyes have been studied. The major finding has been that high energy and low exposure time in microwave oven gives comparable results to those by pad batch method in terms of K/S values, bleaching in post-dyeing wash-off and dry wet rub fastness. Several bulk trials have been taken successfully (Nanda & Patel 2002).

Thermosetting is an important part of the finishing of thermoplastic poly (ethylene terephthalate) (PET) fabrics and garments that confers stability in dimensions and shape as well as appropriate hand to the final product. Conventional thermosetting methods for PET include hot air and steaming treatments. In the present work we used solid state NMR as well DSC methods in order to investigate any differences in the behavior of PET chips when annealed with either a conventional or microwave technique. (D'Arrigo et al. 2002).

2.2 Electromagnetic devices in textile finishing

There are three types of devices for microwave processing of flexible materials. The device based on the resonant cavity principle can be used on discontinuing principle. Therefore it is suitable for lab research of small quantities of textile materials. The major part of the research was conducted on this type of a device. Devices based on the open resonator and waveguide applicator principle operate according to a continuing principle, and they are still being tested. These devices for microwave textile finishing are prevalently laboratory apparatus. Their main problem is reduced spreading of microwaves into the environment through gaps for flexible material. The only devices using electromagnetic waves that are used in textile industrial applications are radio-frequency dryers.

2.2.1 Resonant cavity

The frequencies used in microwave ovens were chosen based on two constraints. The first is that they should be in one of the industrial, scientific, and medical (ISM) frequency bands set aside for non-communication purposes. Three additional ISM bands exist in the microwave frequencies. Two of them are centered on 5.8 GHz and 24.125 GHz, but are not used for microwave cooking because of the very high cost of power generation at these frequencies. The third, centered on 433.92 MHz, is a narrow band that would require expensive equipment to generate sufficient power without creating interference outside the

band, and is only available in some countries. For household purposes, 2.45 GHz has the advantage over 915 MHz in that 915 MHz is only an ISM band in the ITU Region while 2.45 GHz is available worldwide.

Most microwave ovens allow users to choose between several power levels. In most ovens, however, there is no change in the intensity of the microwave radiation; instead, the magnetron is turned on and off in duty cycles of several seconds at a time. This can actually be heard (a change in the humming sound from the oven), or observed when microwaving airy foods which may inflate during heating phases and deflate when the magnetron is turned off. For such an oven, the magnetron is driven by a linear transformer which can only feasibly be switched completely on or off. Newer models have inverter power supplies which use pulse width modulation to provide effectively-continuous heating at reduced power so that foods are heated more evenly at a given power level and can be heated more quickly without being damaged by uneven heating.

The cooking chamber itself is a Faraday cage which prevents the microwaves from escaping. The oven door usually has a window for easy viewing, but the window has a layer of conductive mesh some distance from the outer panel to maintain the shielding. Because the size of the perforations in the mesh are much less than the microwaves' wavelength, most of the microwave radiation cannot pass through the door, while visible light (with a much shorter wavelength) can.

This type of device has precisely determined dimensions depending on the characteristics of microwaves. Until now, the use of different types of resonant cavities has been tested for the purpose of microwave treatment and one of them is a domestic oven. A magnetron operating most often in the 2.45 GHz band (ISM) generates microwave power between a few hundred watts and few kilowatts, depending upon the application. It is connected by means of a waveguides to resonant cavity oven, which contains the materials to be heated or dried: food, wood, paper, plastics chemicals textiles, building materials. A mode stirrer distributes the microwave energy among the different resonant modes of the cavity, ensuring homogeneous heating. Main problems related to the use of such resonant cavities are the

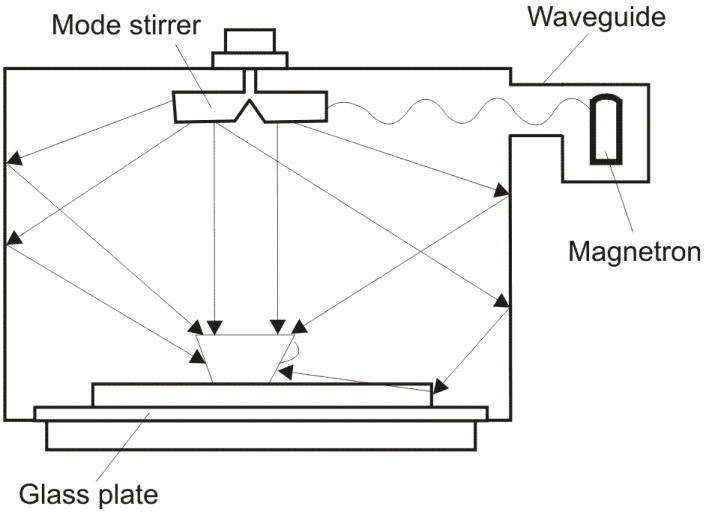

Fig. 6. Microwave oven

non-uniform energy distribution and possible MW leakage from the door seals in the case of inadequate chokes. The distribution of microwave energy within the cavity is always imperfect and the rotator (turntable) will cause the passage of the material through hotter and cooler spots, averaging out the exposure to microwaves. (Thewlis & Barnold 1999), (Hong & Thompson 1998), (Enderling 1988).

2.2.2 Open-resonator

The second reported microwave drying machine consist of many drying cells (17 in their prototype machine), which are positioned above the moving textile material. Each of the drying cells is based on the idea of an open resonator. These cells have their own magnetron placed in a waveguide holder. This applicator, which derives from the Fabry-Perot open resonator, has a magnetron as a source of high electromagnetic power. Dried textile material is located in the middle plane between the parallel conductive plates and the distance between these plates is equal to 3/2 λ. The use of this device is mostly for drying in the factory production of fabrics. This type of semi industrial dryer was developed at the Czech Technical University, Prague, Research Institute of Textile Machines Liberec and Technical University of Liberec (Pourova & Vrba 2006) (Vrba et al. 2005).

In their research of the open applicator they determined the position of the magnetron. In the same manner they also found the distribution of the electric field strength in drying textile materials. This applicator has a magnetron as a source of high electromagnetic power, placed in the waveguide holder. The power of the used magnetrons is 800 W and its working frequency is 2.45 GHz.

Their drying resonant system is optimized by criteria to create the maximum electric field strength in the plane of the drying textile. They described this structure by means of an oriented graph, which is represented in the Figure 8.

Drying resonant system is optimized by criteria to create the maximum electric field strength in the plane of the dying textile. We can describe this structure by means of an oriented graph, and we can also create a diagram of the electromagnetic waves inside this structure. By modifying the diagrams we can arrive at the resulting expression for calculating the E-field strength in the textile plane:

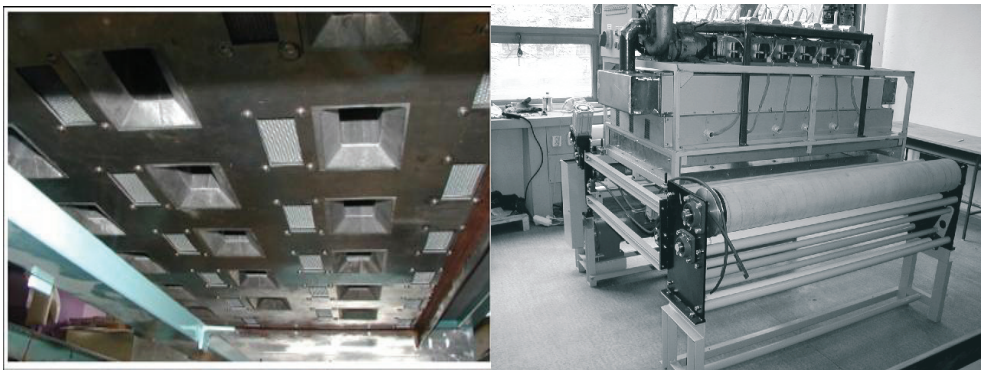

a) b)

Fig. 7. Open-resonator a) Interior the microwave drying machine, b) Prototype of semi-industrial microwave drying machine

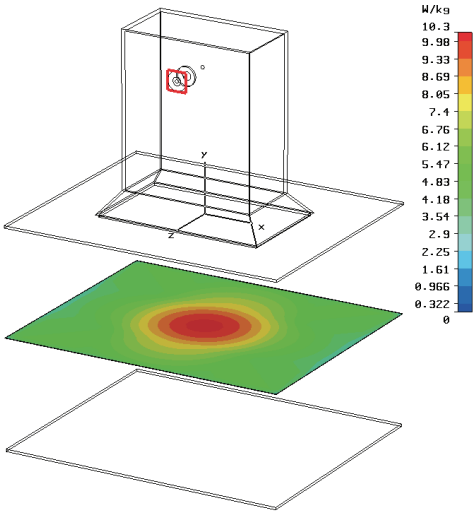

Fig. 8. Distribution of electric field strength in one applicator

$$E(l, p_2, \alpha_{tex}) = \sum_{n=0}^{\infty} p_1^n (p_2 + \delta_2 e^{-x})^n \cdot e^{-j\beta l(l+2n)} \tag{2}$$

parameters p_2 and $\dot{\alpha}_{tex}$ are given by the dielectric properties of the textile, so we can write the electric field strength depended on relative permittivity ε_{tex} and loss factor tg δ_{tex} as follows

$$E(l, p_2, \alpha_{tex}) = \frac{e^{(j\beta l + \alpha_{tex} \cdot t)}}{e^{(j\beta l + \alpha_{tex} \cdot l)} - p_1 p_2 \cdot e^{(\alpha_{tex} \cdot t)} - p\sqrt{1 - p_2^2}} \tag{3}$$

Electric field strength with respect to distance l and to relative permittivity ε_{tex} (tg δ = 0.566)
Were p_1 is reflection coefficient of metallic plate; p_2 is reflection coefficient of textile; $\dot{\alpha}_{tex}$ is attenuation factor of textile; β is phase constant of free space; tg δ_{tex} - loss factor; l is distance between reflective plate and textile; t is thickness of textile; δ is $\sqrt{1 - p^2}_2$ – transmission factor; e- is $e^{(j- \dot{\alpha} \text{ tex } t)}$ – absorption in textile; ε_{tex} – relative permittivity

2.2.3 Waveguide applicator

Waveguide are metallic tube, in the section-plane rectangle or circle. They transport electromagnetic energy from magnetron that runs along the waveguide. Waveguides work according to the principle of waves reflecting from the waveguide from one part to another. Fields in the waveguide can bee seen as a group of planar waves. They reflect from one part to another part, distributing in the direction of waveguide shown in the figure 9.
There are two characteristic wave lengths:

- one in the direction of vertical with the waveguide:

$$\lambda_n = \lambda / \cos\theta \tag{4}$$

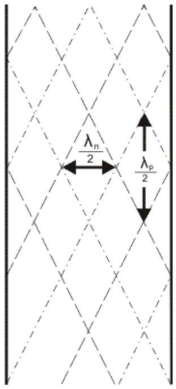

Fig. 9. Characteristic wave length in waveguide

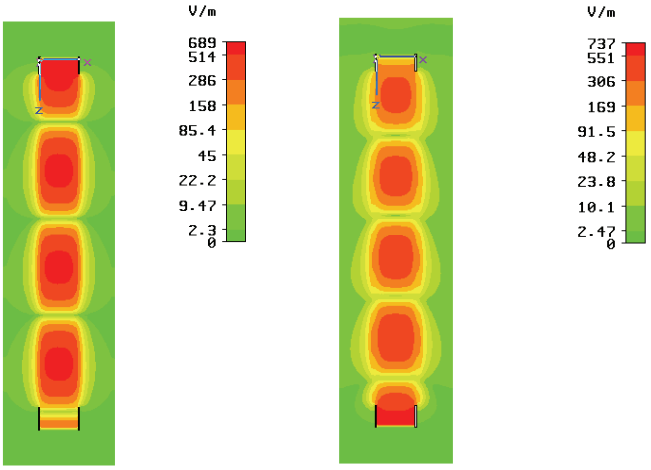

a) b)

Fig. 10. 2D distribution of electric field strength in one waveguide a) without the textile material, b) with textile material

- one in the direction of parallel with the waveguide:

$$\lambda_p = \lambda / \sin\theta \quad (5)$$

Were λ is wave length appointed signal; λ_n - is wave length in the direction vertical with the waveguide; λ_p I wavelength in the direction parallel with waveguide; θ is entrance angle (angle of incidence).

This drying system for the treatment of flexible textile material consists of rectangular waveguides centrally slotted in order to obtain planar passage of textile mater in wide state (Katovic et al. 2008). With proper design of the waveguides and supporting equipment, a specific environment (at the particular wavelength) can be created in order to provide controlled distribution of the microwave energy, making it possible to achieve uniform

exposure to material passed through a channel. The leakage of microwave energy is inherently small due to the fact that waveguide slots are oriented along the waveguide line of symmetry, and therefore they cannot act as efficient slot antennas. Furthermore, in this way the material lies in the maximum of the electric field that assures effective coupling to the flowing microwave energy. In a case that request for slots symmetry is fulfilled, only the load (textile material) which passes through the waveguides has an influence on energy loss. The amount of microwave energy absorbed by the textile in each waveguide pass depends on the material thickness and moisture content. This laboratory drying system for the treatment of flexible textile material consists of 6 rectangular waveguides (4 x 8 cm) centrally slotted in order to obtain planar passage of textile material in a wide state.

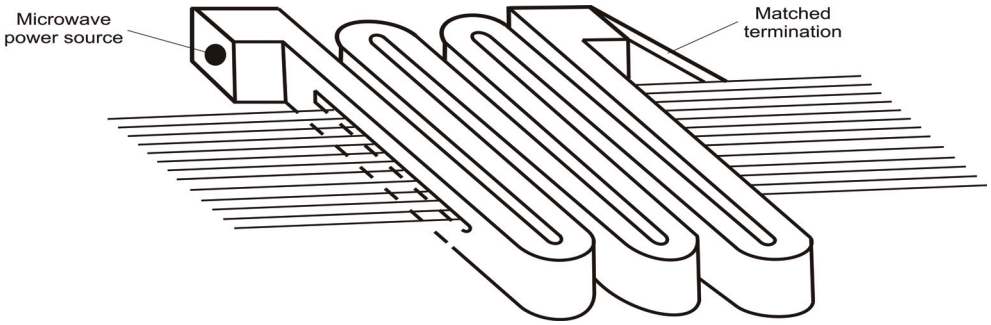

Fig. 11. Scheme of the textile material passing through the waveguides

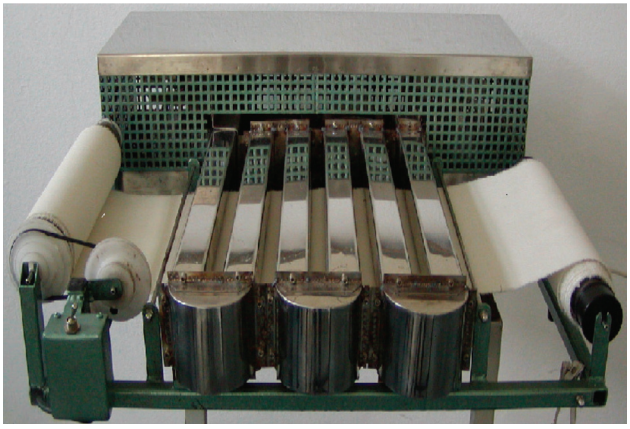

Fig. 12. Laboratory microwave device for the treatment of textile materials

In a case of single pass applicator, exponential decay of electric field might cause non-uniform heat distribution.
To prevent this negative tendency, the material is passed through a number of waveguide passes. In order to
obtain a uniform absorption of microwave energy on the whole material an even number of waveguides must always be used. Number of waveguides used depends on the desired speed of the textile material passing and the amount of water on the material. Due to special

design of waveguide slot for textile materials there is only minimal leakage of microwave energy into the environment. Namely, passing of the textile material through the waveguides leads to transition of the part of energy out of the waveguide together with the material. In order to reduce this energy transition as much as possible, waveguide slots are elongated and beveled which enables the return of microwave energy into the waveguide. Reduced energy is guided through the waveguide to the absorber of microwave energy (water) (Katovic et al. (2005).

Fig. 13. The modular microwave unit

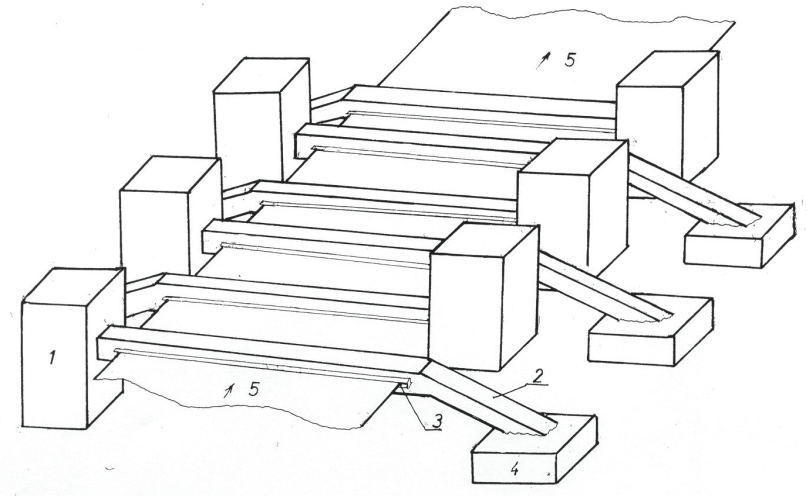

Fig. 14. Modular microwave units
1. Microwave unit box 2. Waveguides 3. Slots 4. Absorber of microwave energy (water)
5. Textile material.

For paper manufacturing, textiles, and other flat materials, American company Industrial Microwave System (IMS) offer an exceptional improvement over other drying alternatives.

A completely scalable configuration of slotted separated waveguides in combination with high power microwave generators can accommodate materials up to 5 cm in thickness and 10 m wide. Because of the efficiency of microwaves along with the uniform energy distribution, production speed can be dramatically increased and product quality improved.

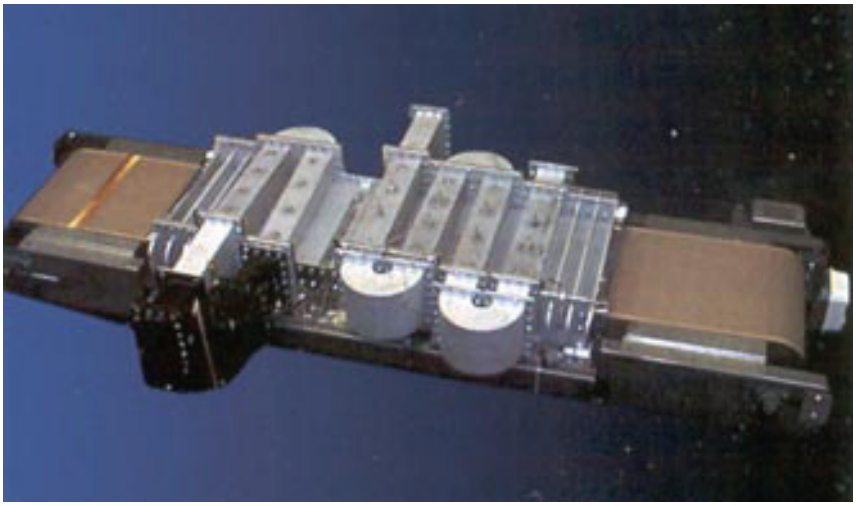

Fig. 15. IMS Planar System (prospect of company *Industrial Microwave System*)

3. Radio frequency dryers

Radio frequency (RF) and microwaves (MW) are forms of electromagnetic energy but differ in operating frequency and wavelength. Both are allocated specific bands of operation by international governments. Industrial radio frequencies typically operate between 10 and 30 MHz with wavelengths of 30 to 10 meters. Radio frequency dryers are operating with power from 10 till 100 kW. Generally speaking, the efficiency of power utilization is far lower in a RF generator than a microwave unit, although the initial capital cost per KW of power output is higher. Selection of RF or microwave heating will depend on product physical properties and required process conditions for a particular application. Where penetration depth in excess of 15 cm is required and control of uniformity of heating is not a major issue, radio frequency offers a good solution. However, where uniformity of drying and moisture control is essential. For planar applications requiring belt widths in excess of 100 cm, where edge-to-edge uniformity is essential, control of microwave energy is superior to RF. Low moisture levels and high production belt speeds, such as those encountered in the textile industry, are far better suited to IMS microwave heating due to their characteristics of control and response time respectively. Electromagnetic waves have been used in the textile industry finishing the purpose of drying of thick materials, performed at radio frequency (RF) dryers, which are operating at different frequencies between 10 and 30 MHz. In textile processing, radio frequency waves are used in dryers for thick and multi-layered materials. In these machines, energy is transferred by means of two metal electrodes plates, between which the fabric is transported on a conveyer belt. An alternating electric field is created between the electrodes, with alternating voltage created by on RF generator.

Under the influence of the alternating electric field, dipole water molecules start vibrating, which causes them to heat up and be transformed into water vapor. A wet fabric submitted to a radiofrequency fields absorbs the electromagnetic energy, so that its internal temperature increases. If a sufficient amount of a energy is supplied, the water is converted into steam, which leaves the product; that is to say, the wet product is dried. Radiofrequency dyers have some specific design and construction features which allow their users to obtain the maximum benefits from the radio frequency technology in terms of quality of the dried products, reduced operating cots flexibility and reliability. The RF generators are of the „lumped components" type, having high efficiency (Q quality factor) and outstanding reliability. The cooling system of triodes is made up of a double water circuit; it is designed to allow the longest possible life of the triodes and does not require periodic maintenance operation. The RF power adjustment is accomplished by means of a semi-automatic circuit which controls the power supplied to the product being dried through a variable capacitor, located in the generator. The electrode is fixed or automatically positioned at pre-set heights. The range of power density for textile industry is from is 3 (nylon) to 18 kW/m^2 (cotton, viscose) of electrode surface.

Fig. 16. Radio frequency dryer (Prospect of company *Stalam*)

4. Future development

The main advantage of the microwave energy application is that the energy consumption is 60-70 % lower respect to conventional heating treatments. Another advantage is its influence on the reaction kinetics: a reaction that takes place in two days under conventional treatment methods terminates after a few minutes applying MW energy.
Recent studies have documented a significantly reduced time for fabricating zeolites, mixed oxide and mesoporous molecular sieves by employing microwave energy. In many cases,

microwave syntheses have proven to synthesize new nanoporous structures. By reducing the times by over an order of magnitude, continuous production would be possible to replace batch synthesis. This lowering of the cost would make more nanoporous materials readily available for many chemical, environmental, and biological applications. Further, microwave syntheses have often proven to create more uniform (defect-free) products than from conventional hydrothermal synthesis.

The main disadvantage of a wide application of microwave energy in textile finishing is the negative influence of electromagnetic irradiation on the environment. It means that preventive security measures are needed to be developed prior to microwave energy use on a larger scale. The exposure to an excessive level of radiation can produce hazards. The microwave radiation is non-ionizing, its main effect being of a thermal nature, commonly used in applications. The body absorbs radiation and automatically adapts to the resulting temperature increase, excess heat being removed by the blood flow. However, should the radiation become too intense, the thermal balance no longer could be restored by the body processes, and burns would then occur. As microwaves tend to heat deeply into the body, one might fear deep burns would occur while the surface temperature remained acceptable. There exists a certain radiation threshold, beyond which irreversible changes do occur. A considerable number of studies were carried out to determine this threshold. No permanent effect was observed for power level lower than 100mW/cm^2. Severe overexposure of non-uniform energy distribution may provide excessive focus of heat build up resulting in burnt material or a fire hazard. Another disadvantage is the depth of penetration achievable using microwave energy. This is a function of microwave frequency, dielectric properties of the material being heated and its temperature. As a general rule, the higher the frequency, the lower the depth of penetration.

5. References

Anonymus (1996). Microwave Processes for the Combined Desizing, Scouring and Bleaching of Grey Cotton Fabrics, *J.Text. Institute*, 3, *pp. 602-607,* ISSN 0400-5000

Barantsev, V.M., Larionov, O.S., Pavlov, N.N. (2007). Prospects for modification of para-aramid fibres with metal complex salts in conditions of microwave exposiure, *Fibre Chemistry* 39, *pp.193-196*, ISSN 0018-3830

Bischof Vukusic, S., Schramm, C., Katovic, D. (2003). Influence of Microwaves on Nonformaldehyde DP Finished Dyed Cotton Fabrics, *Textile Research Journal, 73, pp.733-738*, ISSN 0040-5175

Bischof Vukusic, S., Katovic, D. (2004). Textile finishing treatments influenced with microwaves, *The Textile Institute 83rd World Conference,* Shangai*, China, pp.1165-1169,* ISBN 1-8703-7261-1

Bischof Vukusic, S., Katovi D., Flincec Grgac S. (2004). Effect of microwave treatment on fluorocarbon finishing, *Colourage Annual, 51, pp.1000 -1004,* ISSN 0010-1826

Cablewski, T. et al (1994). Development and Application of Continuous Microwave Reactor for Organic Synthesis*, J. Org.Chem 59 pp. 3408 – 3412,* ISSN022-3263

Chang, H-T., Chang S-T.: (2003) Improvements in dimensional stability and lighfastnedd of wood by butyrylation using microwave heating *J.Wood Sci (2003) 49 p.455-460* ISSN 1435-0211

D'Arrigo, Focher, B., Pellacani, G.C., Cosentino, C.Torri, G. (2002). Textiles Thermosetting by Microwaves*, Macromol. Symp. 180 pp. 223-239*, ISNN 1022-1360

Enderlig, R., (1988). US Patent 4,907,310

Englert, R.D., Berriman, L.P. (1974), Curing chemically treated cellulosic fabrics, *US Patent 3846845, 1974. 1112*

Fouda, M. El Shafei, A., Hebeish, A. (2009). Microwave curing for producing cotton fabrics with care and antibacterial properties, *Carbohydrate Polymers 77, pp. 651-655,* ISSN 0144-8617

Hong, S., Thompson, D. (1998), Canadian Patent CA 2 235 439

Hou, A., Wang, X., Wu, L. (2008). Effect of microwave irradiation on the physical properties and morphological structures of cotton cellulose*, Carbonate Polymers 74 pp. 934-937,* ISSN 0144-8617

Katovic, D., Bischof Vukusic, S., Soljacic, I., Stefanic, G. (2000). Application of Electromagnetic Waves in Durable Press Finishing with Polycarboxylic Acid, *AATCC International Conference & Exhibition, Winston-Salem, NC, USA, 17-20 September 2000, CD-ROM,*

Katovic, D., S. Bischof Vukusic, (2002), Application of Electromagnetic Waves in Durable Press Finishing with Polycarboxylic Acid, *AATCC Review 2 (2002) 4,pp. 39-42*, ISSN 1532-8813

Katovic, D. Bischof Vukusic S., Versec, J. (2002), The application of microwave energy in Durable Press Finishing, *International Textile Clothing & Design Conference Dubrovnik 6-9 October (2002) 283-287*, ISBN 953-96408-8-1

Katovic, D., Bischof Vukusic, S. Flincec Grgac, S. (2005). Application of Microwaves in Textile Finishing Processes, *Tekstil 54(7) 313-318,* ISSN 0492-5882

Katovic, D., Bischof Vukusic, S., Hrabar, S., Bartolic, J. (2005). *Microwaves in Chemical Finishing of Textiles* 18th International Conference on Applied Electromagnetics and Communications 12-14 October (2005), Dubrovnik, 255-25, ISBN 953-6037-44-0

Katovic, D., Kovacevic, S., Bischof Vukusic, S., Schwarz, I., Flincec Grgac, S. (2007), Influence of Drying on Psysico-mechanical Properties of Sized Yarn, *Tekstil 56,8, pp .479 - 486,* ISSN 0492-5882

Katović, D. Kovacevic, Bischof Vukusic, S., Schwarz I., Flincec Grgac, S. (2008). The Effect of Microwave on Warp Sizing, *Textile Research Journal 74, pp. 353-360,* ISSN 0040-5175

Kaynak A., Hakansson E., Amiet A. (2009) The influence of polymerization time and dopant concentration on the absorption of microwave radiation in conducting polypyrrole coated textiles, *Synthetic Metals 159 (2009) pp.1373-1380,* ISSN 0379-6779

Metaxas, A.C., Meredith, R.J. (1983). Industrial Microwave Heating, *Peter Peregrinus, pp. 111-150,* ISBN 0-90604-889-3, London

Nanda, R., Patel, G. (2002). *Microwave oven*: *A tool for quick response in shade development and lab-to bulk shade translation in reactive dyeing* 7th International & 58th All India Textile Conference, Mumbai 14 -15 Dec 2002 pp. 83-88

Nanda, R., Patel, G. (2002). Microwave Oven: A tool for guide response in shade translation in reactive dyeing*, Colourage* 49,12, *pp.83-88, ,* ISSN 0010-1826

Neral, B., Sostar Turk, S., Schneider, R (2007). Efficiency of Microwave Fixation of Digital Prints of the Reactive Dyestuff, *Tekstil 56, 6, pp.358-367,* ISSN 0492-5882

Pourova, M., Vrba, J. (2006). Microwave Drying of Textile Materials and Optimization of Resonant Applicator *Acta polytechnica 46 5, pp. 3-7,* ISSN 0323-7648

Reagan, B.M. (1982*),* Eradication of insects from wool textiles, *Journal of the American Institute for Conservation 21, 2, pp. 1-34,* ISSN 0197-1360

Rouette, H.K. (2001). Encyclopedia of Textile Finishing, *Springer-Verlag, Berlin Heidelberg pp. 1399-1401,* ISBN 3-540-65031-8

Saito,Y., Nakano,K., Shida S., Soma,T., Arima, T. (2004). Microwave-enhanced release of formaldehyde from plywood *Holzforschung 58, pp. 548-551,* ISSN 1437-434

Satge,C., Verneuil, B., Brandland, P. Granet, R. Krausz P., Rozier, J., Petit, C. (2002). Rapid homogeneneous esterification of cellulose induced by microwave irradiation Carbonate *Polimers 49 pp. 373-376,* ISSN 1385-772

Strizhah, P.E., Tripol`shii A.I., Gurnik T.N., Tuzikov, F.V., Moroz, E.M. Konstandinova, T.E., Tuzikova,N.A., Kol`ko, V.P., Danilenko,I.A. Gorban, O.A. (2008). Effect of temperature on the structural characteristics ofd zirconium dioxide nanoparticles produced under conditions of microwaver treatment, *Theoretical and Experimental Chemistry,44, 3, p.144-148,* ISSN 0040-5760

Therdthai, N., Zhou,W., (2009). Characterzation of microwave vacuum drying and hot air drying of mint leaves (Mentha cordifolia Opiz ex Fresen), *Journal of Food Engineering 91 pp.482-489,* ISBN 0260-8774

Thewli, R., Barnoldswick (1999). European Patent EP 0 974 693 A1 (1999)

Thiry, M. (2000), The Magic of Microwave, *Textile Chemist and Colorist–American Dyestaf Reporter 32, 10, pp. 2-4,* ISSN 0040-490

Tomljenovic, A., Katovic, D. (2008). *Microwaves – solution for improving Polyester woven fabric UV protective properties* 4 rd International Textile, Cloting & Design Conference October 5th to 8th 2008; Dubrovnik, 898-903 ISBN 978-953-7105-26-6

Tompsett G., Conner W.C., Yngresson K.S. (2006). Microwave Synthesis of Nanoporous Materials *ChemPhysChem 7,296-319* ISSN 1439-764

Varma, R. (2001). Solvent- free accelerated organic syntheses using microwaves*, Pure Appl. Chem 73, pp.193- 198* ISSN 0033-4545

Vrba, J., Stejskal, M., Klepl, R., Richter, A., Pourova, M., Žak, O., Herza, J., Oppi, L. (2005). *Microwave Drying Machine for Textile Materials* European 35th Microwave Conference ISBN 2-9600551-2-8

Wang H., Takashima H., Miyakawa Y., Kanno Y. (2005) Development of catalyst materials being effective for microwave sterilization *Science and Technology of Advanced Materials 6 pp. 921-926* ISBN 1878-5514

Zubizarreta, L.,Arenillas,A, Menéndez,J.A., Pis,J.J., Pirard,J.P., Job,N. (2008). Microwave Drying as an effective method to obtain porous carbon xerogels, *Journal of Non-Crystalline Solids 354 pp. 4024-4026,* ISSN 0022-3093

17

Composites Based on Natural Fibre Fabrics

Giuseppe Cristaldi, Alberta Latteri, Giuseppe Recca and Gianluca Cicala
University of Catania – Department of Physical and Chemical Methodologies for Engineering, Catania
Italy

1. Introduction

In the latest years industry is attempting to decrease the dependence on petroleum based fuels and products due to the increased environmental consciousness. This is leading to the need to investigate environmentally friendly, sustainable materials to replace existing ones. The tremendous increase of production and use of plastics in every sector of our life lead to huge plastic wastes. Disposal problems, as well as strong regulations and criteria for cleaner and safer environment, have directed great part of the scientific research toward eco-composite materials. Among the different types of eco-composites those which contain natural fibers (NF) and natural polymers have a key role. Since few years polymeric biodegradable matrices have appeared as commercial products, however their high price represents the main restriction to wide usage. Currently the most viable way toward eco-friendly composites is the use of natural fibres as reinforcement. Natural fibres represent a traditional class of renewable materials which, nowadays, are experiencing a great revival. In the latest years there have been many researches developed in the field of natural fibre reinforced plastics (Bledzki & Gassan, 1999). Most of them are based on the study of the mechanical properties of composites reinforced with short fibers. The components obtained therefore are mostly used to produce non-structural parts for the automotive industry such as covers, car doors panels and car roofs (Magurno, 1999, John at al., 2008) (Fig.1,2).

Fig. 1. Mercedes-Benz A natural fibre composites components (source: DaimlerChrysler AG)

Few studies deal with structural composites based on natural reinforcements. These studies are mainly oriented to the housing applications where structural panels and sandwich beams are manufactured out of natural fibres and used as roofs (Saheb & Jog., 1999).

Considering the high performance standard of composite materials in terms of durability, maintenance and cost effectiveness, the application of natural fiber reinforced composites as construction material holds enormous potential and is critical for achieving sustainability. Due to their low density and their cellular structure, natural fiber posses very good acoustic and thermal insulation properties and demonstrate many advantageous properties over glass or rockwool fibre (e.g. handling and disposal).

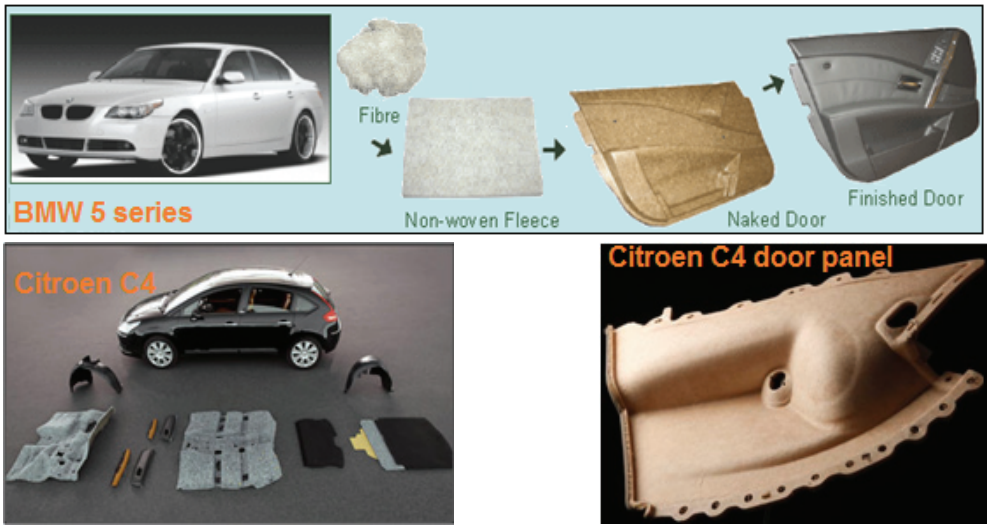

Fig. 2. Examples of applications of Natural Fibres in the automotive field

Nowadays natural fibre composites are not exploited only in structural and semi-structural applications of the automotive sector, but in other fields too (Fig.3).

Fig. 3. Examples of use of Natural Fibres in several applications

Natural fibres (Fig.4) can be divided, according to their origin, into: animal, vegetable and mineral. The most used are the vegetable ones due to their wide availability and renewability in short time respect to others, so when we say "natural fibres" We refer here to the vegetables ones. In the past, natural fibres were not taken into account as reinforcements for polymeric materials because of some problems associated with their use:

- Low thermal stability, in other terms the possibility of degradation at moderate temperature (230-250 ° C).
- Hydrophilic nature of fibre surface, due to the presence of pendant hydroxyl and polar groups in various constituents, which lead to poor adhesion between fibres and hydrophobic matrix polymers (John et al., 2008, Kalia et al., 2009). The hydrophilic nature can lead to swelling and maceration of the fibers. Furthermore, moisture content decreases significantly fibre's mechanical properties.
- Properties variability depending on the quality of the harvest, age and body of the plant from which they are extracted, the extraction techniques and the environmental conditions of the site.

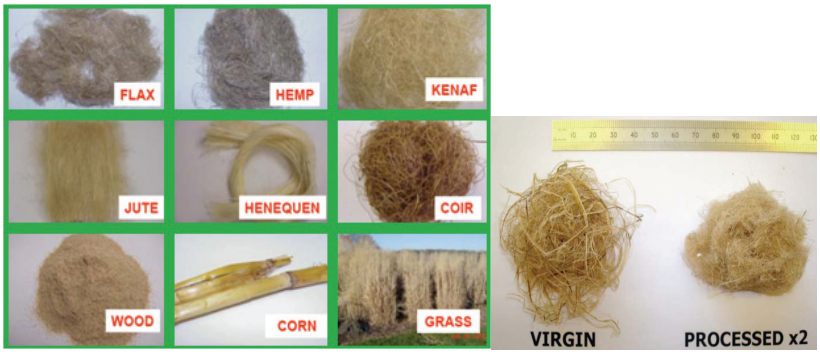

Fig. 4. (a) Some natural fibre, (b) Unprocessed and Processed hemp fibres (source: University of Exeter)

Lack of good interfacial adhesion, low degradation temperature, and poor resistance towards moisture make the use of natural fibre reinforced composites less attractive than synthetic fibre (glass, carbon, aramid, etc.) that have been up to now the only choice for reinforcing polymeric composites, due to their superior mechanical properties. However, the production of composites reinforced with synthetic fibres and matrices requires a large amount of energy which is only partially recovered with incineration of fibre reinforced composites. This has once again drawn the attention towards natural fibres due to their environmental advantages. It has been demonstrated that the energy needed for production of natural fibres is, on average, more than half of the amount needed for synthetic fibres (Fig.5). Thus, the renewed interest in the natural fibers, due to their lightweight, nonabrasive, non irritating, combustible, nontoxic, biodegradable properties (Saheb & Jog, 1999), low energy consumption for production, budget zero CO_2 emissions if burned, low cost (Table 1), main availability and renewability compared to synthetic fibres, has resulted in a large number of applications to bring it at par and even superior to synthetic fibers. Because of such properties natural fibers are fast emerging as a viable choice as reinforcing material in composites (kalia et al., 2009).

Even if natural fibre has a very low energy consumption for production compared to other synthetic fibre, such as glass or carbon, careful environmental impact evaluation must be

take in consideration in order to make the right choice. In fact, the validity of "green" case for substitution of synthetic fibre by natural ones is dependent on the type of reinforcement and related production processes. A parameter which better describe the environmental impact is the *embodied energy* calculated with reference to all related agricultural operations (from ploughing to harvest), fibre extraction operations (retting and decortication), fibre preparation operations (hackling and carding), fibre processing operations (spinning or finishing) and materials used for these operations. The use of embodied energy parameter reveals that not any kind of natural fibre reinforcement is "greener" then synthetic ones. Fig. 6 shows that, even if adopting the most environmental friendly option (no-till and water retting) for flax fibre production, only mat fabrics are, in energetic terms, "greener" while flax yarns has a higher embodied energy respect to glass fibre continuous filament production.

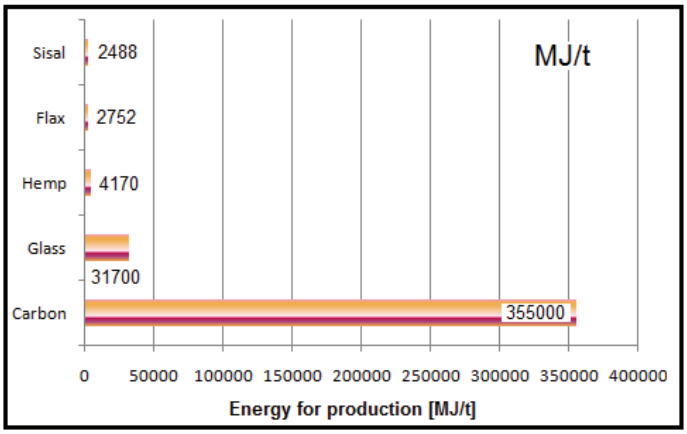

Fig. 5. Energy for production of some fibre *(sources: SachsenLeinen; Daimler 1999; BAFA; NOVA; AVB; CELC; REO)*

Fiber	Price	Specific Gravity	Price
	$ /m³	Kg/m³	$ /kg
Wood	420	1600	0,26
Flax	600	1500	0,40
Glass	4850	2600	1,87
PP	650	900	0,72

Table 1. Cost comparison between natural and synthetic fibre *(Source: Georgia Institute of Technology www.me.gatech.edu/jonathan.colton/me4793/natfiber.pdf)*

Natural fibres can be classified according to their origin and grouped into *leaf:* abaca, cantala, curaua, date palm, henequen, pineapple, sisal, banana; *seed*: cotton; *bast*: flax, hemp, jute, ramie; fruit: coir, kapok, oil palm. Among them flax, bamboo, sisal, hemp, ramie, jute, and wood fibres are of particular interest (Kalia et al., 2009). The most important physical and mechanical properties are summarized in Table 2.

Physical and mechanical properties depend on the single fibre chemical composition (Cellulose, hemicelluloses, lignin, pectin, waxes, water content and other minors) according to grooving (soil features, climate, aging conditions) and extraction/processing methods

conditions. Grooving conditions is recognized as the most influent parameter for the variability of mechanical properties of the fibres. The chemical composition of several natural fibres is summarised in Table 3.

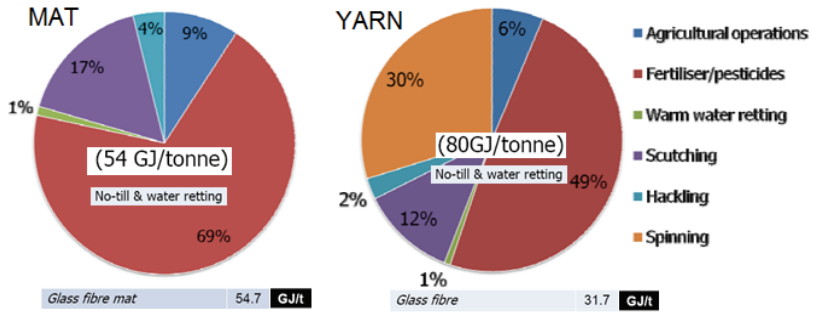

Fig. 6. Embodied energy of flax fibre mat and yarn (source: ACMC Advanced Composites Manufacturing Centre – University of Plymouth)

Plant fibre	Tensile strength (MPa)	Young's modulus (GPa)	Specific modulus (GPa)	Failure strain (%)	Length of ultimates, l (mm)	Diameter of ultimates, d (μm)	Aspect ratio, l/d	Microfib angle, θ (°)	Density (kg.m^{-3})	Moisture content (eq.) (%)
Cotton[s]	300-700	6-10	4-6.5	6-8	20-64	11.5-17	2752	20-30	1550	8.5
Kapok[s]	93.3	4	12.9	1.2	8-32	15-35	724	-	311-384	10.9
Bamboo[b]	575	27	18	-	2.7	10-40	9259	-	1500	-
Flax[b]	500-900	50-70	34-48	1.3-3.3	27-36	17.8-21.6	1258	5	1400-1500	12
Hemp[b]	310-750	30-60	20-41	2-4	8.3-14	17-23	549	6.2	1400-1500	12
Jute[b]	200-450	20-55	14-39	2-3	1.9-3.2	15.9-20.7	157	8.1	1300-1500	12
Kenaf[b]	295-1191	22-60	-	-	2-61	17.7-21.9	119	-	1220-1400	17
Ramie[b]	915	23	15	3.7	60-250	28.1-35	4639	-	1550	8.5
Abaca[l]	12	41	-	3.4	4.6-5.2	17-21.4	257	-	1500	14
Banana[l]	529-914	27-32	20-24	1-3	2-3.8	-	-	11-12	1300-1350	-
Pineapple[l]	413-1627	60-82	42-57	0-1.6	-	20-80	-	6-14	1440-1560	-
Sisal[l]	80-840	9-22	6-15	2-14	1.8-3.1	18.3-23.7	115	10-22	1300-1500	11
Coir[f]	106-175	6	5.2	15-40	0.9-1.2	16.2-19.5	64	39-49	1150-1250	13

Table 2. Natural fibre properties. Source: Natural fibre'09 Proceedings (University of Bath)

%	Jute	Flax	Hemp	Kenaf	Sisal	Cotton
Cellulose	61-71	71-75	70,2-74,4	53-57	67-78	82,7
Hemicellulose	13,6-20,4	18,6-20,6	17,9-22,4	15-19	10-14,2	5,7
Lignin	12-13	2,2	3,7-5,7	5,9-9,3	8-11	-
Pectin	0,2	2,2	0,9	-	10	-
Others	-	3,8	6,1	7,9	1	-
Waxes	0,5	1,7	0,8	-	2,0	0,6
Water	12,6	10,0	10,8	-	11,0	-

Table 3. Natural fibre composition (Williams et al., 2000; Bogoeva-Gaceva et al., 2007)

Natural fibre mechanical properties depends on the type of cellulose and the geometry of the elementary cell. The celluloses chains are arranged parallel to each other, forming bundles each containing forty or more cellulosic macromolecules linked by hydrogen bonds and through links with amorphous hemicelluloses and lignin which confer stiffness to fibre called microfibrils. More interwoven microfibrils form a rope-like structure (Rong at al., 2001) (Fig.7).

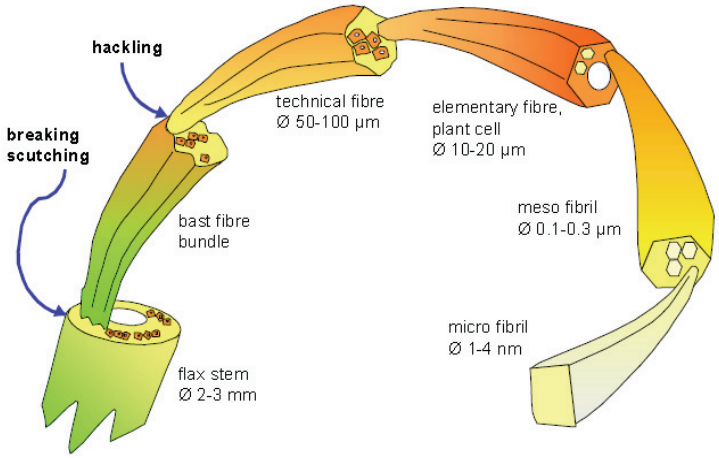

Fig. 7. Natural fibre hierarchal structure

Among natural fibres the bast fibres, extracted from the stems of plants such as jute, kenaf, flax, ramie and hemp are widely accepted as the best candidates for reinforcements of composites due to their good mechanical properties. Hemp was shown to have very promising tensile properties for applications where mechanical properties are a requisite (Nair et al., 2000)

As many authors agree, the two basic parameters that allow to characterize mechanical behavior of natural fibers are the cellulose content and the spiral angle. In general, the tensile strength of the fibers increases with increasing cellulose content and with decreasing angle of helix axis of the fibers.

The strength of natural fibre composites in on average lower compared to the synthetic fibre reinforced composites, even under optimised fibre-matrix interaction (Heijenrath & Peijs, 1996 , Berglund & Ericson, 1995), but their lower density and cost make them competitive in terms of specific and economic properties. This is basically due to the composite-like structure of natural fibres (Van den Oever et al., 1995); they are generally not single filaments as most manmade fibres but they can have several physical forms, which depend on the degree of fibre isolation. Composite strength depends also on fibre diameter (smallest diameter could achieve higher mechanical resistance due to larger specific contact surface with matrix) and fibre length.

2. Natural fibre fabric types

The possibility to have long or short fibres depends on the material under consideration, in fact, for synthetic fibre it is easy and common to have long continuous fibres out of

production plant, while, for natural fibres, the fibre's length is an inherent limit for the material itself due to their natural origin which limits their length (for example the plant stem). This is a basic reason why natural fibres are usually found as short reinforcements which are used to produce mat fabrics. Discontinuous fibres (*chopped*) are generally used for a randomly oriented reinforcement (*mat*) when there is not any preferential stress direction and/or there is a low stress/strain level in the composite (Fig.8). As it will be shown in the case studies mats, due to the random fibre orientation, are non-optimised fabric for mechanical performances.

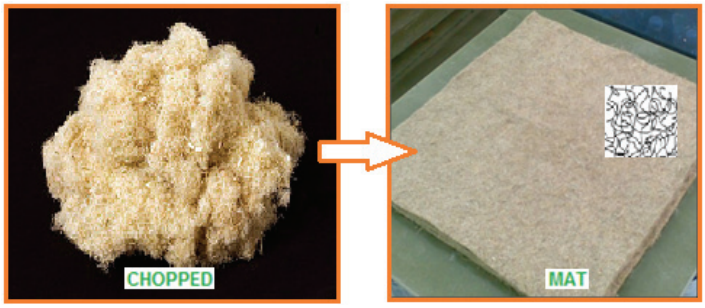

Fig. 8. Hemp mat

The alternative to the use of short fibres is the manufacture of long yarns. Yarn is a long continuous assembly of relatively short interlocked fibres, suitable for use in the production of textiles, sewing, crocheting, knitting, weaving, embroidery and ropemaking that are twisted with an angle to the yarn axis in order to provide axial strength to the yarn. Spun yarns are made by twisting or otherwise bonding staple fibres together to make a cohesive thread and may contain a single type of fibre or a blend of various types. Two or more spun yarns, if twisted together, form a thicker twisted yarn. Depending on the direction of this final twist, the yarn will be known as s-twist or z-twist (Fig.9). Two or more parallel spun yarns can form a *roving*. The main advantage of using natural yarns is the possibility to weave them into 2D and 3D fabrics with tailored yarn orientations.

A common measure unit used to classify fibres and yarns is the *denier* which corresponds to the linear mass density of the yarns. Denier is defined as the mass in grams per 9000 meters. In the International System of Units the tex is used instead, defined as the mass in grams per 1000 meters. The most commonly used unit is actually the decitex, abbreviated dtex, which is the mass in grams per 10000 meters. Similar to tex and denier, yield is a term that helps describe the linear density of a roving of fibres. However, unlike tex and denier, yield is the inverse of linear density and is usually expressed in yards/lb. Linear mass of twisted yarn is expressed by a fraction where the numerator is the yarn count and the denominator is simply the number of ends (e.g. 30/3).

Spun yarns obtained from natural fibres present usually some short fibres protruding out of the main yarn body (Fig.10). This short fibres are commonly referred to as yarn hairiness. Although not desirable in many cases, the hairiness can lead to better mechanical yarn/resin interlocking in composites. Another advantage of natural yarns is the increased surface roughness of yarns compared to fibres, which increases the interfacial strength due to mechanical interlocking, improving the transverse properties. In addition, twisting localizes the micro damages within the yarn leading to higher fracture strength.

Fig. 9. Hemp twisted yarn and scanning electron microscope image of hemp twisted yarn

Fig. 10. Hemp and flax fibre rovings

An important control parameter for such natural yarns is the twist level. It has been shown (Goutianos & Peijs , 2003) that very low twisted yarns display a very low strength when tested in air and therefore they cannot be used in processes such as pultrusion or textile manufacturing routes like knitting or weaving.(Fig.11) where heavy loading is experienced by the yarns while processing. In the case of short staple (length) fibres, higher twist level is necessary to prevent fibre slippage and to develop sufficient strength.

Besides yarn strength, the amount of twist also affects the inter-yarn impregnation while fabricating reinforced composites. With increased twist level yarns become more compact making it difficult for the resin to penetrate into the yarn. Dry yarns lead to lower bonding between yarns and resin thus leading to delamination and lowering of the composite tensile properties. Several authors showed that when highly twisted yarns are impregnated in a polymer resin, their strength may decrease significantly with decreases similar to the drop in strength of an off-axis composite (Goutianos & Peijs , 2003; Baley, 2002). Thus, there is an optimum level of twist, which should be kept as low as possible for optimal composite mechanical properties to allow for proper yarn's wetting to be achieved.

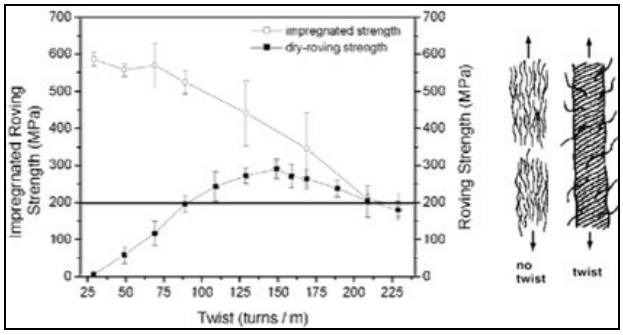

Fig. 11. Effect of twist level on mechanical properties (Goutianos at al., 2006)

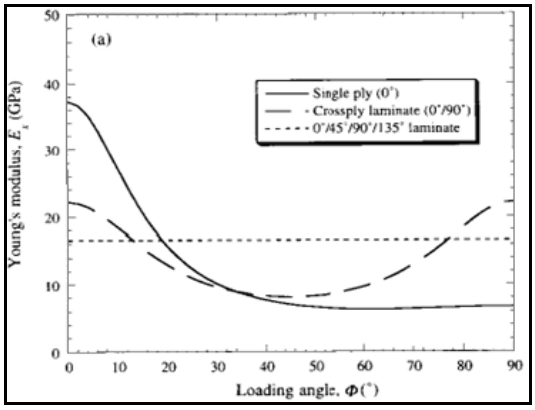

Fig. 12. Effect of fibre orientation on elastic modulus. Data for 50% fibre volume fraction of glass-epoxy laminate (source: Hull & Clyne)

The fibre contribution to composite mechanical properties improvement is emphasized when the stresses have components along the fibre direction (Fig. 12). However, most of the studies reported in literature are focused on the use of mat which are the cheapest alternative (Paiva et al., 2004) among technical fabrics. Several studies showed that the random orientation of the fibres in mat fabrics leads to lowering of the reinforcing efficiency (Baiardo et al., 2004).

Yarns offer a viable and interesting alternative to the use of short fibres as multiple filament yarns can be weaved into 2- or 3-Dimension textiles. Weaving is a textile production method which involves interlacing a set of longer threads, twisted yarn or roving, (called the warp) with a set of crossing threads (called the weft) (Fig.13). This is done on a frame or machine known as a loom, of which there are a number of types. Some weaving is still done by hand, but the vast majority is mechanised. The main advantage of using weaved fabrics is the possibility to pre-orient the filaments in the designed directions. Natural yarns differ from multifilament of synthetic fibres (ie.tow) because they are an assembly of short fibre instead of an assembly of aligned continuous fibres. However, the fibres which constitute the yarn have a preferential orientation along an helical trajectory which make the use of natural yarns attractive compared to short fibres because in such yarns fibres are mostly along the load direction.

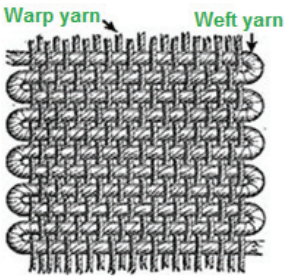

Fig. 13. Warp and weft in plain weaving

The manner in which the warp and weft threads are interlaced is known as the *weave style*. The three basic weaves styles or architectures are:

- plain weave
- satin weave
- twill weave

Plain weave is the most basic type of textile weaves.The warp and weft are aligned so they form a simple criss-cross pattern. Each weft thread crosses the warp threads by going over one, then under the next, and so on (Fig.14, 15). The next weft thread goes under the warp threads that its neighbour went over, and vice versa. In balanced plain weaves the warp and weft are made of threads of the same weight (size) and the same number of ends per inch. *http://en.wikipedia.org/wiki/Plain_weave - cite_note-1*

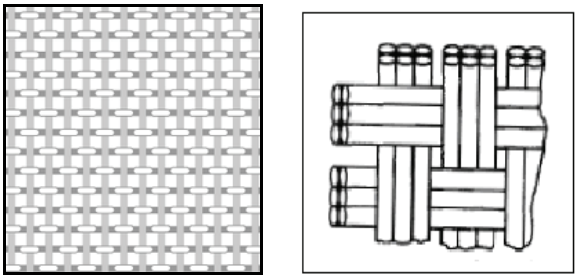

Fig. 14. Plain woven yarn and woven roving schemes (0°/90° reinforcement directions)

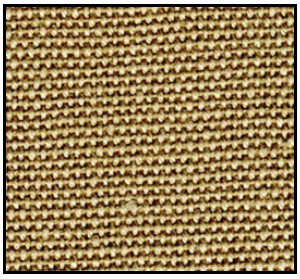

Fig. 15. Examples of plain woven flax yarns. H-181 100% Hemp Canvas weave 18oz/sq yd Wide 59" 5N/2 x 8N/2 x23x21. *Source: dongpinghemp.com*

The satin weave is characterized by four or more weft yarns floating over a warp yarn or vice versa, four warp yarns floating over a single weft yarn (Fig.16).
Twill is a type of fabric woven with a pattern of diagonal parallel ribs. It is made by passing the weft thread over one or more warp threads and then under two or more warp threads and so on, with a "step" or offset between rows to create the characteristic diagonal pattern (Fig.17,18). Because of this structure, twills generally drape well. In a twill weave, each weft or filling yarn floats across the warp yarns in a progression of interlacings to the right or left, forming a distinct diagonal line. This diagonal line is also known as a wale. A float is the portion of a yarn that crosses over two or more yarns from the opposite direction.

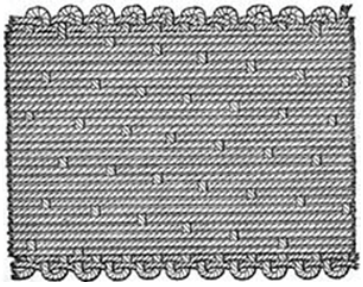

Fig. 16. Satin weave with 16 warp yarns floating over each weft yarn.

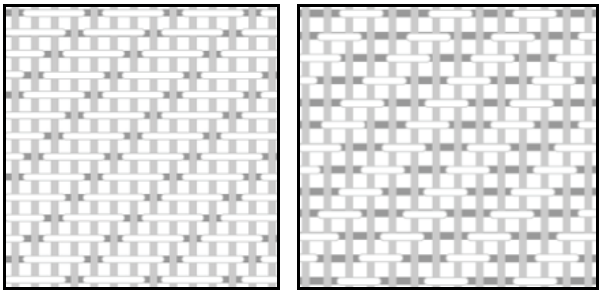

Fig. 17. Structure of a 3/1 and 2/2 twills

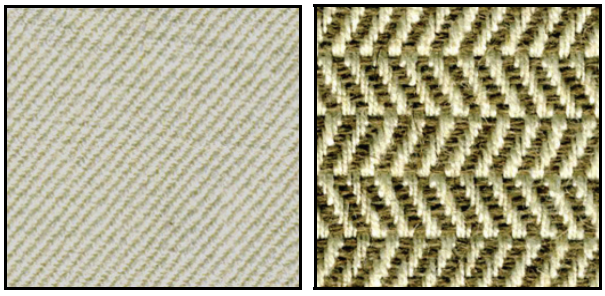

Fig. 18. Examples of plain woven flax yarns. (A) Natural Twill Weave 100% Hemp 12oz Width 57/58" (B) Natural Herringbone Weave 52% Hemp 48% Flax 20oz Width 57/58".
Source: EnviroTextile.com

A twill weave can easily be identified by its diagonal lines. and is often designated as a fraction—such as 2/1—in which the numerator indicates the number of harnesses that are raised, in this example, two, and the denominator indicates the number of harnesses that are lowered when a filling yarn is inserted, in this example one. The fraction 2/2 would be read as "two up, two down." with two warp threads crossing every two weft threads. The offset at each row forms the diagonal pattern. The minimum number of harnesses needed to produce a twill can be determined by totalling the numbers in the fraction.
The fewer interlacings in twills allow the yarns to move more freely, and thus they are softer and more pliable, and drape better. Twills also recover better from wrinkles than plain-weave fabrics. When there are fewer interlacings, yarns can be packed closer together to produce high-count fabrics.
There is an increasing number of producers of natural fibre fabrics around the world which are tailoring their products for composites technology. Table 4 shows some costs for a selection of fabrics commercialized in U.S.A. by the company EnviroTextile LLC.

Fabric Descriptions and Specifications	Units = Yards					
	1-49	50-99	100-499	500-999	1K-2999	3K-4999
Natural 100% Hemp Canvas Plain Weave, 16n/2x7n, 41x28, Width 57/58" 12oz Semi-Bleached, Preshrunk, Cationic Softener, SBP® 100%	$14.60	$12.00	$11.10	$10.30	$10.00	$9.65
Natural 100% Hemp Canvas Basket Weave, 10n/3x 10nm/3, 30x20, Width 57/58" 18.5oz Semi-Bleached, Preshrunk, Cationic Softener, SBP® 100%	$16.45	$13.50	$12.55	$11.60	$11.30	$10.90
Black 100% Hemp Canvas Basket Weave, 10n/3x 10nm/3, 30x20, Width 57/58" 18.5oz, Preshrunk, No Softener, SBP® 100%	$17.60	$14.45	$13.40	$12.40	$12.05	$11.65
Dark Brown 100%Hemp Canvas Basket Weave, 10n/3x 10n/3, 30x20, Width 57/58" 18.5oz Semi-Bleached, Preshrunk, No Softener, SBP® 100%	$17.60	$14.45	$13.40	$12.40	$12.05	$11.65
Sand 100 % Hemp Canvas Basket Weave, 10n/3x 10n/3, 30x20, Width 57/58" 18.5oz Semi-Bleached, Preshrunk, No Softener, SBP® 100%	$17.60	$14.45	$13.40	$12.40	$12.05	$11.65
Natural 100% Hemp Herringbone Weave, 16nm/2x8.5nm, 41x27, Width 55/56" 10.5oz Soft Finish, SBP® 100%	$14.95	$12.30	$11.40	$10.55	$10.25	$9.90

Table 4. Costs of some fabrics sold by EnviroTextile

Other examples of commercial products available on the market are the flax fabric (Fig. 19) manufactured by Biotex (http://www.compositesevolution.com) which are also available as pre-impregnated fabric with PLA (polylacticacid) and PP (polypropylene). Other products available are the pre-impregnated fabrics (FLAXPLY©) produced by Lineo. The products sold by Lineo have pre-treated fibers for increased fiber-matrix adhesion. The FLAXPLY© are proposed to be used for internal layer of mixed carbon/flax design for improved vibration absortion (Fig.20).
As mentioned before, yarns and rovings can be weaved in 3-Dimension fabrics, even if they are not so widespread as plain ones. To date no commercial example of 3D weaved fabric based on natural yarns is available.

Fig. 19. Biotex Flax 3H Satin 420gsm

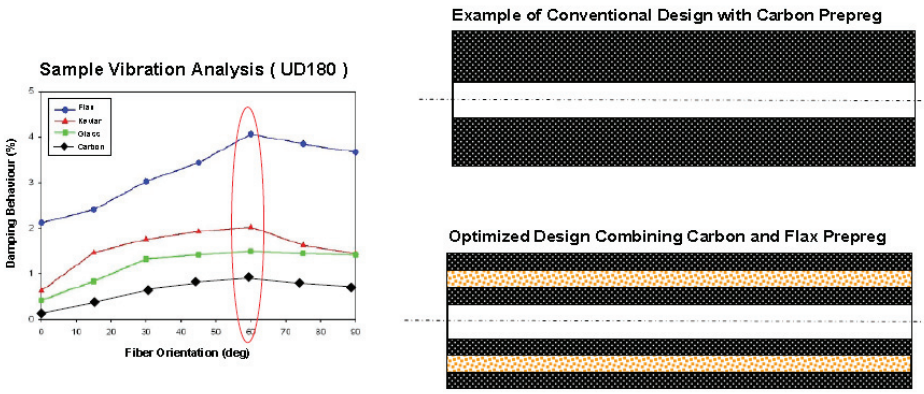

Fig. 20. Example of the use of FLAXPLY© for vibration absorption

3. Fiber surface treatments

The contribution of fibres to the final properties of the composite depends on:

- Mechanical properties of fibres;
- Type (continuos/discontinuos) and orientation of fibres in the composite (anisotropy).
- Volume fraction of fibres;
- Fibre-matrix interface;
- Processing technique used for composite manufacturing.

Shortcomings associated with natural fibres have to be overcome before using them in polymer composites. The most serious concern with natural fibres is their hydrophilic nature due to the presence of pendant hydroxyl and polar groups in various constituents, which can lead poor adhesion between fibres and hydrophobic matrix polymers (Rong et al., 2001, Bledzki & Gassan, 1996). The hydrophilic nature of the fibre surface lead also to high moisture up take for the natural fibres which can seriously lower the mechanical properties of the fibres themselves.

The natural fibres are inherently incompatible with nonpolar-hydrophobic thermoplastics, such as polyolefins. Moreover, difficulty in mixing because of poor wetting of the fibres with the matrix is another problem that leads to composites with weak interface (John & Anandjiwala, 2008).

There are some physical fibre treatments (e.g Plasma), but nowadays when we speak about surface treatments we almost mean chemical ones. These treatments can clean the fibre surface, modify the chemistry on the surface, lower the moisture up take and increase the surface roughness. As the natural fibres bear hydroxyl groups from cellulose and lignin they are amenable to chemical modification. The hydroxyl groups may be involved in the hydrogen bonding within the cellulose molecules thereby reducing the activity towards the matrix. Chemical modifications may activate these groups or can introduce new moieties that can effectively lead to chemical interlock with the matrix. Mercerization, isocyanate treatment, acrylation, permanganate treatment, acetylation, silane treatment and peroxide treatment with various coupling agents and other pretreatments of natural fibres have achieved various levels of success for improving fiber strength, fiber fitness and fiber-matrix adhesion. In the following section we report a review of the main preteatments techniques.

3.1 Alkali treatment

Alkali treatment of natural fibers, also called mercerization, is the common method to produce high-quality fibers. The scheme of the reaction is:

$$\text{FIBER-OH} + \text{NaOH} \rightarrow \text{FIBER-O}^{-}\text{Na}^{+} + \text{H}_2\text{O}.$$

Mercerization leads to fibrillation which causes the breaking down of the composite fibre bundle into smaller fibres. Mercerization reduces fibre diameter, thereby increases the aspect ratio which leads to the development of a rough surface topography that results in better fibre/matrix interface adhesion and an increase in mechanical properties (Kalia at al., 2009). Moreover, mercerization increases the number of possible reactive sites, allows better fibre wetting and gets an effect on the chemical composition of the hemp fibres, degree of polymerization and molecular orientation of the cellulose crystallites due to cementing substances like lignin and hemicelluloses which were removed during the mercerization process. As a result, mercerization had a long-lasting effect on the mechanical properties of hemp fibres, mainly on fibre strength and stiffness. If the treatment is done at high percentage of NaOH there could be an excessive extraction of lignin and hemicelluloses which can results in damage of the ultimate cells walls. Similar reduction of mechanical properties after alkali treatment have been reported in the literature (Rodriguez at al., 2007).Alkali treatment is recognized to hydrolyses the amorphous parts of cellulose present in fibres so that after treatment the material contains more crystalline cellulose (Le Troedec, 2008). Furthermore, it removes waxes and oils from the surfaces (Sgriccia, 2008).

3.2 Acetylation

Acetylation was originally applied to wood cellulose to stabilize the cell walls against moisture, improving dimensional stability and environmental degradation and to introduce plasticization to cellulosic fibers by esterification. Acetylation is based on the reaction of cell wall hydroxyl groups of lignocellulosic materials with acetic or propionic anhydride at elevated temperature (Fig.21). Pretreatment of fibers with acetic anhydride substitutes the polymer hydroxyl groups of the cell wall with acetyl groups, modifying the properties of these polymers so that they become hydrophobic (Andersson & Tillman, 1989; Murray, 1998; Rowell, 1991) Hydroxyl groups that react with the reagent are those of lignin and hemicelluloses (amorphous material), whereas the hydroxyl groups of cellulose (crystalline material) are being closely packed with hydrogen bonds, prevent the diffusion of reagent and thus result in very low extents of reaction (Rowell, 1998).

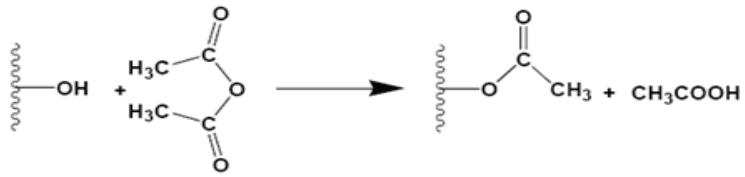

Fig. 21. Scheme of acetylation reaction

3.3 Peroxide treatment

Peroxide treatment of cellulose fibre has attracted the attention of various researchers due to easy processability and improvement in mechanical properties. Organic peroxides tend to decompose easily to free radicals, which further react with the hydrogen group of the matrix and cellulose fibers. In peroxide treatment, fibers are treated with 6% benzoyl peroxide or dicumyl peroxide in acetone solution for about 30 min after alkali pretreatment (Sreekala at al., 2002; Sreekala et al., 2002; Paul et al., 1997) conducted at a temperature of 70°C to support the decomposition of the peroxide.

3.4 Graft copolymerization

Synthesis of graft copolymers by creation of an active site, a freeradical or a chemical group which may get involved in an ionic polymerization or in a condensation process, on the preexisting polymeric backbone is one of the common methods. Polymerization of an appropriate monomer (e.g. benzoyl chloride, maleated polypropylene/maleic anhydride MAH-PP, acrylation, titanate) onto this activated back-bone polymer leads to the formation of a graft copolymer with a higher surface energy and wettability and adhesion interface by polymer matrix. It has been reported that maleic anhydride treatment reduced the water absorption to a great extent in hemp, banana and sisal fibers and their composites (Mysra et al.2000).

Modification of cellulosic fibers by etherification enhances certain new ranges of properties and makes it more useful and acceptable in diversified applications. Sodium hydroxide plays an important role in forming a charged intermediate species with the fiber, which allows the faster nucleophilic addition of epoxides, alkyl halides, benzyl chloride, acrylonitrile, and formaldehyde (Matsuda, 1996).

Benzoyl chloride is the most often used benzoylation pretreatment. Benzoyl ($C_6H_5C=O$) groups react with the cellulosic OH group of fiber decreasing hydrophilic nature of the treated fiber (Joseph et al., 2000) after a 30 min pre-soaking with NaOH solution to activate the hydroxyl groups of the cellulose and lignin in the fiber, followed by filtration and washing with water (Fig.22).

Fig. 22. Possible reaction between cellulosic-OH and benzoyl chloride (Joseph et al., 2000)

A number of methods can be used for the generation of active sites on the polymeric backbone and can be described as: physical, chemical, physicomechanical, radiation method

and enzymatic grafting. The conventional techniques of grafting of natural fibers require significant time and energy. It has been found that grafting under microwave radiations is the best method in terms of time consumption and cost effectiveness. Microwave radiation technique reduces the extent of physicochemical stresses to which the fibers are exposed during the conventional techniques (Kaith & Kalia 2008).

3.5 Coupling agents

Coupling agents usually improve the degree of crosslinking in the interface region and offer a perfect bonding. Among the various coupling agents, silane coupling agents were found to be effective in modifying the natural fiber-matrix interface. Silane grafting is based on the use of reactancts that bear reactive end groups which, on one end, can react with the matrix and, on the other end, can react with the hydroxyl groups of the fiber (Fig.23). The alkoxy or ethoxy are the end groups which can form stable covalent bonds reacting with the hydroxyl groups of the fiber. The end groups which can react with the matrix vary according to the polymer matrix type. If unsaturated polyester is used silanes bearing methacryl-, amine- and vinyl- can be used (Soo-Jin et al., 2001; Li Hu at al., 2009). Efficiency of silane treatment was high for the alkaline treated fiber than for the untreated fiber because more reactive site can be generated for silane reaction. Therefore, fibers are pretreated with NaOH for about half an hour before its coupling with silane. Fibers are then washed many times in distilled water and finally dried. Silane coupling agents may reduce the number of cellulose hydroxyl groups in the fiber-matrix interface minimizing fibre sensitivity to humidity. In the presence of moisture, hydrolizable alkoxy group leads to the formation of silanols. The silanol then reacts with the hydroxyl group of the fiber, forming stable covalent bonds to the cell wall that are chemisorbed onto the fiber surface (Agrawal et al., 2000). Therefore, the hydrocarbon chains provided by the application of silane restrain the swelling of the fiber by creating a cross-linked network because of covalent bonding between the matrix and the fiber.

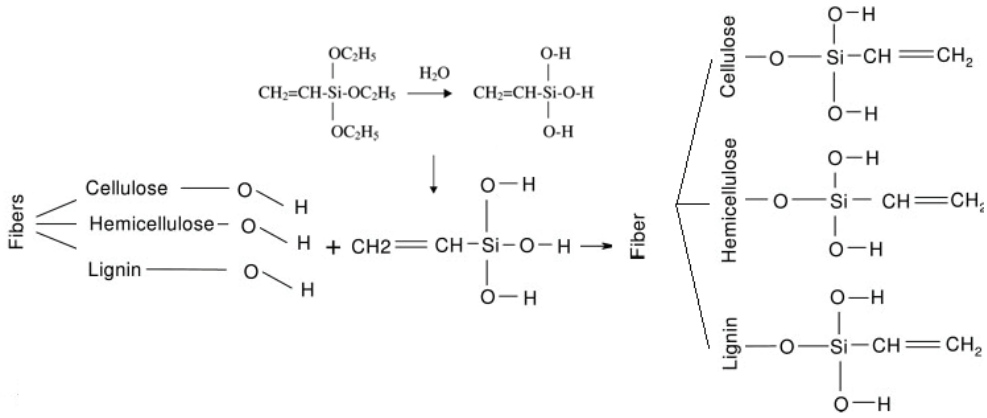

Fig. 23. Reaction of silane with OH groups of natural fiber

Silanes are effective in improving the interface properties (Coutinho at al., 1997; Gonzales et al., 1997). Alkoxy silanes are able to form bonds with hydroxyl groups. Fiber treatment with toluene dissocyanate and triethoxyvinyl silane could improve the interfacial properties.

Silanes after hydrolysis undergo condensation and bond formation stage and can form polysiloxane structures by reaction with hydroxyl group of the fibers. Silane grafting can modify the mechanical performances of fiber as a consequence of the use of acid solution for the treatment.
Isocyanate has –N=C=O functional group, which is very susceptible to reaction with the hydroxyl group of cellulose and lignin in the fibers and forms strong covalent bonds, thereby creating better compatibility with the binder resin in the composites (Kokta et al. 1990).

3.6 Permanganate treatment

Pretreatments with permanganate are conducted by using different concentration of potassium permanganate ($KMnO_4$) solution in acetone with soaking duration from 1 to 3 min after alkaline pretreatment. As a result of permanganate treatment, the hydrophilic tendency of the fibers is reduced, and thus, the water absorption of fiber-reinforced composite decreases with increase in $KMnO_4$ concentration (Sreekala et al., 2000; Paul et al., 1997). Permanganate treatment is indicated as one of the best method to improve the bonding at the fiber-polymer interface.

3.7 Physical plasma treatment

Plasma treatment is an effective method to modify the surface of natural polymers without changing their bulk properties. The plasma discharge can be generated by either corona treatment or cold plasma treatment. Both methods are considered as a plasma treatment when ionized gas has an equivalent number of positive and negative charged molecules that react with the surface of the present material. The distinguishing feature between the two categories of plasmas is the frequency of the electric discharge. High-frequency cold plasma can be produced by microwave energy, whereas a lower frequency alternating current discharge at atmospheric pressure produces corona plasma. The type of ionized gas and the length of exposure influenced the modification of the wood and synthetic polymer surfaces (Young et al., 1992; Goring & Bolam, 1976).

3.8 Chemical treatments on natural fibre: effect on mechanical properties

Chemically treated fibers can show a considerable decrease in tensile properties and this decrease is attributed to the substantial delignification and degradation of cellulosic chains during chemical treatment. The extension at break of these fibers does not change much. Most of the chemical treatments have been found to decrease the fiber strength due to breakage of the bond structure, and disintegration of the noncellulosic materials but silane and acrylation treatment leave to strong covalent bond formation and the stiffness is enhanced marginally due to the crystalline region (cellulosic) of the fiber.
The alkali treatment can produce a drop in both tensile strength and Young's modulus of the fibers if a very high percentage treatment is adopted. This result is attributed to the damage induced in the cell walls and the excessive extraction of lignin and hemicellulose, which play a cementing role in the structure of the fibers.
Morphological studies showed that the silane, benzoylation and peroxide pretreatment of flax fiber improved the surface properties. Silane and peroxide treatment of flax led to a higher tensile strength than that of untreated flax (Wang et al., 2007).

4. Case study: hybrid glass/natural fibre composites for curved pipes

4.1 Case study outline

The case study presented here refers to the analysis of the hybridization of glass fibres with natural fibres for applications in the piping industry (Cicala et al, 2009). The natural fibres studied were hemp, flax and kenaf. The pipe selected for the study was a curved fitting (90°) flanged at both ends designed to withstand an internal pressure of 10 bar and in the presence of acid aqueous solutions. This type of fitting is widely used in chemical plants which bear acid solution. The actual fittings are manufactured by hand layup with a complex sequence of glass mats and fabrics impregnated with epoxy vinyl ester resins. The problem was how to save cost without significant loss in mechanical properties and solvent resistance. Natural fibres mats were investigate as an alternative to glass mats.

4.2 Experimental

A commercial epoxy vinyl ester resin was used as thermoset matrix. Several glass fabrics were used varying from E-glass woven to E-glass random mat and C-glass liner (Table 5). The hemp mat was purchased by Hempcore Ltd., United Kingdom. Kenaf and Flax mats were kindly offered by Sachseinleinen Gmbh.

Component	Cost (€/m^2)	Areal weight (g/m^2)
E-glass woven	2.80	600
E-glass mat	2.13	600
C-glass liner	0.50	30
Hemp mat	0.31	600–650
Flax mat	0.37	750
Kenaf mat	0.33	630–650

Table 5. Technical data of the fabrics used

The lamina for mechanical testing were impregnated by hand lay-up and cured at room temperature for 48 h. The fittings were also manufactured by hand lay-up by wrapping the fabric onto a steel mandrel which is shown for reference in Fig. 24.

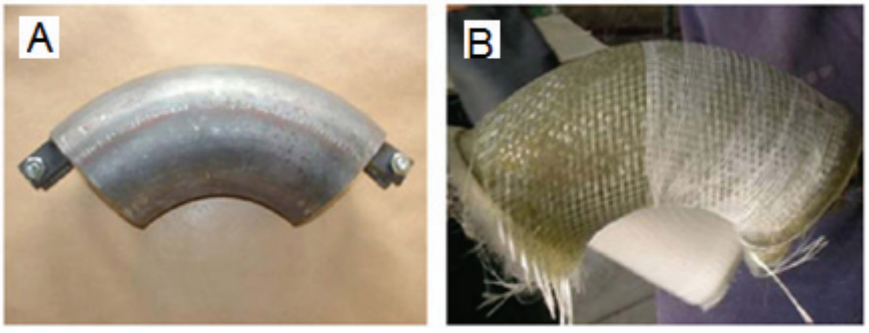

Fig. 24. (A) Steel mandrel used and (B) example of the fabric wrapping step

Tensile tests of single fibres (free fibre length was 15 mm), manually extracted from each mat, were carried out with a speed of 1 mm/min.

The cured laminas were tested accordingly to EN ISO 527 either on laminas obtained from a single fabric or on laminates obtained with a lay-up similar to those used for the fitting.
Some laminate specimens were also conditioned in different HCl solutions with pH varying from 1 to 7. The specimens were immersed for 40 days and then tested to analyze the effect on mechanical properties. This test was designed to predict the mechanical behaviour of the specimens in real working conditions. All the specimens were wrapped with C-glass liner to simulate the real surface of the interior of the fittings which is usually exposed to acid solutions.

4.3 Results and discussion

The results of tensile testing on single ply lamina are summarized in Fig. 25 for the tensile strength and modulus respectively normalized with respect to the density of each lamina. Bending showed similar results. The lamina reinforced with glass woven fabric showed the best performances in terms of tensile strength and modulus. This result is the consequence of the presence of long and aligned continuous glass fibres. The glass mat showed better mechanical properties compared to the natural fibre mats. The decrease of tensile strength compared to neat resin was observed for the lamina obtained from natural fibre mats. However, slight improvements of tensile modulus were observed compared to neat resin for the same samples. This behaviour can be explained as a consequence of the low fibre volume fraction (V_f) achieved for the lamina reinforced with the natural fibres and of the scarce adhesion between fibre and matrix. The latter and matrix were due to the absence of surface treatment on the fibres used in the present study. The natural fibre surface was not treated because this choice avoids to increase the price of the natural fibre. Measurements of V_f were performed on the natural fibre mat samples and an average of 8–11% was obtained. The reason for such low V_f are twofold: the hand lay-up method does not allow to achieve high compaction pressure and poor control on resin quantity is obtained; the natural fibres have a porous structure that increase the amount of resin adsorbed when lamina are impregnated. Moreover, the architecture of the natural fibre mats is quite open and thus higher percentages of resin are allowed to impregnated the mat. If liquid molding techniques like RTM (Resin Transfer Moulding) were employed for the manufacturing a V_f of 30% could be achievable. Table 6 reports the mechanical data of Fig. 25 after normalization to a V_f of 30%. The data clearly show that natural fibres can compare to glass fibres also in terms of mechanical performances if higher volume fraction of natural fibres are achieved.
The laminate sequence leads to a thickness of 11.92 mm and a cost for the fittings of 15.74€ in terms of raw materials cost) with a weight of 2.97 kg.
The laminates for fittings which are currently manufactured present the following ply sequence: [C/C/M/W/M/W/M/M/W/M/W/M] where C stands for C-glass liner, M for E-glass mat and W for E-glass woven.
The resistance of the laminate sequence was verified accordingly to the Tsai–Hill criterion and to the maximum tension criterion using the data from single lamina testing for the calculations. The calculations were carried out for each single ply considering the relative position in the lay-up sequence (table 7).
Accordingly to this finding and taking into account the cured ply thickness of the hemp mat the following alternative design was proposed for the fittings in order to achieve a pipe thickness similar to the original pipe construction: [C/C/M_n/W/W/M_n] where M_n stands for the natural fibre mat.

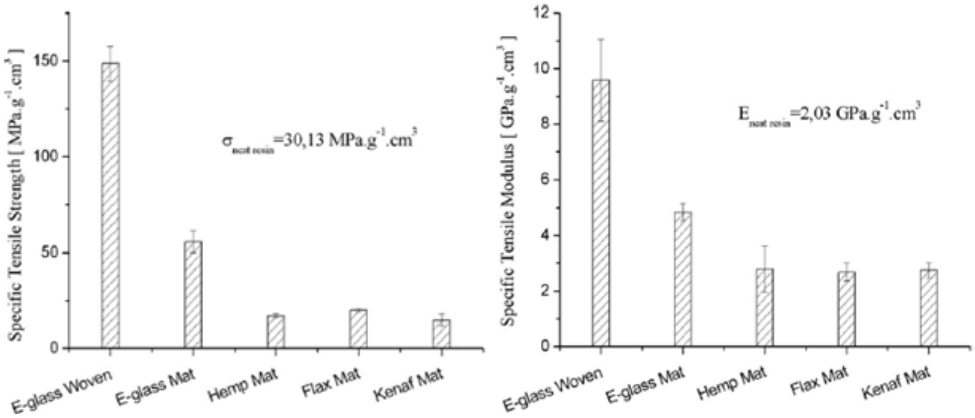

Fig. 25. Specific tensile strength and modulus on single lamina

Material	V_f (%)	Tensile strength (MPa g^{-1} cm^3)	Tensile modulus (GPa g^{-1} cm^3)
E-glass woven	35	127.64	8.22
E-glass mat	20	83.78	7.26
Hemp mat	12	42.95	7.00
Flax mat	10	60.24	8.04
Kenaf mat	9	49.50	9.17

Table. 6. Mechanical properties of single lamina after normalization to V_f of 30%

Ply	R (mm)	Maximum tension criterion			Tsai–Hill criterion			
		σ (MPa)	Res. (MPa)	Verify	σ (MPa)	Res (MPa)	Value R	Verify
Liner 1	50	–	–	–	–	–	–	–
L1	50	51.9	74.8	OK	51.9	74.8	0.36	OK
L2	51.54	123.1	240.2	OK	123.1	240.2	0.20	OK
L3	52.21	54.2	74.8	OK	54.2	74.8	0.39	OK
L4	53.75	128.4	240.2	OK	128.4	240.2	0.21	OK
L5	54.42	56.5	74.8	OK	56.5	74.3	0.43	OK
L6	55.96	58.1	74.8	OK	58.1	74.8	0.45	OK
L7	57.5	137.3	240.2	OK	137.3	240.2	0.25	OK
L8	58.17	60.4	74.8	OK	60.4	74.8	0.49	OK
L9	59.71	142.6	240.2	OK	142.6	240.2	0.26	OK
L10	60.38	62.7	74.8	OK	62.7	74.8	0.53	OK

Table. 7. Calculations according to the maximum tension and the Tsai-Hill criterion

The novel hybrid lay-up has been used to predict the cost (raw material) and the weight of the fittings produced using natural mat as replacement of glass mat. The results are summarized in Figs. 26 and 27 where the data for the original lay-up (named Glass) is reported for comparison purposes.

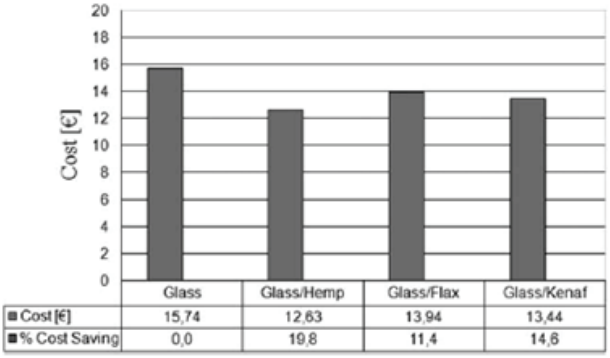

	Glass	Glass/Hemp	Glass/Flax	Glass/Kenaf
Cost [€]	15,74	12,63	13,94	13,44
% Cost Saving	0,0	19,8	11,4	14,6

Fig. 26. Cost comparison for different lay-up solutions

The comparison shows that the novel lay-up allows for the reduction of cost and weight for all the types of the natural fibres selected. The best performances were obtained with the hemp mat. A prototype of the fitting was build with the proposed laminate sequence using the hemp mat and it was tested under pressure up to 16 bar without any significant deformation or fluid leakage.

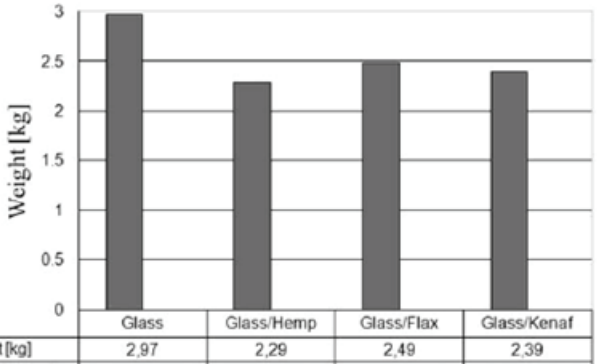

	Glass	Glass/Hemp	Glass/Flax	Glass/Kenaf
Weight [kg]	2,97	2,29	2,49	2,39
% Weight Saving	0,0	22,9	16,2	19,5

Fig. 27. Weight comparison for different lay-up solutions

Finally some laminates were tested after immersion in aqueous acid solutions for 40 days. In order to have significant data that laminates were wrapped with C-glass liner impregnated with the resin. This construction of the test lamina allows reproducing the conditions of the internal layer of the pipe which is usually exposed to the acid solution. The mechanical test showed that only small variations of the mechanical properties after immersion were obtained. The resistance to acid solution is a consequence of the barrier effect of the liner wrapping.

5. Case study: twisted hemp fabric versus hemp fabric

5.1 Case study outline

The objective of this case study is to compare the mechanical properties of twisted hemp fabric with hemp mats as viable reinforcement for composites. It has been mentioned

previously that hemp mats do not represent a fabric with optimised properties for composites reinforcement due to their random fibre orientation. To overcome the limitation offered by mats the use of fabric made with aligned yarn has been investigated. Two fabric architectures were considered: unidirectional and twill 2x2.

5.2 Experimental

The general purpose unsaturated polyester resin ECMALON 4411, purchased by Ecmass Resins Pvt. Ltd, India, was used as thermoset matrix. Methyl ethyl ketone peroxide (MEKT) and cobalt naphthenate were purchased by Aldrich, Italy, and used as catalyst and accelerator respectively. 3-aminopropyltriethoxysilane (A1100) was purchased from Aldrich, Italy, and used without further purification.

Several hemp fabrics were used in this study, varying from random mat fabric, purchased by Hempcore Ltd., United Kingdom, to unidirectional [0°] and bidirectional [0°/90°] woven fabrics purchased by Canipificio Italiano, Italy. The woven fabrics were obtained weaving yarns of natural fibres made of stable filaments twisted together.

Methyl ethyl ketone peroxide (MEKT) and cobalt naphtenate were added at room temperature at percentages of 1.5 wt% and 0.07 wt% respectively. Hand layup was used to prepare the laminates for mechanical testing. Each composite was cured at room temperature for 48 h.

The cured laminas were tested accordingly to EN ISO 527 for tensile test. Five replicas for each specimen were tested. Tensile test was carried out with a Zwick universal testing machine (model Z050) equipped with a 50 kN load cell. The experiment was performed in displacement-control mode at a stroke rate (i.e. cross-head displacement rate) of 2 mm/. All output data (strain, displacement of cross-head, and load) were collected by an acquisition system and transferred to the PC.

5.3 Results and discussion

The mechanical properties of the laminates reinforced by mat are reduced by a factor of about 3/8 because of the random distribution of the fibres. To overcome this limitation the use of weaved fabrics made of twisted yarns has been considered here. Two architectures, namely, unidirectional (UD) and 0/90 were considered (Fig.28). The laminates were obtained by hand layup. The results of tensile testing obtained for laminates prepared with these fabrics are summarized in Fig. 29.

Fig.29 clearly shows that both modulus and strength are greatly enhanced when twisted yarns are used despite their low mechanical properties in dry form compared to single fibres extracted from hemp mats. This finding is the outcome of the impregnation of the yarns with the resin which, upon curing, stabilizes the yarn reducing the sliding effect of the filaments. The good properties measured for the composites reinforced with hemp is the results of the favourable orientation, along the loading direction, of the staple fibres of the yarns. As it can be expected the 0/90 fabrics present lower mechanical performances compared to unidirectional fabrics. This result is due to the presence in the 0/90 fabric of yarns directed transversely compared to loading tensile direction. The modulus and strength reported in Fig. are slightly lower than the values found in literature because of the manufacturing method (ie. hand layup) selected and of the low fibre volume fraction achieved.

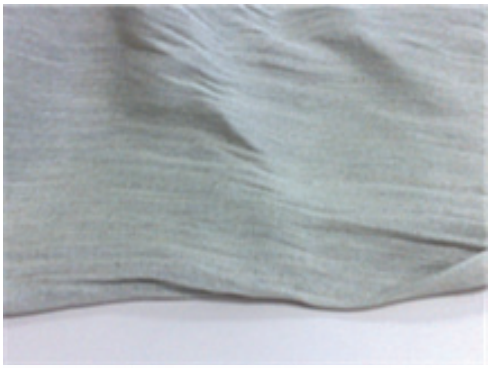

Fig. 28. Weaved fabric (0/90) with twisted yarns

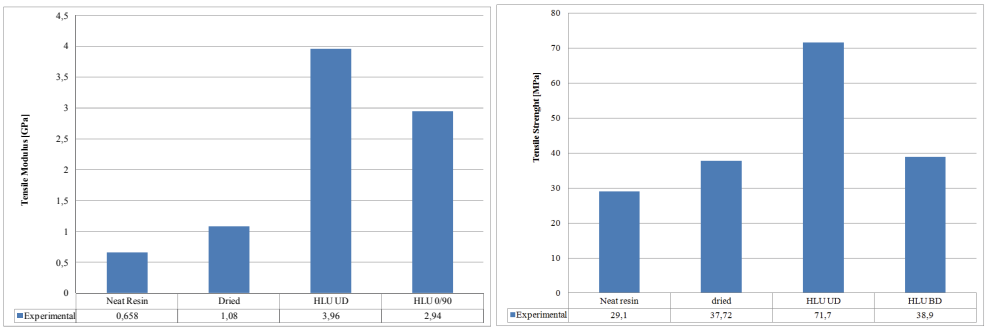

(a) (b)

Fig. 29. Tensile testing of weaved fabrics: Modulus (a), Strength (b)

6. Conclusions

The present chapter was focused on the use of natural fibre fabric as reinforcement for composite materials. The environmental and cost benefits connected with the use of natural fibre based fabrics are at the basis of their wide success. However, several limitations must be overcome in order to exploit the full potential of natural fibres. At first proper fibre surface treatment should be developed and implemented at industrial scale. Secondly, the use of mats should be investigated and the hybridization of mats with different textile further improved by analysing the effects of different layup and manufacturing techniques. Finally, the use of advanced textile based on twisted yarn should be developed further by optimising the yarn manufacturing and realising 3D architectures which are still missing from the market.

7. References

Bledzki AK & Gassan J. (1999). Composites reinforced with cellulose based fibres. *J Prog Polym Sci*; 24, 221–74.

Magurno A. (1999). Vegetable fibres in automotive interior components. Die Angew Makromol Chem; 272, 99–107.

John M.J., Francis B., Varughese K.T. & Thomas S. (2008), Effect of chemical modification on properties of hybrid fiber biocomposites. Composites: Part A – Applied Science and Manufacturing, 39 (2008) 352-363.

Saheb DN & Jog JP. (1999) Natural fiber polymer composites: A review. Adv Polym. Technol., 18, 351–63.

Kalia S., Kaith B.S. & Kaura I. (2009), Pretreatments of Natural Fibers and their Application as Reinforcing Material in Polymer Composites – A Review. Polymer Engineering and Science, 49, 1253-1272.

Williams G.I. & Wool R.P.(2000), Composites from Natural Fibers and Soy Oil Resins. Appl.Compos. Mater., 7, 421.

Bogoeva-Gaceva G., Avella M., Malinconico M., Buzarovska A., Grozdanov A., Gentile G. & Errico M.E. (2007), Natural Fiber Eco-Composites. Polymer Composites, 28, 98-107.

Rong. M.Z., Zhang M.Q., Liu Y., Yang G.C. & Zeng H.M. (2001), The effect of fiber treatment on the mechanical properties of sisal-reinforced epoxy composites. *Compos.Sci.Technolo.*, 61, 1437.

Nair KCM, Kumar RP, Thomas S, Schit SC & Ramamurthy K. (2000) Rheological behavior of short sisal fiber-reinforced polystyrene composites. Composites Part A. 31, 1231–40.

Heijenrath R. & Peijs T. (1996), Natural-fibre-mat-reinforced thermoplastic composites based on flax fibres and polypropylene, Adv. Comp. Let, 5, 81-85.

Berglund L.A. & Ericson M.L. (1995), Glass mat reinforced polypropylene in: Polypropylene: Structure, blends and composites, Vol 3, J. Karger-Kocsis (ed.), 202-227, Chapman & Hall, London.

Van den Oever M.J.A, Bos H.L. & van Kemenade M.J.J.M. (1995), Influence of the physical structure of flax fibres on the mechanical properties of flax fibre reinforced polypropylene composites, Appl. Comp. Mat. 7, 387-402.

Paiva MC, Cunha AM, Ammar I & Ben Cheikh R. (2004), Alfa fibres: mechanical, morphological, and interfacial characterisation, In: Proceedings of ICCE-11, pag. 8–14 USA, August 2004.

Baiardo M, Zini E & Mariastella S. (2004), Flax fibre-polyester composites. Composites: Part A ; 35, 703–10.

Goutianos, S. & Peijs, T. (2003) The optimisation of flax fibre yarns for the development of high performance natural fibre composites. Adv. Compos. Lett. 12, 237–241.

Baley, C. (2002) Analysis of the flax fibres tensile behaviour and analysis of the tensile stiffness increase. Composites A, 33, 939–948.

Goutianos S., Peijs T. & Nystrom B. (2006), Development of Flax Fibre based Textile Reinforcements for Comnposite Applications, Appl. Compos. Mater., 13, 199-215.

John M.J. & Anandjiwala R.D. (2008), Chemical modification of flax reinforced polypropylene composites, Polym. Compos., 29, 187.

Bledzki AK & Gassan J. (1996), Natural fiber reinforced plastics. Kassel, Germany: University of Kassel; 1996.

Rodriguez E.S., Stefani P.M. & Vazquez A. (2007), Effects of Fibers'Alkali Treatment on the Resin Transfer Moulding Processing and Mechanical Properties of Jute-Vinylester Composites, Journal of Composite Materials, Vol. 41, No. 14.

Le Troedec M., Sedan D., Peyratout C., Bonnet J.P., Smith A., Guinebretiere R., Gloaguen V. & Krausz P. (2008), Influence of various chemical treatments on the composition and structure of hemp fibres, Composites- Part A: applied science and manufacturing, 39, 514-522.

Sgriccia N., Hawley M.C. & Misra M. (2008), Characterization of natural fiber surfaces and natural fiber composites, Composites- Part A: applied science and manufacturing, 39, 1632-1637.

Andersson M. & Tillman A.M. (1989), Acetylation of jute: Effects on strength, rot resistance, and hydrophobicity, *J. Appl. Polym. Sci.*, 37, 3437.

Murray J.E. (1998), Acetylated Natural Fibers and Composite Reinforcement, *21st International BPF Composites Congress*, Publication Number 293/12, British Plastics Federation, London.

Rowell R.M. (1991), Natural Composites, Fiber Modification, in *International Encyclopedia of composites*, 4, S.M. Lee, Ed., VHC, New York,.

Rowell R.M. (1998), Property Enhanced Natural Fiber Composite Material based on Chemical Modification, in *Science and Technology of Polymers and Advanced Materials*, Prasad P.N., Mark J.E., Kendil S.H. & Kafafi Z.H Eds., pag. 717-732, Plenum Press, New York.

Matsuda H. (1996), Chemical Modification of Solid Wood in Chemical Modification of Lignocellulosic Materials, D. Hon Ed., pag. 159, Marcel Dekker, New York.

Sreekala M.S., Kumaran M.G., Joseph S., Jacob M & Thomas S. (2000), Appl. Compos. Mater., 7, 295.

A. Paul, K. Joseph, and S. Thomas, Compos. Sci. Technol., 57, 67 (1997).

M.S. Sreekala, M.G. Kumaran, and S. Thomas (2002), Compos. Part A: Appl. Sci. Manuf., 33, 763.

Joseph K., Mattoso L.H.C., Toledo R.D., Thomas S., de Carvalho L.H., Pothen L., Kala S. & James B. (2000), Natural Fiber Reinforced Thermoplastic Composites in *Natural Polymers and Agrofibers Composites*, Frollini E., Leao A.L. & Mattoso L.H.C. Eds., 159, San Carlos, Brazil, Embrapa, USP-IQSC, UNESP.

Kaith B.S. & Kalia S. (2008), *Polym. Compos.*, 29, 791.

Soo-Jin Park & Joong-Seong Jin (2001), Effect of Silane Coupling Agent on Interphase and Performance of Glass Fibers/unsaturated Polyester Composites, *Journal of Colloid and Interface Science,* 242, 174-179.

Li Hu, Yizao Wana, Fang He, H.L. Luo, Hui Liang, Xiaolei Li & Jiehua Wang (2009), Effect of coupling treatment on mechanical properties of bacterial cellulose nanofibre-reinforced UPR ecocomposites, *Materials Letters,* 63: 1952–195.

Mishra S.,. Naik J.B &. Patil Y.P (2000), *Compos. Sci. Technol.*, 60, 1729.

Agrawal R., Saxena N.S., Sharma K.B. (2000), Thomas S. &. Sreekala M.S, *Mater. Sci. Eng. A*, 277, 77.

Coutinho F.M.B., Costa T.H.S. & Carvalho D.L. (1997), *J. Appl. Polym. Sci.*, 65, 1227.

Gonzalez L., Rodriguez A., de Benito J.L.& Marcos-Fernandez A. (1997), *J. Appl. Polym. Sci.*, 63, 1353.

Sreekala M.S., Kumaran M.G., Joseph S., Jacob M. & Thomas S. (2000), *Appl. Compos. Mater.*, 7, 295.

Kokta B.V., Maldas D., Daneault C. & Beland P. (1990), *Polym.-Plast. Technol. Eng.*, 29, 87.

Wang B., Panigrahi S., Tabil L. & Crerar W. (2007), *J. Reinf. Plast. Compos.*, 26, 447.

Young R., Rowell R., Shulz T.P. & Narayan R. (1992), Activation and Characterization of Fiber Surfaces for Composites in *Emerging Technologies for Materials and Chemicals from Biomass*, Eds., American Chemical Society, pag.115 Washington D.C., 115.

Goring D. & Bolam F. (1976), Plasma-Induced Adhesion in Cellulose and Synthetic Polymers in *The Fundamental Properties of Paper Related to its uses*, Ed., Ernest Benn Limited, pag.172, London.

Cicala G., Cristaldi G., Recca G., Ziegmann G., ElSabbagh A. & M.Dickert (2009). Properties and performances of various hybrid glass/natural fibre composites for curved pipes, *Materials & Design,* 30, 2538-2542.

18

Crashworthiness Investigation and Optimization of Empty and Foam Filled Composite Crash Box

Dr. Hamidreza Zarei[1] and Prof. Dr.-Ing. Matthias Kröger[2]
[1]*Aeronautical University, Tehran,*
[2]*Institute of Machine Elements, Design and Manufacturing,*
University of Technology Freiberg,
[1]*Iran*
[2]*Germany*

1. Introduction

Metallic and composite columns are used in a broad range of automotive and aerospace applications and especially as crash absorber elements. In automotive application, crashworthy structures absorb impact energy in a controlled manner. Thereby, they bring the passenger compartment to rest without subjecting the occupant to high decelerations. Energy absorption in metallic crash absorbers normally takes place by progressive buckling and local bending collapse of columns wall. A distinctive feature of such a deformation mechanism is that the rate of energy dissipation is concentrated over relatively narrow zones, while the other part of the structure undergoes a rigid body motion. In comparison to metals, most composite columns crush in a brittle manner and they fail through a sequence of fracture mechanism involving fiber fracture, matrix crazing and cracking, fiber-matrix debonding, delamination and internal ply separation. The high strength to weight and stiffness to weight ratios of composite materials motivated the automobile industry to gradual replacement of the metallic structures by composite ones. The implementation of composite materials in the vehicles not only increases the energy absorption per unit of weight (Ramakrishna, 1997) but also reduces the noise and vibrations, in comparison with steel or aluminum structures (Shin et al., 2002). The crashworthiness of a crash box is expressed in terms of its energy absorption E and specific energy absorption SEA. The energy absorption performance of a composite crash box can be tailored by controlling various parameters like fiber type, matrix type, fiber architecture, specimen geometry, process condition, fiber volume fraction and impact velocity. A comprehensive review of the various research activities have been conducted by Jacob et al. (Jacob et al., 2002) to understand the effect of particular parameter on energy absorption capability of composite crash boxes.

The response of composite tubes under axial compression has been investigated by Hull (Hull, 1982). He tried to achieve optimum deceleration under crush conditions. He showed that the fiber arrangement appeared to have the greatest effect on the specific energy absorption. Farley (Farley, 1983 and 1991) conducted quasi-static compression and impact tests to investigate the energy absorption characteristics of the composite tubes. Through his

experimental work, he showed that the energy absorption capabilities of Thornel 300-fiberite and Kevlar-49-fiberite 934 composites are a function of crushing speed. He concluded that strain rate sensibility of these composite materials depends on the relationship between the mechanical response of the dominant crushing mechanism and the strain rate. Hamada and Ramakrishna (Hamada & Ramakrishna, 1997) also investigate the crush behavior of composite tubes under axial compression. Carbon polyether etherketone (PEEK) composite tubes were tested quasi-statically and dynamically showing progressive crushing initiated at a chamfered end. The quasi-staticlly tested tubes display higher specific energy absorption as a result of different crushing mechanisms attributed to different crushing speeds. Mamalis et al. (Mamalis et al., 1997 and 2005) investigated the crush behavior of square composite tubes subjected to static and dynamic axial compression. They reported that three different crush modes for the composite tubes are included, stable progressive collapse mode associated with large amounts of crush energy absorption, mid-length collapse mode characterized by brittle fracture and catastrophic failure that absorbed the lowest energy. The load-displacement curves for the static testing exhibited typical peaks and valleys with a narrow fluctuation amplitude, while the curves for the dynamically tested specimens were far more erratic. Later Mamalis et al. (Mamalis et al., 2006) investigated the crushing characteristics of thin walled carbon fiber reinforced plastic CFRP tubular components. They made a comparison between the quasi-static and dynamic energy absorption capability of square CFRP.

The high cost of the experimental test and also the development of new finite element codes make the design by means of numerical methods very attractive. Mamalis et al. (Mamalis et al., 2006) used the explicit finite element code LS-DYNA to simulate the crush response of square CFRP composite tubes. They used their experimental results to validate the simulations. Results of experimental investigations and finite element analysis of some composite structures of a Formula One racing car are presented by Bisagni et al.(Bisagni et al., 2005) . Hoermann and Wacker (Hoermann & Wacker, 2005) used LS-DYNA explicit code to simulate modular composite thermoplastic crash boxes. El-Hage et al. (El-Hage et al., 2004) used finite element method to study the quasi-static axial crush behavior of aluminum/composite hybrid tubes. The hybrid tubes contain filament wound E glass-fiber reinforced epoxy over-wrap around an aluminum tube.

Although there is several published work to determine the crash characteristics of metallic and composite columns, only few attempts have been made to optimize those behaviors. Yamazaki and Han (Yamazaki & Han, 1998) used crashworthiness maximization techniques for tubular structures. Based on numerical analyzes, the crash responses of tubes were determined and a response surface approximation method RSM was applied to construct an approximative design sub-problems. The optimization technique was used to maximize the absorbed energy of cylindrical and square tubes subjected to impact crash load. For a given impact velocity and material, the dimensions of the tube such as thickness and radius were optimized under the constraints of tube mass as well as the allowable limit of the axial impact force. Zarei and Kroeger (Zarei & Kroeger, 2006) used Multi design objective MDO crashworthiness optimization method to optimize circular aluminum tubes. Here the MDO procedure was used to find the optimum aluminum tube that absorbs the most energy while has minimum weight.

This study deals with experimental and numerical crashworthiness investigations of square and hexagonal composite crash boxes. Drop weight impact tests are conducted on composite crash boxes and the finite element method is used to reveal more details about crash process. Thin shell elements are used to model the tube walls. The crash experiments

show that tubes crush in a progressive manner, i.e. the crushing starts from triggered end of the tubes, exhibit delamination between the layers. Two finite element models, namely single layer and multi layers, are developed.
In the single layer model, the delamination behavior could not be modeled and the predicted energy absorption is highly underestimated. Therefore, to properly consider the delamination between the composite layers, the tube walls are modeled as multi layer shells and an adequate contact algorithm is implemented to model the adhesion between them. Numerical results show that in comparison to the one layer method, the multi layer method yield more meaningful and accurate experimental results. Finally the multi design optimization MDO technique is implemented to identify optimum tube geometry that has maximum energy absorption and specific energy absorption characteristics.
The length, thickness (number of layers) and width of the tubes are optimized while the mean crash load is not allowed to exceed allowable limits. The D-optimal design of experiment and the response surface method are used to construct sub-problems in the sequentially optimization procedure. The optimum tube is determined that has maximum reachable energy absorption with minimum tube weight. Finally the optimum composite crash box is compared with the optimum aluminum crash box. Also the crash behaviour of foam filled composite crash boxes are investigated and compared with empty ones.

2. Experimental and numerical results

Axial impact tests were conducted on square and hexagonal composite crash boxes. The nominal wall thicknesses of the composite tubes are 2 mm, 2.4 mm and 2.7 mm. Square tubes with length of 150 mm and hexagonal tube with the length of 91 mm are used, see Figure 1. The specimens are made from woven glass-fiber in a polyamide matrix, approximately 50% volume fiber. Equal amount of fibers are in the two perpendicular main orientations. They are produced by Jacob Composite GmbH. Similar tubes are used in the bumper system of the BMW M3 E46 as well as E92 and E93 model as crash boxes.
A 45 degree trigger was created at the top end of the specimens. Generally injection moulding can be used to produce complex reinforced thermoplastics parts with low fiber length/fiber diameter aspect ratio. With increasing aspect ratio the crush performance increases but the flow ability of the material decreases. For this reason continuous reinforced thermoplastic have to be thermoformed. In this way and by using other post processing technologies like welding, complex composite parts with an excellent crush performance can be realized (Hoermann & Wacker, 2005). Here, the crash boxes are produced from thermoplastic plates by using thermoforming technique. The square specimens have overlap in one side and the overlaps have been glued by using a structural adhesive. The hexagonal crash boxes consist of two parts that are welded to each other.
The experimental tests have been conducted on the drop test rig, see Fig. 2, which is installed in the Institute of Dynamics and Vibrations at the Leibniz University of Hannover. This test rig has an impact mass which can be varied from 20 to 300 kg. The maximum drop height is 8 m and maximum impact speed is 12.5 m/s. The force and the displacement are recorded with a PC using an AD-converter. The force is measured using strain gauges and laser displacement sensors provide the axial deformation distance of the tubes. Here an impact mass of 92 kg was selected. The interest in this study is the mean crashing load P_m and the energy absorption E. The mean crash load is defined by

$$P_m = 1/\delta \int_0^{\delta} P(\delta)\, d\delta \tag{1}$$

where P(δ) is the instantaneous crash load corresponding to the instantaneous crash displacement d. The area under the crash load–displacement curve gives the absorbed energy. The ratio of the absorbed energy to the crush mass of the structure is the specific energy absorption. High values indicate a lightweight absorber. Figure 1 shows the geometry of the specimens.

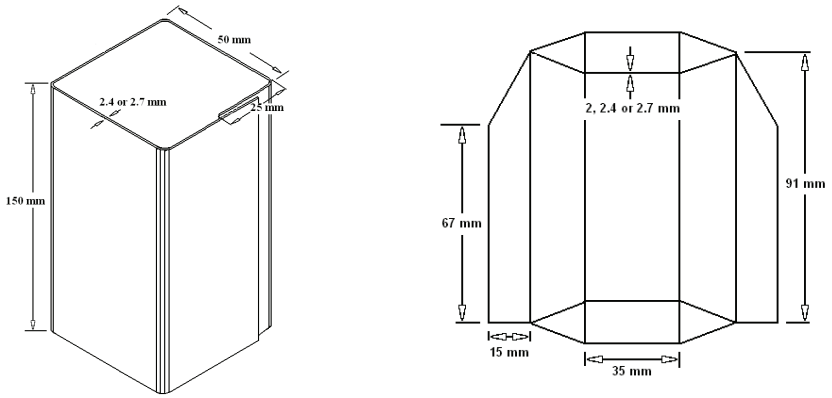

Fig. 1. (a) Square crash box (b) hexagonal crash box

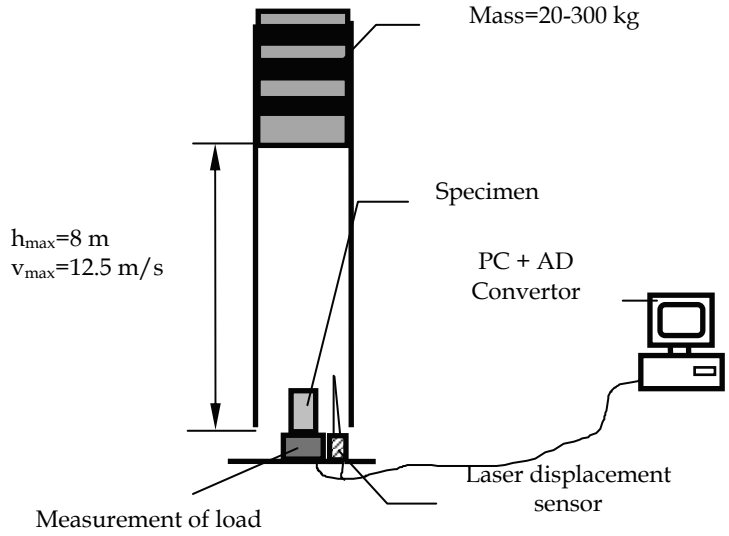

Fig. 2. Test rig

Numerical simulations of crash tests are performed to obtain local information from the crush process. The modeling and analysis is done with the use of explicit finite element

code, LS-DYNA. The column walls are built with the Belytschko-Tsay thin shell elements and solid elements are used to model the impactor. The contact between the rigid body and the specimen is modeled using a node to surface algorithm with a friction coefficient of μ= 0.2. To take into account the self contact between the tube walls during the deformation, a single surface contact algorithm is used. The impactor has been modeled with the rigid material. The composite walls have been modeled with the use of material model #54 in LS-DYNA. This model has the option of using either the Tsai-Wu failure criterion or the Chang-Chang failure criterion for lamina failure. The Tsai-Wu failure criterion is a quadratic stress-based global failure prediction equation and is relatively simple to use; however, it does not specifically consider the failure modes observed in composite materials (Mallick, 1990). Chang-Chang failure criterion (Mallick, 1990) is a modified version of the Hashin failure criterion (Hashin, 1980) in which the tensile fiber failure, compressive fiber failure, tensile matrix failure and compressive matrix failure are separately considered. Chang and Chang modified the Hashin equations to include the non-linear shear stress-strain behavior of a composite lamina. They also defined a post-failure degradation rule so that the behavior of the laminate can be analyzed after each successive lamina fails. According to this rule, if fiber breakage and/or matrix shear failure occurs in a lamina, both transverse modulus and minor Poisson's ratio are reduced to zero, but the change in longitudinal modulus and shear modulus follows a Weibull distribution. On the other hand, if matrix tensile or compressive failure occurs first, the transverse modulus and minor Poisson's ratio are reduced to zero, while the longitudinal modulus and shear modulus remain unchanged. The failure equations selected for this study are based on the Chang-Chang failure criterion. However, in material model #54, the post-failure conditions are slightly modified from the Chang-Chang conditions. For computational purposes, four indicator functions e_f, e_c, e_m, e_d corresponding to four failure modes are introduced. These failure indicators are based on total failure hypothesis for the laminas, where both the strength and the stiffness are set equal to zero after failure is encountered,

(a) Tensile fiber mode (fiber rupture),

$$\sigma_{aa} > 0, \text{ and } e_f^2=(\sigma_{aa}/x_t)^2 + \zeta(\sigma_{ab}/S_c)^2 - 1 \begin{cases} \geq 0 \Rightarrow \text{faild} \\ > 0 \Rightarrow \text{elastic} \end{cases} \tag{2}$$

Where ζ is a weighting factor for the shear term in tensile fiber mode and $0<\zeta<1$. $E_a=E_b=G_{ab}=\upsilon_{ab}=\upsilon_{ba}=0$ after lamina failure by fiber rupture.

(b) Compressive fiber mode (fiber buckling or kinking),

$$\sigma_{aa} > 0, \text{ and } e_c^2=(\sigma_{aa}/x_c)^2 - 1 \begin{cases} \geq 0 \Rightarrow \text{faild} \\ > 0 \Rightarrow \text{elastic} \end{cases} \tag{3}$$

$E_a=\upsilon_{ab}=\upsilon_{ba}=0$ after lamina failure by fiber buckling or kinking.

(c) Tensile matrix mode (matrix cracking under transverse tension and in-plane shear),

$$\sigma_{bb} > 0, \text{ and } e_m^2=(\sigma_{bb}/y_t)^2 + \zeta(\sigma_{ab}/S_c)^2 - 1 \begin{cases} \geq 0 \Rightarrow \text{faild} \\ > 0 \Rightarrow \text{elastic} \end{cases} \tag{4}$$

$E_a=G_{ab}=\upsilon_{ab}=0$ after lamina failure by matrix cracking

(d) Compressive matrix mode (matrix cracking under transverse compression and in-plane shear),

$$\sigma_{bb}>0,\ \text{and}\ e_d^2=(\sigma_{bb}/2S_c)^2+\left[(y_c/2S_c)^2-1\right]\sigma_{bb}/y_c+(\sigma_{bb}/2S_c)^2-1\begin{cases}\geq 0\Rightarrow \text{faild}\\ >0\Rightarrow \text{elastic}\end{cases} \quad (5)$$

$E_b=\upsilon_{ab}=\upsilon_{ba}=0\rightarrow G_{ab}=0$ after lamina failure by matrix cracking

In Equations (2)–(5), σ_{aa} is the stress in the fiber direction, σ_{bb} is the stress in the transverse direction (normal to the fiber direction) and σ_{ab} is the shear stress in the lamina plane aa-bb. The other lamina-level notations in Equations (2)–(5) are as follows: x_t and x_c are tensile and compressive strengths in the fiber direction, respectively. Y_t and y_c are tensile and compressive strengths in the matrix direction, respectively. S_c is shear strength; E_a and E_b are Young's moduli in the longitudinal and transverse directions, respectively. Here, to model the trigger, two elements with progressively reduced thicknesses were placed in the triggers zone. The tied surface to surface contact algorithm has been used to glue the overlapping walls.

Tables 1 and 2 show the test results of the square and hexagonal composite tubes . Here, the area under crush load-displacement curve is considered as energy absorption E. The maximum crush load P_{max} is a single peak at the end of the initial linear part of the load curve. The mean crush load P_m has been determined with the use of Equation (1). The maximum crush displacement S_{max} is the total displacement of the impactor after contact with the crash box. The values of specific energy absorption SEA, which is the energy absorption per crush weight, and the crush load efficiency η, which is the ratio of the mean crush load and maximum crush load, are also presented in these tables.

Figure 3 shows the specimen (S-67) and (S-75) after crush, respectively. Relatively ductile crush mode can be recognized. The tubes are split at their corners. This splitting effect is initiated at the end of the linear elastic loading phase, when the applied load attains its peak value P_{max}. The splitting of the corners of the tube is followed by an immediate drop of the crush load, and propagation parallel to the tube axis results in splitting of the tube in several parts. Simultaneous of splitting, some of these parts are completely splayed into two fronds which spread outwards and inwards and some parts are split only partially. Subsequent to splitting, the external and internal fronds are bended and curled downwards and some additional transverse and longitudinal fracture happened.

Photographs from high speed camera for different impact moments are presented in Figures 4 and 5. Here it can be seen that local matrix and fiber rupture results in a formation of pulverized ingredients material just after initial contact between impactor and crash boxes. As compressive loading proceeds, further fragments are detached from the crash box. Furthermore, the crush performance of tests has been simulated with the use of LS-DYNA explicit code. Figure 6 shows the experimental and simulated crush load-displacement and energy absorption-displacement curves of tests (S-67) to (S-69).

The same results for hexagonal crash boxes, tests (S-75) to (S-77), are presented in Figure 7. The crush-load displacement curves indicate that the mean crush load of simulation is obviously lower than experimental results. The numerical simulation can not cover the experiments very good.

Test No.	V [m/s]	t [mm]	P_{max} [kN]	P_m [kN]	S_{max} [mm]	E [J]	SEA [J/kg]	η [%]
S-67	10.3	2.4	77.2	40.6	126.9	4956	41844	53
S-68	10.4	2.4	75.3	46.03	118.9	5053	45533	61
S-69	10.2	2.4	83.7	43.3	117.3	4923	44967	52
S-70	10.4	2.7	82.2	58.7	86.2	5075	55542	71
S-71	10.4	2.7	92.3	59.3	84.7	5024	55957	64

Table 1. Experimental dynamic test on square composite tube

Test No.	V [m/s]	t [mm]	P_{max} [kN]	P_m [kN]	S_{max} [mm]	E [J]	SEA [J/kg]	η [%]
S-72	7.3	2.0	51	42.6	72.8	3103	35681	83
S-73	7.3	2.0	55	45.5	68.3	3109	35750	83
S-74	7.3	2.0	46	37.9	78.2	2964	34083	82
S-75	8.4	2.4	72	53.7	76.95	4133	39604	75
S-76	8.4	2.4	81	69.4	61.03	4235	40582	86
S-77	8.9	2.4	72	65.6	71.4	4683	44875	91
S-78	8.3	2.7	83	66.9	59.96	4012	34173	81
S-79	8.3	2.7	80	68.4	58.6	4008	34139	86
S-80	8.8	2.7	84	58.8	75.5	4442	37836	70

Table 2. Experimental dynamic test on hexagonal composite tube

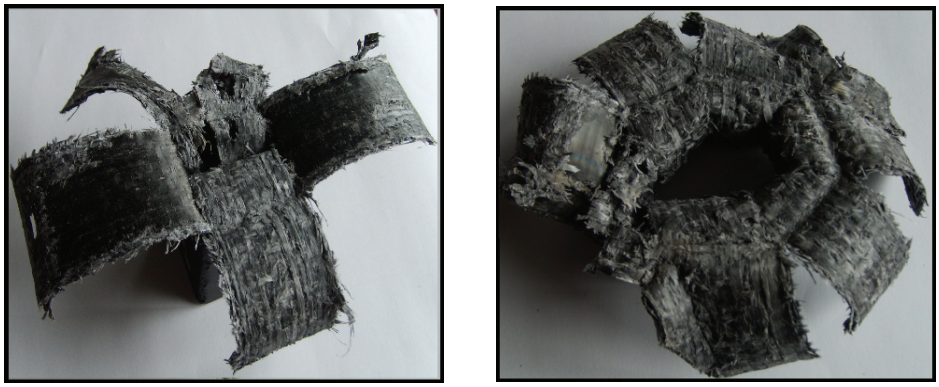

Fig. 3. Crush pattern of square tube S-67 (left) and hexagonal tube S-75 (right)

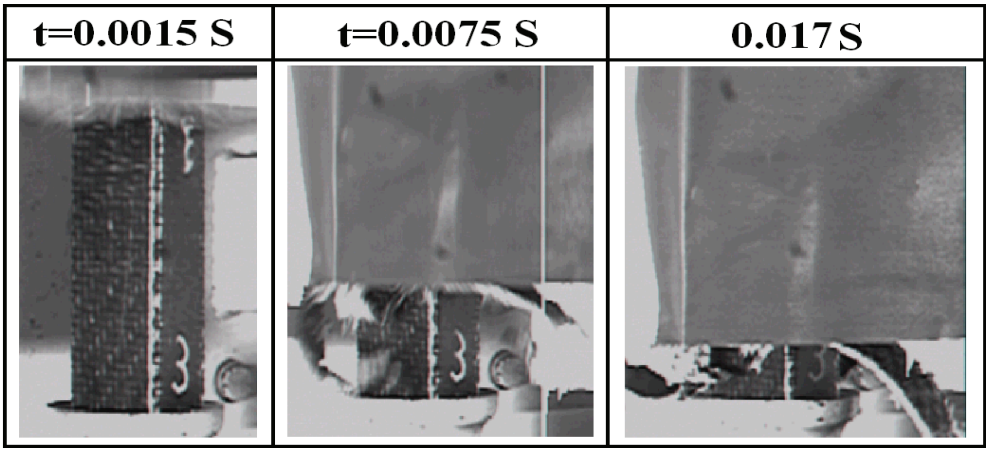

Fig. 4. Crush pattern of a square composite tube (S-67) for different crush moments

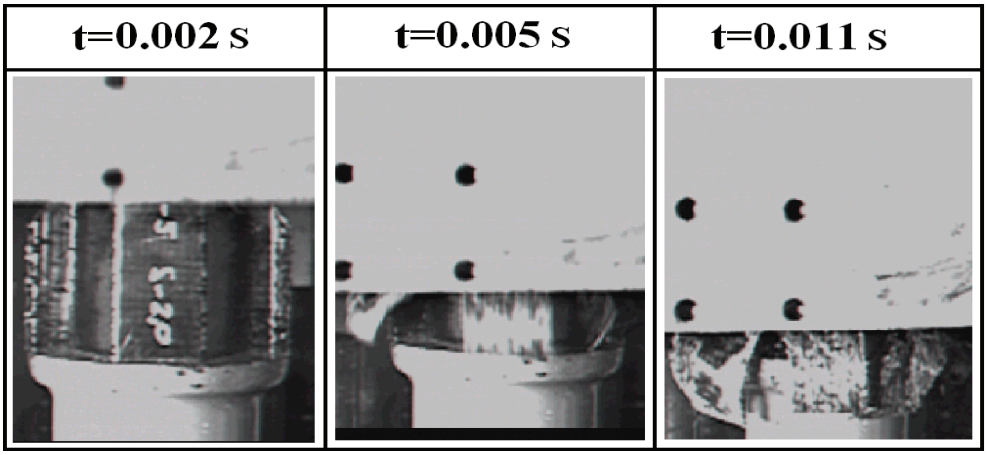

Fig. 5. Crush pattern of a hexagonal composite tube (S-75) for different crush moments

The energy absorption E and specific energy absorption SEA of the experiments and simulations at the same crush length (80 mm for square tubes and 60 mm for hexagonal ones) are presented in Table 3. Here, index S indicates simulation results. Again, it can be seen that the numerical simulations highly underestimate the tube crush behavior. The numerical crush patterns show the tube experiences the progressive crushing with some damages in tube walls instead of splitting and spreading, see Figure 8 and 9. It is evident that the total energy absorption of the composite tube is the sum of the energy needed for splitting of the tube corners, delamination and spreading of tube walls into two inwards and outwards fronds, bending and curling of each fronds, fracture and damage created in fronds during bending, fragmentations of tube walls and friction between the impactor and inwards and outwards fronds. The single layer finite element model does not have the capability to consider all aspects of crushing damages observed experimentally. Therefore, a new finite element model has to be developed to overcome this problem.

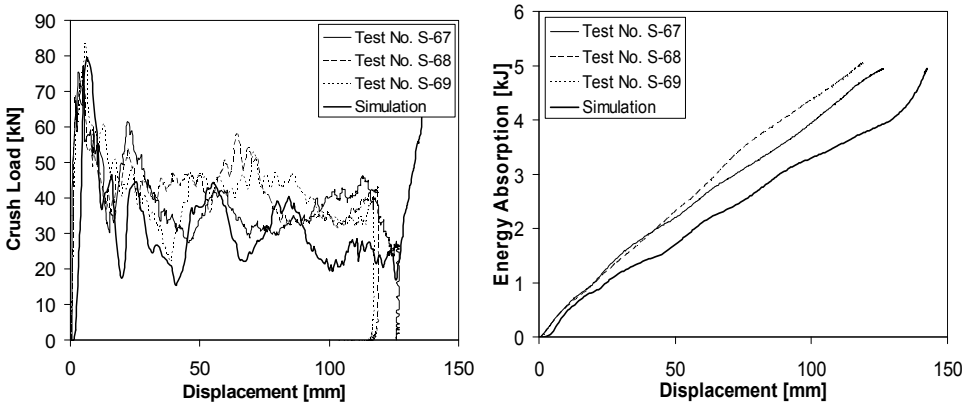

Fig. 6. Comparison between experimental and numerical (single layer method) crush load-displacement curves (left) and energy absorption-displacement curves (right) of square composite tubes

Test No.	E [J]	SEA [J/kg]	Es [J]	SEAS [J/kg]	Difference [%]
S-67	3259	43647	2686	35973	-17.6
S-68	3682	49313	-	-	-27.1
S-69	3520	47143	-	-	-23.7
S-75	3718	54035	2890	42002	-22.3
S-76	4170	60604	-	-	-30.7
S-77	3930	57116	-	-	-26.5

Table 3. Comparison between experimental and numerical (single layer method) energy absorption and specific energy absorption of the square and hexagonal tubes

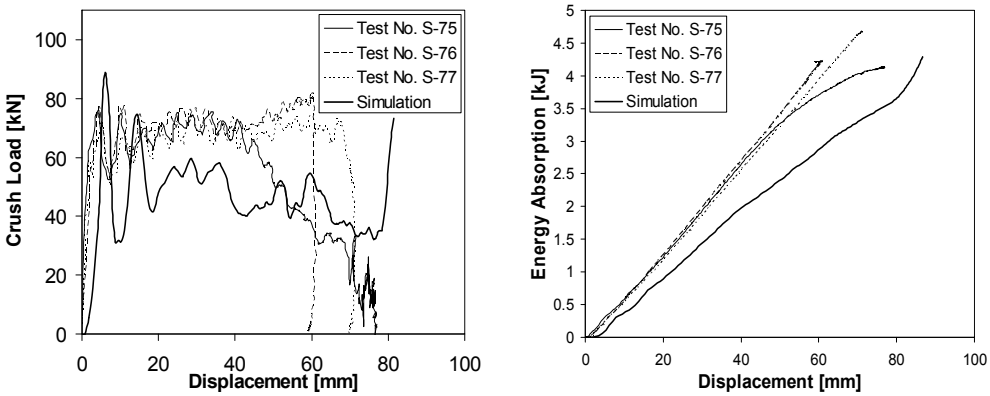

Fig. 7. Comparison between experimental and numerical (single layer method) crush load-displacement curves (left) and energy absorption-displacement curves (right) of hexagonal composite tubes

3. Advanced finite element model

The numerical crush behavior of the composite crash box are shown above for tube walls modeled with only one layer of shell elements, simulated crush pattern are quite different from experiment. The delamination, a main energy absorption source of composite crash boxes, can not be modeled and, therefore, the predicted energy absorption by the simulation is highly underestimated. Several methods have been used by the researchers to model the delamination growth in composite materials, including the virtual crack extension technique (Farley & Jones, 1992), stress intensity factor calculations (Hamada & Ramakrishna, 1997), stresses in a resin layer (Kindervater, 1995), and, the virtual crack closure technique (Fleming & Vizzini, 1996).

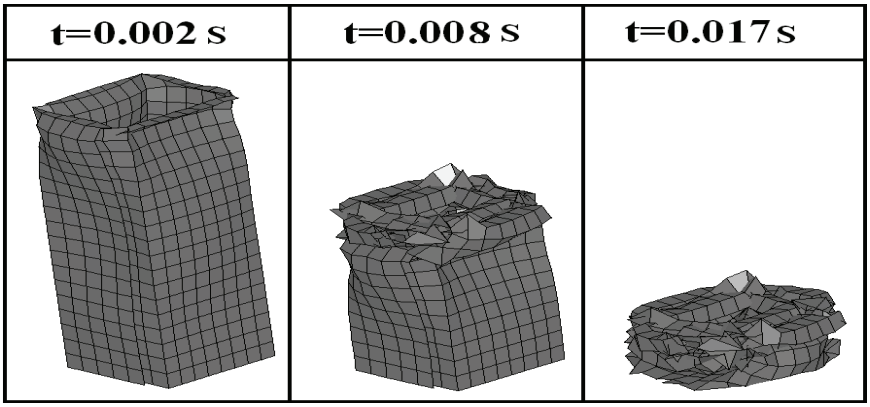

Fig. 8. Crush pattern of single layer finite element model of square composite tube

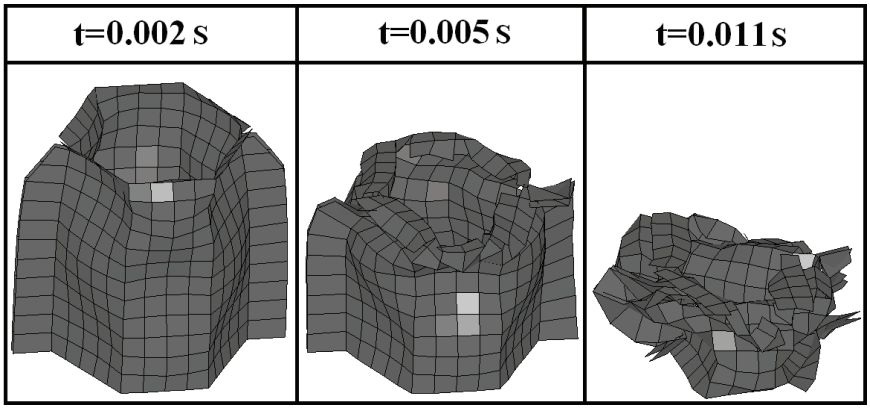

Fig. 9. Crush pattern of single layer finite element model of hexagonal composite tube

However, choices for modeling delamination using conventional finite element crush codes are more limited. Good correlations are obtained in many cases using models that do not fully capture all aspects of crushing damage observed experimentally. They only provide sufficient attention to the aspects of crushing that mostly influence the response. Models of

composite structures using in-plane damaging failure models to represent crushing behavior are used in (Haug et al., 1991), (Johnson et al., 1996 and 1997), (Feillard, 1999) and (Kohlgrueber & Kamoulakos, 1998). These models appear to be effective for structures whose failure modes are governed by large-scale laminate failure and local instability. However, crushing behavior in which wholesale destruction of the laminate contributes significantly to the overall energy absorption cannot be accurately modeled by this approach (Fleming, 2001). Further, if delamination or debonding forms a significant part of the behavior, specialized procedures must be introduced into the model to address this failure mechanism . Kohlgrueber and Kamoulakos (Kohlgrueber & Kamoulakos, 1998)and Kerth et al. (Kerth et al., 1996) used tied connections with a force-based failure method to model the delamination in composite materials. By this method, nodes on opposite sides of an interface where delamination is expected are tied together using any of a variety of methods including spring elements or rigid rods. If the forces produced by these elements exceed some criterion, the constraint is released. The primary disadvantage of this method is that there is no strong physical basis for determining the failure forces. Reedy et al. (Reedy et al., 1997) applied cohesive fracture model for the same reason. This method is similar to the previous method. However, instead of relying on simple spring properties the force-displacement response of the interfacial elements is based on classical cohesive failure behavior. Virtual crack closure technique is often used by researchers in the area of fracture mechanics. Energy release rates are calculated from nodal forces and displacements in the vicinity of a crack front. Although the method is sensitive to mesh refinement, but not so sensitive like the other fracture modelling techniques, those requiring accurate calculation of stresses in the singular region near a crack front. Further, the use of conventional force and displacement variables obviates the need for special element types that are not available in conventional crash codes.

In this study for the delamination, tube walls are modeled with two layers of shell elements. The thickness of each layer is equal to the half of the tube wall thickness [130]. To avoid tremendous increase of the required simulation time, a larger number of layers is avoided. The surface to surface tiebreak contact is used to model the bonding between the bundles of plies of the tube walls. In this contact algorithm the tiebreak is active for nodes which are initially in contact. Stress is limited by the perfectly plastic yield condition. For ties in tension, the yield condition is

$$[\sqrt{(\sigma_n{}^2 + 3|\sigma_s|^2)} / \varepsilon_p] \leq 1 \tag{6}$$

Where ε_p is the plastic yield stress and σ_n and σ_s are normal and shear stresses, respectively. For ties in compression, the yield condition is

$$[\sqrt{(3|\sigma_s|^2)} / \varepsilon_p] \leq 1 \tag{7}$$

The stress is also scaled by a damage function. The damage function is defined by a load curve with starts at unity for crack width of zero and decays in some way to zero at a given value of the crack opening (Hallquist, 1998)], see Figure 10. The surface to surface tied contact is implemented between the overlapped walls and single surface contact is used for each layer. The node to surface contact is applied between rigid impactor and composite layers. To model the rupture at the corners of the tube, the vertical sides of the tube have offset 0.5 mm and deformable spot-welds are used to connect the nodes of the vertical sides.

The spot-welds are defined by the use of material number #100 in LS-DYNA (MAT_SPOTWELD). Based on this material model, beam elements, based on Hughes-Liu beam formulation, are placed between the tube walls and contact-spotweld algorithm ties the beam elements to the tube shell elements. The normal strength of spot-welds is calculated from the transverse tensile strength of the composite material.

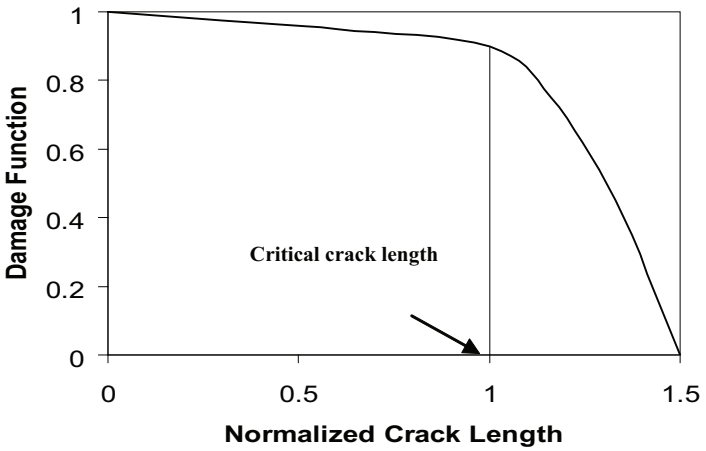

Fig. 10. Variation of damage function

To account for the reduced strength of the composite material at the corners, material strength is reduced by 50%. The shear strength is considered as half of the normal strength. In order to model the trigger, the length of the outer layer of the composite tube is a little bit smaller than the inner layer. The crush patterns of the multi layer square and hexagonal crash boxes are presented in Figures 11 and 12. Here it is possible to see the delamination which starts in some tube walls and propagates during the crush process.

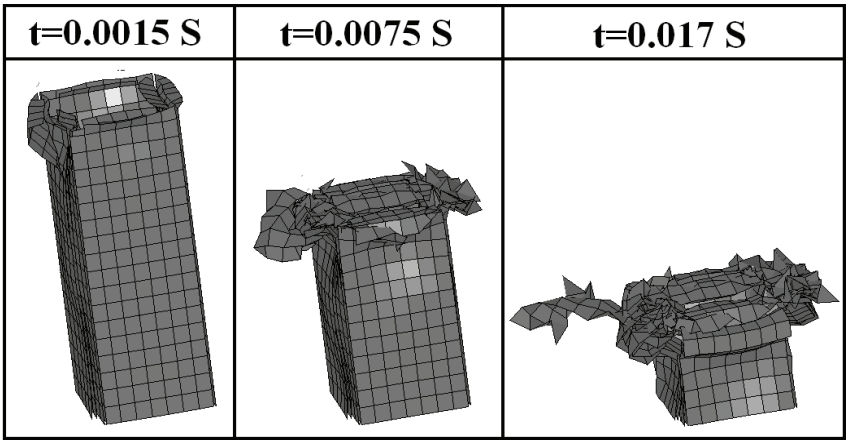

Fig. 11. Crush pattern of multi layer finite element model of square composite tube

The Figures 13 and 14 left compare the crush load-displacement curves of experimental and numerical impact on square and hexagonal crash boxes, respectively. Acceptable correlations are reached between experiments and simulations. In addition the experimental and numerical energy absorption is presented in Figure 13 and Figure 14 right. The multi layers method can predict the energy absorption of the crash box very well.

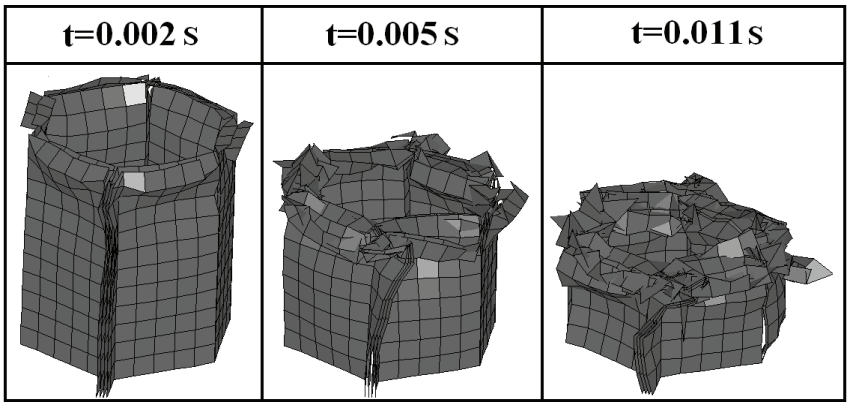

Fig. 12. Crush pattern of multi layer finite element model of hexagonal composite tube

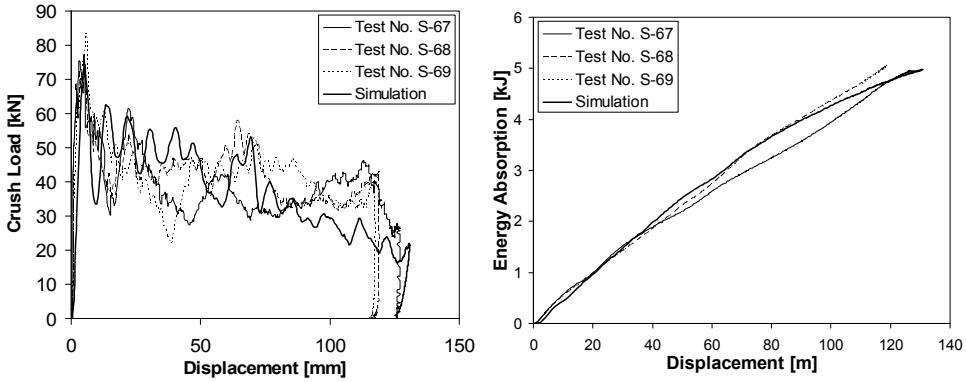

Fig. 13. Comparison between experimental and numerical (multi layers method) crush load-displacement curves (left) and energy absorption-displacement curves (right) of square composite tubes

4. Multi design optimization of crush behavior of square composite crash box

There are high interests to find the effect of composite tube geometry on its energy absorption capability. Generally, variation in tube geometry influences the fracture mechanisms and, therefore, the energy absorption capability. Thornton and Edwards (Thornton and Edwards, 1982) investigated the crush performance of square, rectangular and circular composite tubes. They concluded that for a given fiber lay up and tube geometry, circular tubes have the highest specific energy absorption followed by square and

rectangular tubes. Farley (Farley, 1986) investigated the effect of geometry on the energy absorption capability of the composite tubes. He conducted a series of quasi-static crash tests of Graphite/Epoxy and Kevlar/Epoxy composite tubes with the ply orientation of ±45 degree. He found that the tube diameter to wall thickness ratio d/t has significant effects on the energy absorption capability. The energy absorption was found to be a decreasing nonlinear function of tube d/t ratio. A reduction in d/t ratio increases the specific energy absorption of the tube. Similar result has been reported by Farley and Jones (Farley & Jones, 1992) for elliptical composite tubes.

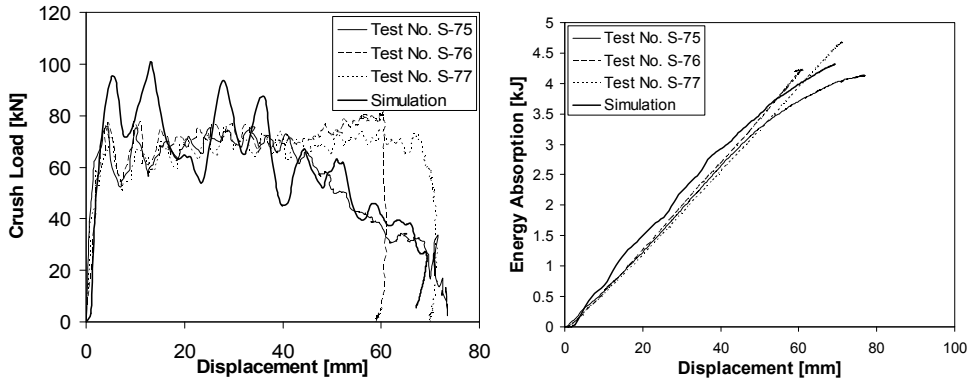

Fig. 14. Comparison between experimental and numerical (multi layers method) crush load-displacement curves (left) and energy absorption-displacement curves (right) of hexagonal composite tubes

Zarei and Kroeger (Zarei & Kroeger, 2006) used Multi design objective MDO crashworthiness optimization method to optimize circular aluminum tubes. Here, the same optimization procedure is used to find optimum composite crash box. The finite element method is used to calculate the absorbed energy and specific absorbed energy of the tubes. The design variables are the tube thickness (number of layers), width and length of the composite tubes. The composite tubes with the thickness between 1 mm and 4 mm are selected while the tube width is varied between 70 mm and 120 mm and the tube length between 100 mm and 350 mm. Here 0.5 mm thickness is considered for each layer of composite tube. To have acceptable crush performance in oblique crash conditions, the tube width lower than 70 mm is not considered. An impact force constraint is usually required to reduce the occupant injury when passenger vehicles are considered. Therefore, in the optimization process, the mean crush load P_m should not exceed the allowable limit P_{ma} i.e.:

$$g = Pm/Pma-1 \leq 0. \quad (8)$$

Where Pma=68.5 kN is selected in this research. The optimization problem can be rewritten as follows

Maximize energy absorption E and specific energy absorption SEA of tube

Subjected to

$$0.5 \text{ mm} \leq t \leq 3.0 \text{ mm},$$
$$100 \text{ mm} \leq l \leq 350 \text{ mm},$$
$$50 \text{ mm} \leq d \leq 120 \text{ mm},$$
$$P_m \leq 68.5 \text{ kN}.$$

The optimization procedure which is presented in Figure 15 is applied to the maximization of absorbed energy and specific absorbed energy of the composite tube under axial impact load. Since the interest is to find the crush behavior of tubes up to the final effective crush length, all tubes are encountered with a large amount of impact energy. Here 75 percent of tube length is considered as effective crush length. In order to reduce the optimization time, the single layer finite element models are used to find the energy absorption of composite tubes in every subproblem and the final optimum tube is modeled as a multi layer composite tube.

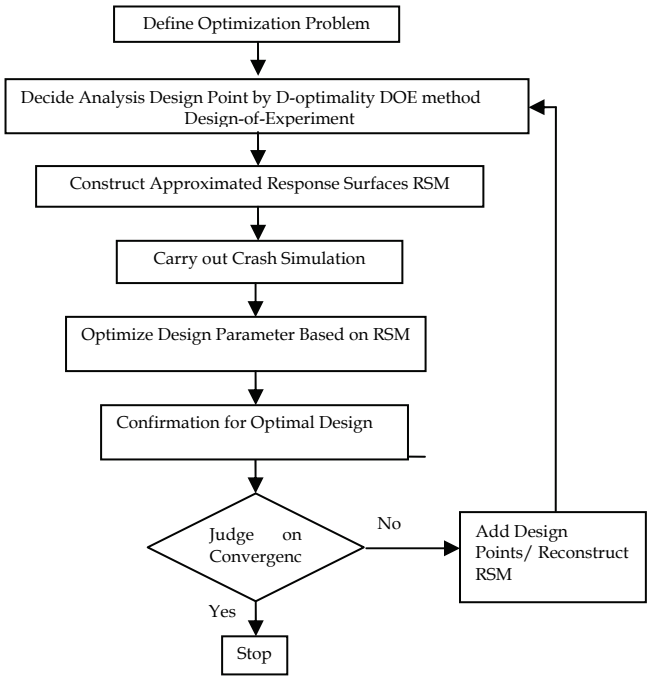

Fig. 15. Flowchart of the optimization process

Table 4 shows the final optimum composite tube that absorbs maximum energy with minimum weight. Here it can be seen that the optimum tube thickness t is 3 mm (N_l=6 layers). The thicker tube will have mean crush load higher than allowable limit. The variable d coincides with the lower bound which shows an increase of the crashworthiness efficiency by reduction of tube width. But here values lower that 70 mm are not allowed to guarantee enough bending resistance of the composite crash box in oblique crash conditions. The tube length coincides with the upper bound but in order to avoid global buckling, longer tubes are not considered. Previously the MDO procedure was used to find optimum aluminum tubes. There, to avoid global buckling in the aluminum tubes the maximum allowed tube length to width ratio is set to $l/d \leq 3$ based on experimental observations (Mamalis et al., 2005) and (Hanssen et al., 1999 and 2000). In order to compare crashworthiness behavior of the optimum composite and aluminum crash boxes, this new optimization constraint is considered for composite crash tube. Table 5 shows the results of optimum composite and

aluminum crash boxes. It can be seen that the composite tube absorbs about 17 percent more energy than aluminum crash box while it has about 27 percent lower weight.

Tube type	T; N_l [mm; -]	d [mm]	l [mm]	E [J]	SEA [J/kg]
Square composite	3; 6	70	350	15316	35580

Table 4. Optimum square composite tube

Tube Type	t [mm]	d [mm]	l [mm]	E [J]	Increase [%]	SEA [J/kg]	Increase [%]
Square aluminum	2.1	70	210	7602	-	26124	-
Square composite	3	70	210	9198	17.4	35716	26.9

Table 5. Comparison between optimum composite and optimum aluminum crash boxes

5. Crush performance investigation of foam-filled composite crash box

Here, Alporas aluminum foam with a relative density of 0.085 is used to produce foam filled square composite crash box. Dynamic compression tests were conducted on them. The composite square tubes with the dimensions which previously presented in Figure 1 are used. The nominal wall thickness of the composite tubes is 2.4 mm. Dynamic tests were done in drop weight test rig. Simply support boundary conditions were applied for the tubes. Table 6 shows the results of experimental tests. The crush pattern of test number (F-37) is shown in the Figure 16. Here, similar to empty composite tubes, the tube is split from its corners. In comparison to the empty composite tubes, lower delamination area can be seen. The tube is ruptured from its corners and the foam filler is crushed progressively. Numerical simulations of crash tests are performed using the explicit finite element code LS-DYNA. The new developed finite element model in this study is used to describe the composite square tubes, see section 4. The foam filler is modeled with solid elements and rigid body elements are used to model the rigid impactor. The contact between the rigid body and the specimen is modeled using a node to surface algorithm with a friction coefficient of μ=0.2. To account for self contact between the tube walls during deformation, a single surface contact algorithm is used. The node to surface contact is implemented between tube walls and foam filler. The composite walls are modeled with the use of material model #54 in LS-DYNA The aluminum foam was modeled with the foam model of Dehspande and Fleck (2000) [19] material number #154 in LS-DYNA. Figure 17 shows that the predicted energy absorption by the simulation is in good agreement with the experimental one.

Table 7 shows a comparison between energy absorption E and specific energy absorption SEA of the empty and foam-filled composite square tubes at the 80 mm crash length. Here, it can be seen that the foam insertion of the composite tube results in higher energy absorption but unlike the aluminum foam-filled tubes, the specific energy absorption in the composite filled tubes is decreased in comparison with empty one. As mentioned in the chapter four, the benefit of using foam inside the crash absorbers is the interaction between foam and crash absorber walls during crush process. But as one can see in the Figure 16, in the foam-filled composite tubes, the composite tube is split into four parts and the tube and foam crushed independently. Here no interaction between tube and foam is taken place. From

Figure 3 it can be seen that the empty composite tubes are split into several parts and each part is splayed into two fronds which spread outwards and inwards. From Figure 16 it is clear that the foam filler forced the tube parts outward during the crush process and prevent from splaying of the parts. Therefore no frond is created and delamination between the composite layers, which is one of the main energy absorption sources of the composite, is not taken placed. Therefore, the specific energy absorption of the filled composite tube is lower than empty tubes.

Another interesting result which is extracted from experimental results of dynamic tests on simple foam filler is that the energy absorption of foam filler is about 4950 J at 80 mm crash length. That means the some of the energy absorption of the empty composite tube alone and foam filler alone is higher than energy absorption of the foam-filled composite tube. In other word not only inserted foam plays no positive roll in the crush process of the filled composite crash box but also it has destructive effect.

Test No.	V [m/s]	t [mm]	P_{max} [kN]	P_m [kN]	S_{max} [mm]	E [J]	SEA [J/kg]	η [%]
F-37	10.4	2.4	85.1	46.9	105.4	4994	34006	55.1
F-38	10.3	2.4	95.1	47.3	97.7	4890	35922	49.7
F-39	10.3	2.4	87.8	46.2	108.5	4954	32770	42.6

Table 6. Experimental dynamic test on foam filed square composite tube

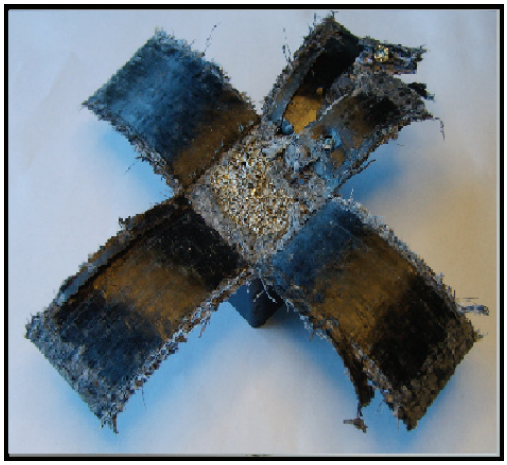

Fig. 16. Crush pattern of foam-filled composite crash box

Test No.	Filler type	E [J]	Increase [%]	SEA [J/kg]	Increase [%]
Average of S-67, S-68, S-69	-	3487	-	46701	-
Average of F-37, F-38-F-39	Foam	3832	9.0	34233	-26.7

Table 7. Comparison between empty and foam-filled composite tubes

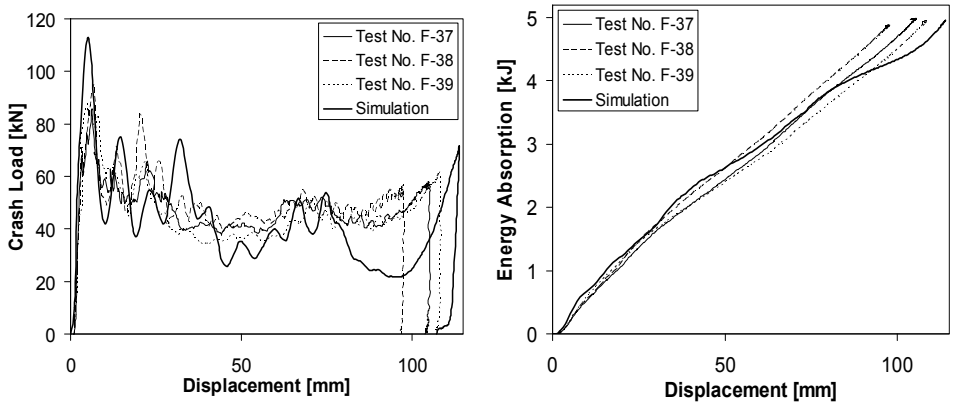

Fig. 17. Comparison between experimental and numerical (multi layers method) crush load-displacement curves (left) and energy absorption-displacement curves (right) of square composite foam-filled tubes

6. Conclusion

Experimental crash tests on square and hexagonal composite crash boxes showed that unlike metallic crash boxes which are crushed in a progressive buckling manner, the composite tubes are crushed in a progressive damaging manner.

A new multi layer finite element model was developed to simulate the crush process of the composite crash box.

The MDO procedure was used to find an optimum design of the composite crash box. The comparison between crashworthiness behavior of the optimum composite and aluminum crash boxes showed that the composite crash box absorbs about 17 percent more energy than the aluminum crash box while it has about 27 percent higher SEA.

For light weight crash box or bumper beam designs, low density metal fillers, such as aluminum honeycomb or foam, are superior to tubes and beams with thicker walls in terms of achieving the same energy absorption. The crush performance of foam-filled square composite crash box was investigated experimentally and numerically. The results showed that the foam insertion results in higher energy absorption but unlike the aluminium foam-filled tubes, the specific energy absorption of the composite filled tubes is decreased in comparison with empty one.

7. References

Bisagni, C.; Pietro, GD.; Fraschini, L. & Terletti, D. (2005). Progressive crushing of fiber-reinforced composite structural component of a formula one racing car. *Compos. Struct*., Vol. 68, 491–503

Chang, FK. & Chang, KY. (1987). Post-failure analysis of bolted composite joints in tension and shear-out mode failure. *J. Compos. Mater*., Vol. 21, 809–33

El-Hagel, H.; Mallick, PK. & Zamani, N. (2004). Numerical modeling of quasistatic axial crash of square aluminum-composite hybrid tubes. *Int. J. Crashworthiness*, Vol. 9, No. 6, 653–64

Farley, G.L. (1991). The effects of crushing speed on the energy-absorption capability of composite tubes. *J. Compos. Mater*., Vol. 25, No. 10, 1314–29.

Farley, G.L. (1983). Energy absorption of composite materials. *J. Compos. Mater.,* Vol. 17, No. 3, 267–79

Farley, GL. (1986). Effect of specimen geometry on the energy absorption capability of composite tubes. *J. Compos. Mater*., Vol. 20, 390–400

.

Farley, GL. & Jones, RM. (1992). Prediction of the energy-absorption capability of composite tubes. *J. Compos. Mater*., Vol. 26, No. 3, 388–404

Fleming, DC. & Vizzini, AJ. (1996). Off-axis energy absorption characteristics of composites for crashworthy rotorcraft design. *J. American Helicopter Soc.,* Vol. 41, No. 3, 239–46

Fleming, DC. (2001). Delamination modeling of composite for improved crash analysis. *J. Compos. Mater*., Vol. 35, No. 19, 1777–92

Feillard, P. (1999). Crash modeling of automotive structural parts made of composite materials, *Proceedings of the SAE international congress and exposition*, March 1–4, Detroit, MI

Jacob, GC.; Simunovic, JFS. & Starbruk, JM. (2002). Energy absorption in polymer composite for automotive crashworthiness. *J. Compos. Mater*., Vol. 36, No.7, 813–50

Johnson, AF.; Kindervater, CM.; Kohlgrueber, D. & Luetzenburger, M. (1996). Predictive methodologies for the crashworthiness of aircraft structures, *Proceedings of the 52nd american helicopter society annual forum*, pp. 1340–52, June 4–6, Washington DC

Johnson, AF. & Kohlgrueber, D. (1997). Modeling the crash response of composite structures. *J. Phys. IV France, Colloque C3, Supple ´ment au Journal de Physique III*, Vol. 7, C3-981–6 (in English).

Hallquist, JO. (1998). *LS-DYNA theoritical manual*. Livermore Software Technology Corporation

Hamada, H.; Ramakrishna, SA. (1997). FEM method for prediction of energy absorption capability of crashworthy polymer composite materials. *J. Reinf. Plast. Compos*., Vol. 16, No. 3, 226–42

Hanssen, AG.; Langseth, M. & Hopperstad, OS. (1999). Static crushing of square aluminum extrusions with aluminum foam filler. *Int. J. Mech. Engng*., Vol. 41, 967-993

Hashin, Z. (1980). Failure criteria for unidirectional fiber composites. *J. Appl. Mech*., Vol. 47, 329–34

Haug, E.; Fort, O.; Tramecon, A.; Watanabe, M. & Nakada, I. (1991). Numerical crashworthiness simulation of automotive structures and components made of continuous fiber reinforced composite and sandwich assemblies. *SAE technical paper series 910152*

Hoermann, M. & Wacker, M, (2005). Simulation of the crash performance of crash boxes based on advanced thermoplastic composite, *Proceedings of the 5th European LS-DYNA users conference*, pp. 25–6, UK, May ,Birmingham

Hull, D. (1982). Energy absorption of composite materials under crash displacement variables obviates the need for special element types that are not available in crash

codes, *Proceeding of the 4th international conference on composite materials: progress in science and engineering of composites*, pp. 861–87, Japan, Tokyo

Kerth, S.; Dehn, A.; Ostgathe, M. & Maier M. (1996) Experimental investigation and numerical simulation of the crush behavior of composite structural parts, *Proceedings of the 41st international SAMPE symposium and exhibition*, pp. 1397–408

Kindervater, CM. (1995). Crash resistant composite helicopter structural concepts thermoset and thermoplastic corrugated web designs, *Proceedings of the AHS national technical specialists meeting on advanced rotorcraft structures*, Williamsburg, VA

Kohlgrueber, D. & Kamoulakos, A. (1998). Validation of numerical simulation of composite helicopter sub-floor structures under crash loading, *Proceedings of the 54th American helicopter society annual forum*, May 20–22 Washington DC

Mamalis, AG.; Manolakos, DE.; Demosthenous, GA. & Ioannidis, MB. (1997). The static and dynamic axial crumbling of thin-walled fiberglass composite square tubes. *Composites Part B*, Vol.28B, No. 4, 439–51

Mamalis, AG.; Manolakos, DE.; Ioannidis, MB. & Papapostolou, DP. (2005). On the response of thin-walled composite tubular components subjected to static and dynamic axial compressive loading: experimental. *Compos. Struct.*, Vol. 69, 407–20

Mamalis, AG.; Manolakos, DE.; Ioannidis, MB. & Papapostolou, DP. (2006).The static and dynamic axial collapse of CFRP square tubes: finite element modeling. *Compos. Struct*., Vol. 74, 2213–50

Mallick, PK. (1990) *Fiber reinforced composites*. 2nd ed. NY, Marcel Dekker

Ramakrishna, S. (1997). Microstructural design of composite materials for crashworthy applications. *Mater. Des*., Vol.18, 167–73

Reedy, ED.; Mello FJ. & Guess, TR. (1997). Modeling the initiation and growth of delaminations in composite structures. *J. Compos. Mater.*, Vol. 31, No. 8, 812–31

Shin, K.C.; Lee, JJ.; Kim, KH.; Song, MC. & Huh, JS. (2002). Axial crash and bending collapse of an aluminum/GFRP hybrid square tube and its energy absorption capability. *Compos. Struct*., Vol. 57, 279–87

Thornton, PH. & Edwards, PJ. (1982). Energy absorption in composite tubes. *J. Compos. Mater*., Vol. 16, 21–45

Yamazaki, K. & Han, J. (1998). Maximization of the crushing energy absorption of tubes. *Struct. Optim*., Vol. 16, 37–49

Zarei, HR. & Kroeger, M. (2006). Multiobjective crashworthiness optimization of circular aluminum tubes. *Thin-Walled Struct. J*., Vol. 44, 301–8

Zarei, HR.; Kröger, M. & Albertsen, H. (2007). Crashworthiness investigation of the composite thermoplastic crash box, *Proceeding of the Sixth Canadian-International Composites Conference*, pp. 1-14, August , Winnipeg

Zarei, HR.; Kröger, M. & Albertsen, H. (2008). An experimental and numerical crashworthiness investigation of the thermoplastic composite crash boxes. *Comp. struc. J*., Vol. 85, 245-258

19

Effects of the Long-Time Immersion on the Mechanical Behaviour in Case of Some E-glass / Resin Composite Materials

Assoc.prof.dr.eng. Camelia CERBU
„Transilvania" University of Braşov, Faculty of Mechanical Engineering, Romania

1. Introduction

The chapter deals with the actual and difficult problem of analysing the mechanical structures from the perspective of using composite materials in aggressive environment. Optimising the mechanical structures, made by composite materials is a great actual and important problem that includes two of the most modern, difficult and demanded aspects in mechanical engineering. If we point out this subject, meaning the aggressive environment, we already have the complete image of an extreme actual, important and special complexity subject.

The major studies in the field of structural optimising of the components made of composite materials, followed to obtain structures of components having higher strength and rigidity, lower weight, under conditions of a lower cost. There have been analysed composite material components, for which have been varied the material structure for fibre and matrix, the orientation of the fibres in layers, the shape of component, etc. The present study proposes an objective and supplementary criterion: the conservation of the mechanical characteristics of strength and rigidity under the long time action of the aggressive environment factors.

The results presented within this chapter address to the researchers and specialists in the field of the composite materials, to the ph.d. students and students from master, etc. Concurrently, reading of this working, may establish a point of start in the researching activity in this direction because it notes some important remarks regarding the effects of the aggressive environment (humidity, basic and acid solutions, temperature, thermal cycles, electrons radiation, UV rays etc) on the degradation of the mechanical characteristics of some composite materials.

The specialists interested in the field of composite materials will find a rich source of information by establishing a method of testing the specimens made of composite materials, subjected to statically forces after maintaining in aggressive environment; recommendations concerning the polymeric composite structure, having long durability under the action of the humidity and variations of temperature.

When an organic matrix composite is exposed to humid air or to a liquid, both the moisture content and temperature of the composite material may change with time. These changes affect the mechanical characteristics (Corum et al., 2001; Pomies et al., 1995; Cerbu, 2007; Takeshige et al., 2007).

Glass fibre reinforced resins are used widely in the building and chemical industry (wall panel, window frames, tanks, bathroom units, pipes, ducts, boat hulls, storage tanks, process vessels), automotive industry, aerospace industry. These structure elements may also be exposed to the environmental conditions (moisture, temperature etc).

In the last years, it was published many scientific papers concerning to the mechanical behaviour in wet environment of the composite materials and of the structure made of composite materials. For example, it was shown that the long-time immersion of the polymeric composite materials in water, seawater or detergent solutions, lead to the degradation of the mechanical characteristics (Corum et al., 2001; Pomies et al., 1995 ; Cerbu, 2005; Cerbu, 2007). Experimental results (Cerbu s.a. 2009) also demonstrated the influence of the immersion time on the degradation of the mechanical characteristics of some polymeric composite materials.

A recent paper (Takeshige et al. 2007) investigated some interactions between mechanical and chemical fatigue in case of some resin composite materials. Therefore, in that research was remarked that the fatigue crack propagation is retarded under humid conditions but accelerated after water immersion.

Some recent works shown the new tendencies from the manufacture field of the composite materials by recycling of the wood wastes (Adhikary s.a. 2008), plastic wastes, polyetilena waste, paper, CDs / DVDs (Cerbu s.a. 2009) and so forth. Consequently, some of the new composite materials were studied from moisture absorption point of view. For example, Adhikary s.a. (2007) analysed the long-term moisture absorption and thickness swelling in case of some specimens made of recycled thermoplastics reinforced with pinus wood flour.

An interesting book (Klyosov 2007) focused on wood-plastic composites regarding the paticularities of their fabrication; the effects of cellulose fillers, mineral fillers and coupling agents on their mechanical properties. It also showed the effects of the moisture absorption on changes of some mechanical characteristics. Thus, it was experimentally demonstrated that the flexural strength and flexural modulus E increased in case of an water-saturated board made of a commercial wood-plastic composite material.

The first of all, the present chapter proposes the analysing of the efffects of moisture absorbed concerning the changing of the mechanical characteristics of four kinds of polymeric composite materials randomly reinforge with chopped glass fibres. Both the nature of resin and the immersion environment, were analysed regarding their effects on the changing of the mechanical characteristics.

On the other hand, it focus on the using of the wood flour obtained by recycling of the wood wastes from industry to manufacture of hybrid composite materials. The new polymeric composite material described within this section, is reinforced with both glass woven fabric EWR145 (145g/m^2) layed in six layers and wood flour.

It will be comparatively shown the results concerning to the mechanical characteristics (tensile strength, flexural modulus E, flexural maximum stress σ_{max}) determinated by tensile tests and flexural tests (method of the three points), before and after immersion in different environments (water, natural seawater, detergent solution). The results will be compared with the ones obtained in case of four kinds of composite materials randomly reinforced only with chopped glass fibres, free of admixture of wood flour. Moreover, it will be comparatively analysed the data concerning the quantity of the moisture absorbed and the its effect on the change of the mechanical characteristics.

2. Materials. Work method

The first of all, it was manufactured six laminated composite plates whose material structures are different. In this work, E-glass fibres (50 mm length) were used to randomly reinforce four kinds of resins: two polyester resins (Heliopol 8431 ATX and Polylite 440-M880); an epoxy resin (LY554); a vinyl-ester resin (Atlac 582). These composite materials had the average volume fibre ratio equal to 26%, while the weight fibre ratio was 40%. Another two plates having the dimensions 350 x 250mm^2 and 8mm in thickness, were manufactured by using a polyester resin reinforced with both glass woven fabrics EWR145 (six layers) and wood flour (oak wood flour or fir wood flour).
Then, the plates were cut to obtain the specimens according to the european standards concerning of determination of the both tensile properties (ISO 527) and flexural properties (SR EN 63). A total number of 164 specimens were manufactured for tensile tests (Table 1) while 194 specimens were prepared for the flexural tests (Table 2).
It may be noted that all sides of a half of the total number of specimens reinforced only with E-glass fibres, were coated using the resins used for the matrix while the others were not coated.

No.	Composite material	Number of specimens			
		Dry	Environment		
			Water	Detergent solution	Seawater (Black Sea)
1	E-glass / polyester Heliopol 8431 ATX	5	12	12	12
2	E-glass / polyester Polylite 440-M880	5	12	12	12
3	E-glass / epoxy LY 554	5	12	12	12
4	E-glass / vinyl-ester Atlac 582	5	12	12	12

Table 1. Specimens for tensile test

No.	Composite material	Number of specimens			
		Dry	Environment		
			Water	Detergent solution	Seawater (Black Sea)
1	E-glass / polyester Heliopol 8431 ATX	5	12	12	12
2	E-glass / polyester Polylite 440-M880	5	12	12	12
3	E-glass / epoxy LY 554	5	12	12	12
4	E-glass / vinyl-ester Atlac 582 composite	5	12	12	12
5	E-glass EWR145 / fir wood flour / polyester Colpoly 7233	5	5	-	5
6	E-glass EWR145 / oak wood flour / polyester Colpoly 7233	5	5	-	5

Table 2. Specimens for flexural test

Then, the specimens were kept at the room temperature and dried environment for three weeks.
Additionally, some specimens were stored in an oven at 30 ± 1°C and weighted to ensure that they were dried prior to the immersion in water (SR EN ISO 62, 2008). Water (Fig. 1, a),

detergent solution (Fig. 1, b) and fresh natural seawater from Black Sea (Fig. 1,c) at room temperature (20 °C) were used as wet environments. Stands were used to maximise the contact surface between specimens and water (see the detail presented in the Fig. 1, c). The salinity of the natural seawater was approximately of 1.6%. The water tanks were covered to minimise evaporation and the water was changed every month to keep conditions constant.

a.

b.

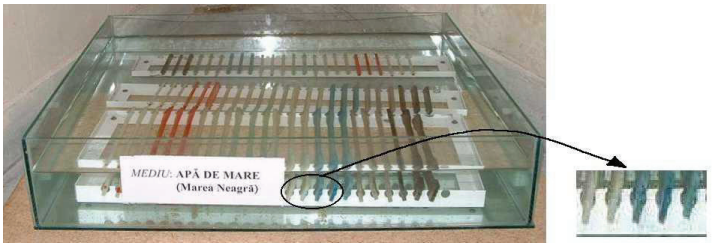

c.

Fig. 1. Environments a. Water ; b. Water / detergent mix c. Seawater (Black Sea);

No.	Composite material	Specimen type	Immersion time *t* (hours)		
			Environment		
			Water	Detergent solution	Seawater (Black Sea)
1.	E - glass / polyester Heliopol 8431 ATX	Uncoated	7197	7134	6987
		Coated	7197	7134	6987
2.	E - glass / polyester Polylite 440-M880	Uncoated	7197	7134	6987
		Coated	1803	1732	2762
3.	E - glass / epoxy LY 554	Uncoated	7197	7134	6987
		Coated	7197	7134	6987
4.	E-glass / vinyl-ester Atlac 582 composite	Uncoated	2975	2865	6987
		Coated	1821	1732	2762
5.	E-glass EWR145 / fir wood flour / polyester Colpoly 7233	Uncoated	5612		5612
6.	E-glass EWR145 / oak wood flour / polyester Colpoly 7233	Uncoated	5853	-	5853

Table 3. Immersion times for the composite materials tested

The times of immersion in water were different in case of the composite materials tested (Table 3). To monitor the uptake of water, quantified by the moisture content *m*, the specimens were periodically removed from tanks, superficially dried with absorbing paper and weighted by using an electronic balance (maximum mass 250 g) accurate within ± 0.0001g.

After long-time immersion, the specimens were subjected to both tensile test and flexural test by the method of the three points (SR EN ISO 178, 2001). LR5K Plus machine manufactured by LLOYD Instruments, was used for mechanical testing of the composite specimens involved. The maximum force provided by the testing machine is $F_{\max} = 5kN$.

The shape and the dimmensions of the tensile specimens are shown in the figure 2. Diagrams having the coordinates force – elongation $(F-\Delta l)$ coordinates were directly recorded from tensile machine.

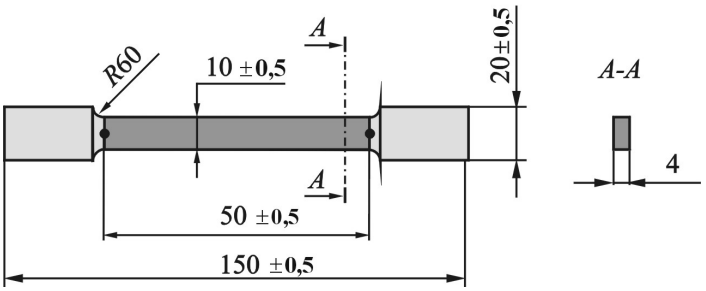

Fig. 2. Specimen for tensile test

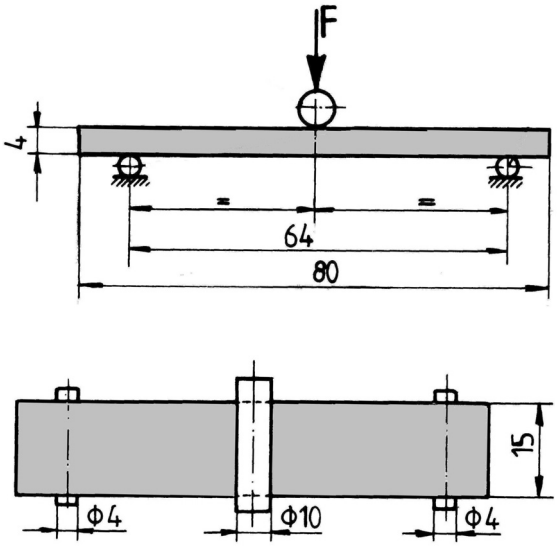

Fig. 3. Specimen used in flexural test

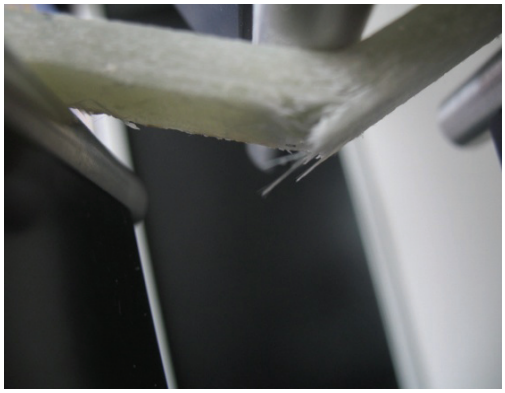

Fig. 4. Specimen made of E-glass / polyester Heliopol 8431 ATX during flexural test

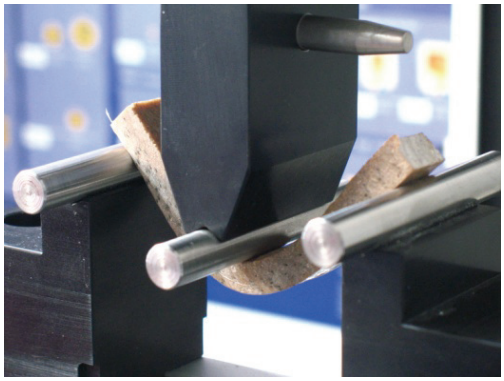

Fig. 5. Specimen made of E-glass EWR145 / oak wood flour / polyester Colpoly 7233 during flexural test

The loading scheme (three-point method) is shown in the figure 3. The dimensions of the specimens are valid only for specimens reinforced only with E-glass fibres because these are functions of the specimen thickness. In case of the flexural tests, the span between the supports was accorded with the specimen thickness (SR EN ISO 62, 2008).
Figures 4 and 5 show two photos of specimens during the flexural test. The specimens shown are made of E-glass / polyester Heliopol 8431 ATX composite material (Fig. 4) and E-glass EWR145 / oak wood flour / polyester Colpoly 7233 (Fig. 5), respectively. It may observe that the deformations are much more greater in case of the specimens made with wood flour (Fig. 5) than in case of the specimens reinforced only with glass fibres (Fig. 4).
The speed of loading was 3mm/min. in case of the specimens made of the composite materials filled with wood flour and 1.5mm/min. in case of the other four kinds of composite materials tested, respectively. The speed of loading was greater in case of additionaly reinforcing with oak wood flour because this composite material is much more flexible. Consequently, the time of the flexural test was approximately 40min. when the speed of loading was equal to 1.5mm/min., in case of this composite material. It was remarked that the the time of the flexural test halved by doubling of the loading speed while

the shape of the curve obtained was approximately the same. It may be mentioned that the time of the flexural test was approximatelly equal to 10min. when the speed of loading was 1.5mm/min., in case of the specimens reinforced only with the E-glass fibres.
Before each mechanical test of a specimen, the dimensions of the cross-section were accurately measured (0.1mm) and then, they were considered as input data in the software program of the machine.
In case of the flexural testing, the testing equipment allowed to record pairs of values (force F and deflection v at midpoint of the specimens) in form of files having up to 3000 recordings. The testing machine also gave the results of a statistical calculus for the set of the specimens tested. Experimental results recorded during the flexural tests, were graphically drawn using F – v coordinates and finally, the following quantities were computed:
- flexural modulus E of the composite material

$$E = \frac{1}{48} \cdot \frac{l^3}{I_z} \cdot \frac{\Delta F}{\Delta v} \tag{1}$$

- flexural strength σ of the composite material:

$$\sigma = \frac{M_{bz\,\max}}{W_z}, \tag{2}$$

where l = 64 *mm* represents the span of the specimen between simple supports (Fig. 3), I_z - moment of inertia, W_z - elastic cross-section modulus, $M_{bz\,max} = Fl/4$ - maximum value of the bending moment. Formula used for the flexural modulus E is a good approximation because $\frac{l}{h} = 16$, where h represents the thickness of the specimen and one can neglect the effect of the shearing force.

3. Results

3.1 Water absorption

The first, moisture behaviour was analysed. The absorption data were shown in the figures 6 – 9 for all composite materials reinforced only with glass fibres. Important remarks are noted by analysing these results.

- Moisture absorption in composite materials depends on the resin used for matrix and type of the wet environment. The absorption process is a long-term process in case of the composite materials tested.
- E - glass / Heliopol 8431 ATX and E-glass / Polylite 440-M880 composites closed the saturation point after 7000 hours of immersion time while the moisture content was approximately the same.
- E-glass / epoxy LY 554 composite does not reach the saturation point after 7000 hours of immersion (Fig. 8) and moisture content is much more greater than in case of the others three composite materials (Fig. 6, 7 and 9). E-glass / epoxy LY 554 composite material absorbs more water than seawater or detergent solution.
- Glass-reinforced polymers absorb more water than seawater. Rate of diffusion of the water through composite materials analysed is greater than that of the seawater.
- Sodium chloride molecules contained in seawater (as well as sulphate) appear to be limiting the diffusion of water into the matrix material.

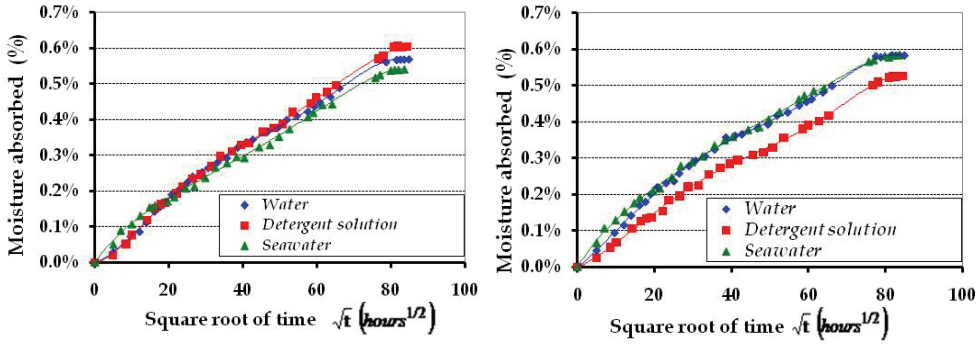

a. Coated specimens b. Uncoated specimens

Fig. 6. Absorption data in case of E-glass / Heliopol 8431 ATX composite material

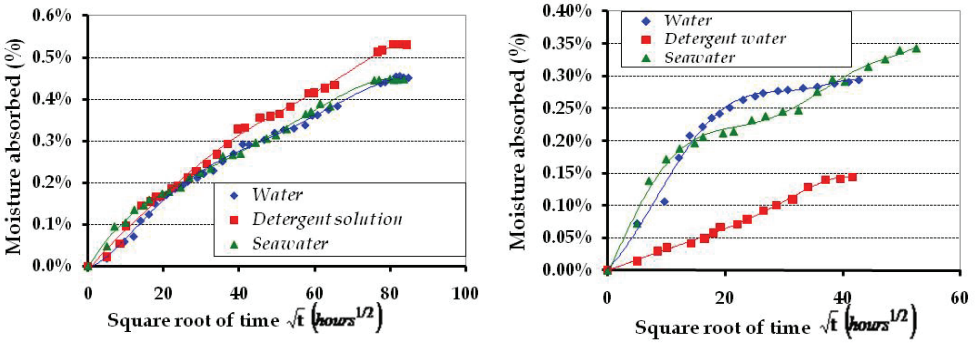

a. Coated specimens b. Uncoated specimens

Fig. 7. Absorption data in case of E-glass / Polylite 440-M880 composite material

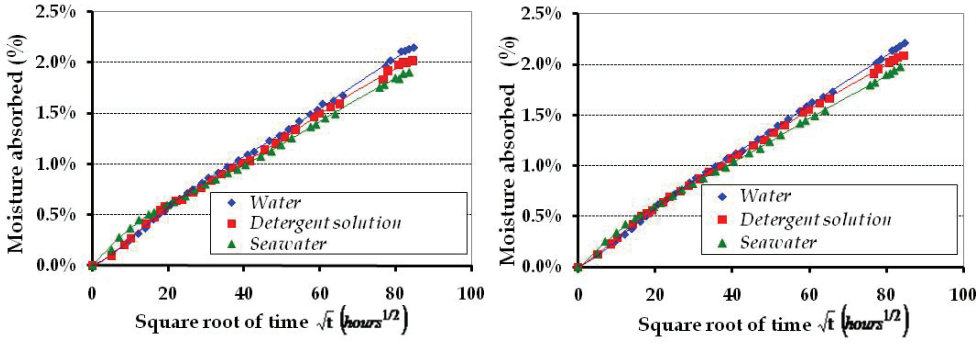

a. Coated specimens b. Uncoated specimens

Fig. 8. Absorption data in case of E-glass / epoxy LY 554 composite material

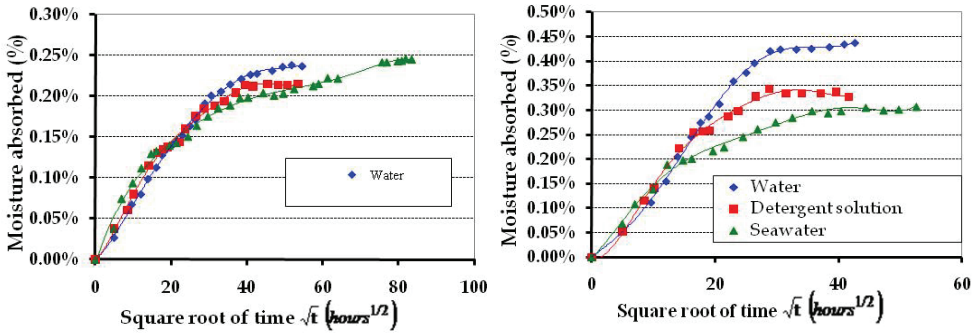

a. Coated specimens b. Uncoated specimens

Fig. 9. Absorption data in case of E-glass / vinyl-ester Atlac 582 composite

The absorption curves recorded in case of the two hybride composites are drawn in the figure 10 in case of the immersion in water and in the figure 11 in case of the immersion in seawater.

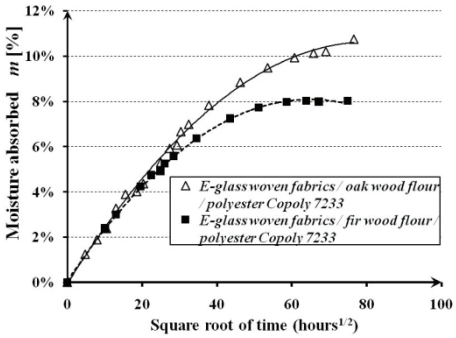

Fig. 10. Data of the absorbed moisture during immersion in water in case of the E-glass woven fabrics / wood flour / polyester

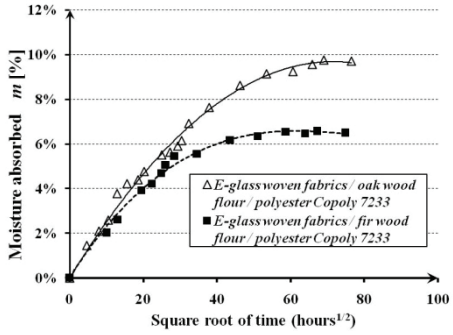

Fig. 11. Data of the absorbed moisture during immersion in seawater in case of the E-glass woven fabrics / wood flour / polyester

It may be easily observed that the two absorption curves recorded in case of the composite material filled with fir wood flour is located below the one recorded in case of the other one composite filled with oak wood flour. The cause may be assigned to resinous nature of the fir wood. Therefore, the greater resin content of the fir wood flour acts as a barrier against the water absorption. The average value of the water content (Fig. 10) was 10.73% while the seawater content (Fig. 11) recorded was 9.72% after immersion during 5853 hours, in case of the composite filled with oak wood flour. In case of the other one composite material filled with fir wood flour, the water content (Fig. 10) was equal to 8.02% while the seawater content was 6.50% after 5612 hours of immersion. Therefore, like the other previous works showed, it was recorded again a smaller quantity of the moisture absorbed during the immersion in seawater than in case of the immersion in water. The salts of the seawater act again like a barrier against the moisture absorption.
There is a small difference between the absorption curves recorded during the first 400-600 hours of immersion. It follows that the diffusivity of the moisture inside the composite material, has approximately the same value in the both cases: water environment and seawater environment.

3.2 Mechanical behaviour in tensile test after immersion in different environments

After approximately 7000 hours of immersion (≈ 10 months) the tensile specimens made of polymer resins reinforced only with glass fibres, were subjected to the tensile test. A photo of these specimens after the tensile test, is shown in the figure 12.

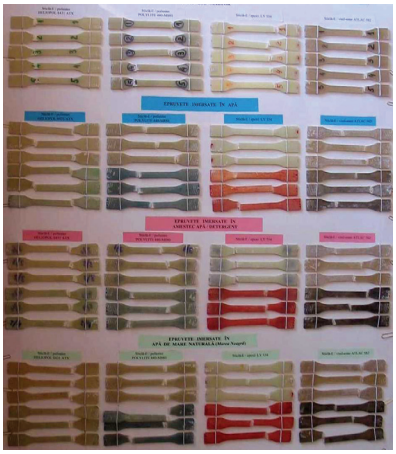

a.

b.

c.

d.

Fig. 12. Tensile Specimens reinforced only with E-glass fibres after flexural test: a. dried specimens; b. specimens after immersion in water; c. specimens after immersion in detergent solution; d. specimens after immersion in seawater

Comparatvely analysing of the experimental results (Fig. 13 - 16) obtained in case of both dried and wet specimens it may observe:

- Tensile strength decreases in case of all composites;
- Decreasing of the tensile strength (40 %) is greater for the specimens made of E-glass / Heliopol 8431 ATX and E-glass / epoxy LY 554 composites after immersion in water than in case of the other two environments (Fig. 10 and 12);

- Conservation of the tensile strength was not very different if all sides of the specimens were coated using the resin of the matrix of the composite;
- Tensile strength of the specimens decreases with 10 – 20 % in case of the immersion in seawater and water / detergent mix (Fig. 10 – 12). The reason could be that moisture content was much smaller in case of these environments.

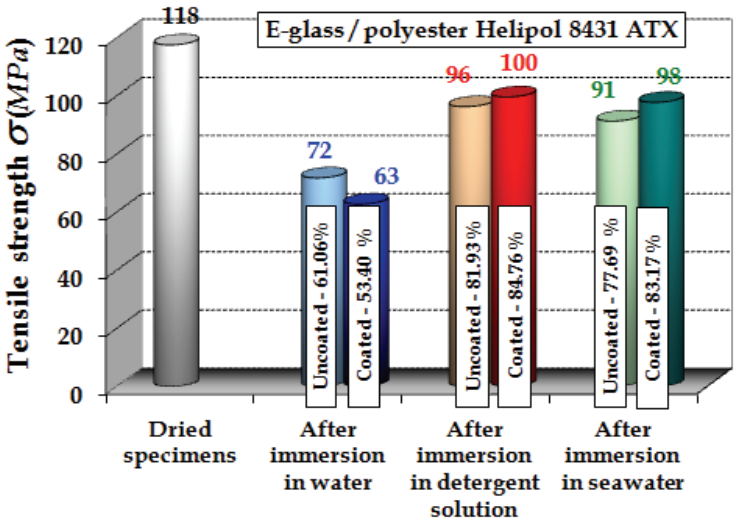

Fig. 13. Changes of the tensile strength in case of E-glass / Heliopol 8431 ATX composite

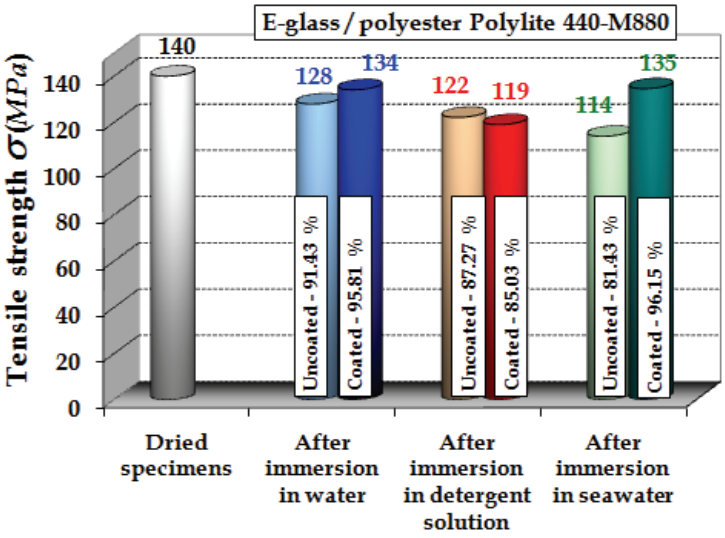

Fig. 14. Changes of the tensile strength in case of E-glass / Polylite 440-M880 composite

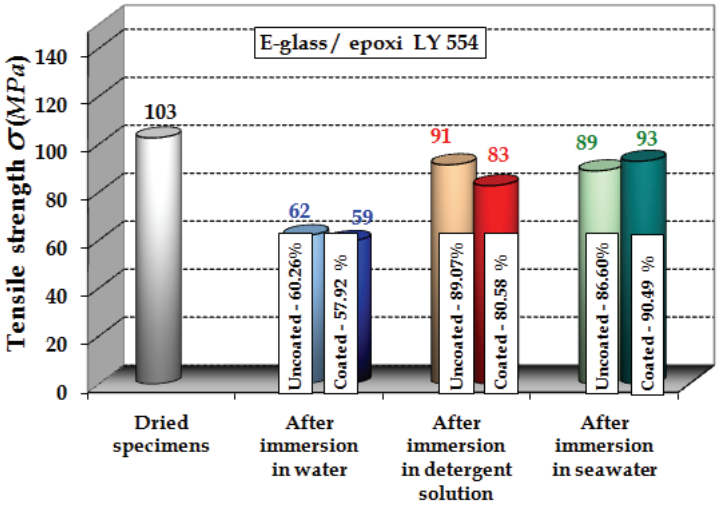

Fig. 15. Changes of the tensile strength in case of E-glass / epoxy LY 554 composite

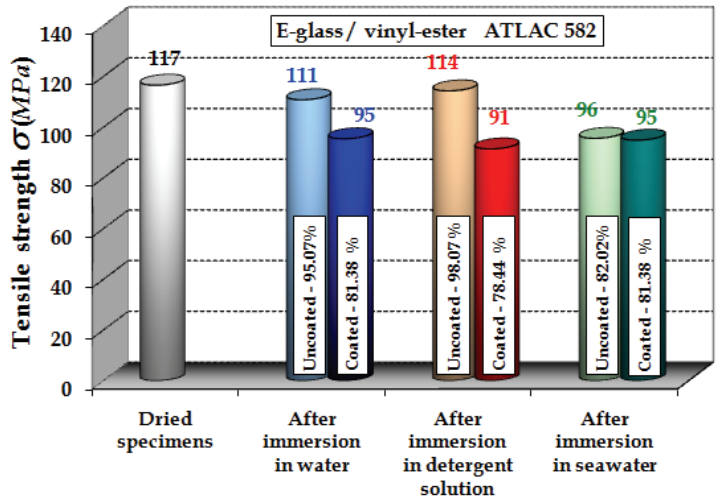

Fig. 16. Changes of the tensile strength in case of E-glass / vinyl-ester ATLAC 582 composite

3.3. Mechanical behaviour in flexural test after immersion in different environments

Then, flexural test by using the three-point method, was considered the immersion in the three kinds of wet environment. The specimens made of polymer resins reinforced with only glass fibres, after they were subjected to the flexural test, are shown in the figure 17. The results obtained in case of the wet specimens were compared with the ones obtained in case of the dried specimens.

Two photos of the flexural specimens filled with both E-glass woven fabrics and wood flour, after immersion in water, are shown in the figures 18 and 19, respectively.
Figures 20 – 23 comparatively show the force – deflection (F-v) curves recorded during the flexural tests, in case of both wet specimens in case of the following composite materials:
- E-glass / polyester Heliopol 8431 ATX (Fig. 20);
- E-glass / polyester Polylite 440-M880 (Fig. 21);
- E-glass / epoxy LY 554 (Fig. 22);
- E-glass / polyester Polylite 440-M880 (Fig. 23).

a.

b.

c.

d.

Fig. 17. Flexural specimens reinforced only with E-glass fibres after flexural test: a. dried specimens; b. specimens after immersion in water; c. specimens after immersion in detergent solution; d. specimens after immersion in seawater

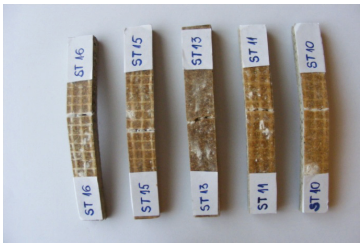

Fig. 18. Flexural specimens made of E-glass EWR145 / oak wood flour / polyester Colpoly 7233 after flexural test

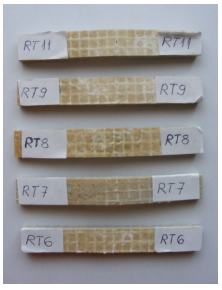

Fig. 19. Flexural specimens made of E-glass EWR145 / fir wood flour / polyester Colpoly 7233 after flexural test

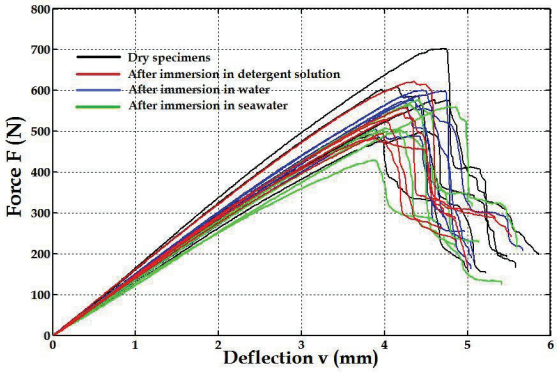

Fig. 20. Curves F-v recorded during the flexural tests in case of E-glass / polyester Heliopol 8431 ATX composite

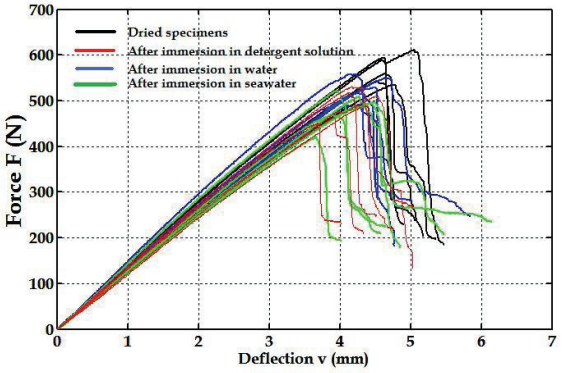

Fig. 21. Curves F-v recorded during the flexural tests in case of E-glass / polyester Polylite 440-M880 composite

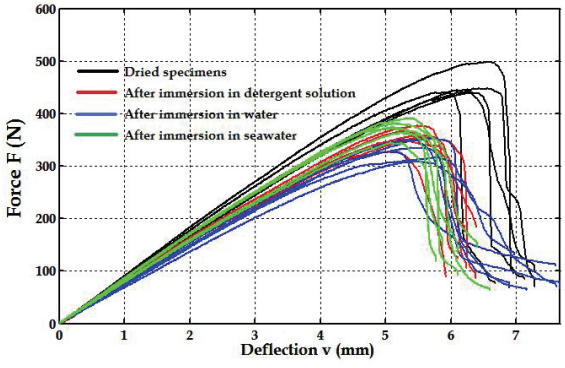

Fig. 22. Curves F-v recorded during the flexural tests in case of E-glass / epoxy LY 554 composite

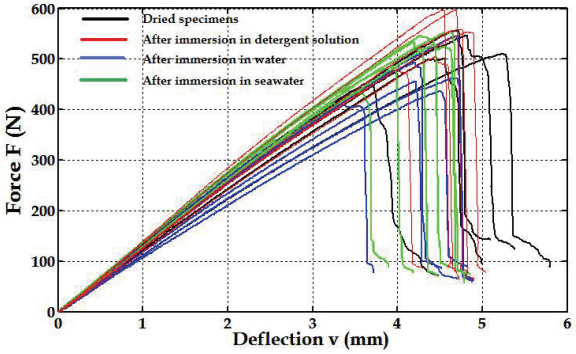

Fig. 23. Curves F-v recorded during the flexural tests in case of E-glass/vinyl-ester ATLAC 582 composite

The flexural modulus was computed on the linear portion of the force-displacement curve. Figures 24 and 25 graphically show the experimental results obtained in case of the glass / polyester composites (E-glass / Heliopol 8431 ATX and E-glass / Polylite 440-M880), figure 26 represents the results in case of E-glass / epoxy LY 554 composite material and figure 27 shows the flexural properties measured in case of the E-glass / vinyl-ester Atlac 582 composite.

Analysing of the results of the experimental research shown in the figures 24 – 27, lead to important remarks that are noted below.

- Effects of the seawater are more pronounced than the action of the water in case of E-glass / polyester composites (E-glass / polyester Heliopol 8431 ATX and E-glass / polyester Polylite 440-M880) as shown in figures 24 and 25.
- Decreasing of the Young's modulus E was ≈ 11 % while the change of the flexural strength was ≈ 12 % in case of the E-glass / polyester Heliopol 8431 ATX composite when the specimens were kept in seawater and detergent solution (Fig. 24). One may observe a good conservation of the flexural characteristics in case of the specimens after 9200 hours of immersion in water.
- Decreasing of the Young's modulus E was ≈ 5 % when the specimens were kept in water and detergent solution while the change was ≈ 10 % when were submerged in seawater in case of the E-glass / Polylite 440-M880 composite (Fig. 25, a).
- A decreasing of the flexural strength was also observed in case of the E-glass / Polylite 440-M880 composite (Fig. 25, b) - about 11%, 23% and 15 % when the specimens were kept in water, seawater and detergent solution, respectively.
- On the other hand, when the E-glass / epoxy LY 554 composite was submerged in water, the decreasing of the Young's modulus was much more pronounced – about 21 % (Fig. 26, a) while the decreasing of the flexural strength was approximately 31 % (Fig. 26, b).
- The decreasing of the flexural strength was about 23%, 26% when the specimens were kept in seawater and detergent solution respectively, in case of the E-glass / epoxy LY 554 composite (Fig. 26, b).
- The decreasing of the Young's modulus E was about 10 %, 15 % when the specimens were kept in seawater and water / detergent mix in case of the E-glass / epoxy LY 554 composite (Fig. 26, a).

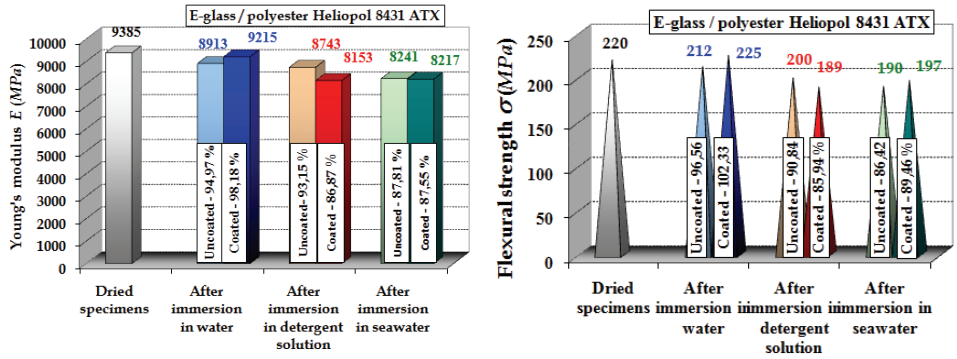

a. b.

Fig. 24. Experimental results of the flexural test in case of E-glass / Heliopol 8431 ATX composite

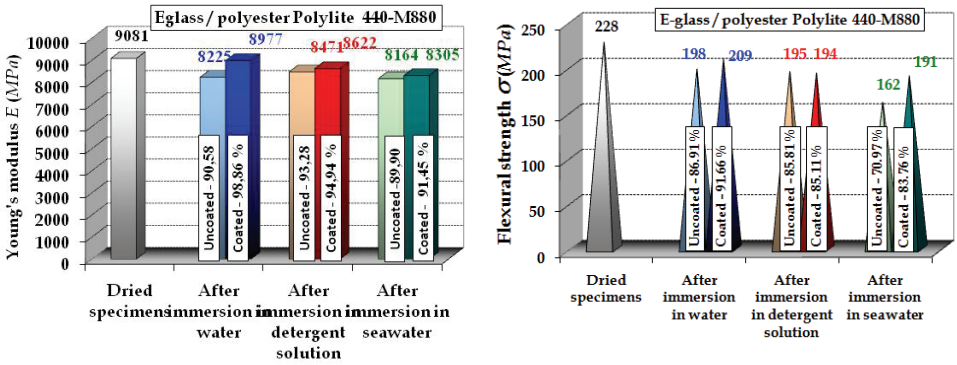

a. b.

Fig. 25. Experimental results of the flexural test in case of E-glass / Polylite 440-M880 composite

Several researchers also found that water absorption causes degradation of matrix-dominated properties such as interface and in-plane shear strengths, compressive strength and transverse tensile strength (Corum et al., 2001; Pomies et al., 1995; Cerbu, 2007; Takeshige et al., 2007). In (Pomies et al., 1995) E-glass / epoxy and carbon / epoxy composites were studied. Finally, the loss in the mechanical properties has been attributed to the plasticity of the matrix by water and degradation of the fibre/matrix interfacial bond due to moisture swelling of the matrix.

In case of the composite materials reinforced only with glass fibres, tested during our experimental research the above reason could be again the cause of the decreasing of the mechanical characteristics of the composite materials.

Experimental results recorded during bending tests, are graphically drawn in case of the hybride composite materials: E-glass EWR145 / fir wood flour / polyester Colpoly 7233 (Fig. 28 and 29) and E-glass EWR145 / oak wood flour / polyester Colpoly 7233 (Fig. 30 and 31). It may be noted that Young's modulus was computed again, for data points located on the linear portion of the F–v curve.

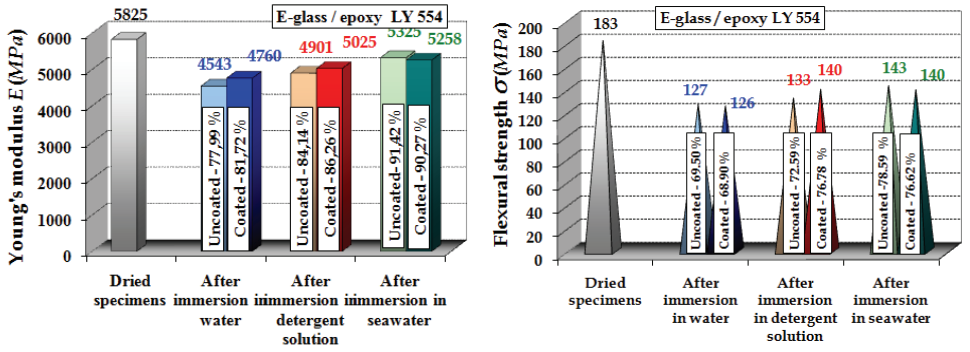

a. b.

Fig. 26. Experimental results of the flexural test in case of E-glass / epoxy LY 554 composite

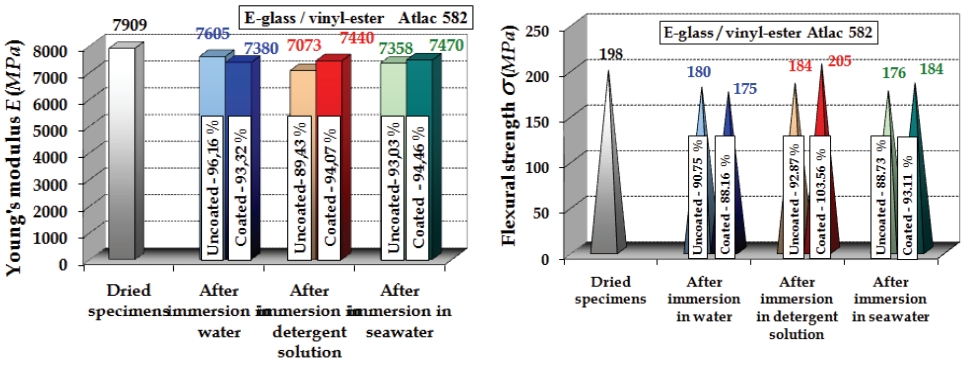

a. b.

Fig. 27. Experimental results of the flexural test in case of E-glass / vinyl-ester Atlac 582 composite

The first of all, it is discussed the changing of the mechanical properties in case of the E-glass / fir wood flour / polyester composite. Young's modulus E (Fig. 28) decreases from 601.1MPa down to 356.2 MPa (with 40.7 %) after 5621 hours of immersion in water while it increases up to 766.0 MPa (with 27.5%) after the same immersion time in seawater. In the same manner, the maximum flexural stress σ_{max} (Fig. 29) decreases from 27.7 MPa down to 16.0 MPa (with 42.2%) after immersion in water and it decreases down to 23.5 MPa (with 15.2%) after immersion in seawater.

In case of the E-glass woven fabric / oak wood flour / polyester composite, it may observe generally speaking, the increasing of both Young's modulus E (Fig. 30) and maximum flexural stress σ_{max} (Fig. 31) after immersion in wet environment. Therefore, this remark confirms once again the well-known property of the oak wood concerning the hardening by aging over the years. In fact, the keeping of the materials completely immersed in water, represents an accelerate process of aging. More exactly, in case of the composite material filled with oak wood flour, Young's modulus E (Fig. 30) increases from 215.0 MPa up to

500.9 MPa (with 132.9%) after 5853 hours of immersion in water while it increases up to 482.0 MPa (with 124.2%) after the same immersion time in seawater. In the same time, the maximum flexural stress σ_{max} (Fig. 31) increases from 21.0 MPa up to 25.0MPa (with 19.05%) after 5853 hours of immersion in water while it decreases down to 17.5MPa (with 16.67%) after the same immersion time in seawater.

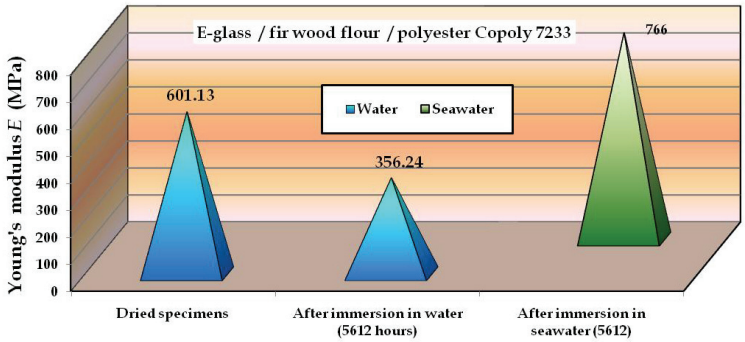

Fig. 28. The effects of water /seawater absorption on *Young*'s modulus E in case of E-glass EWR145 / fir wood flour / polyester Colpoly 7233

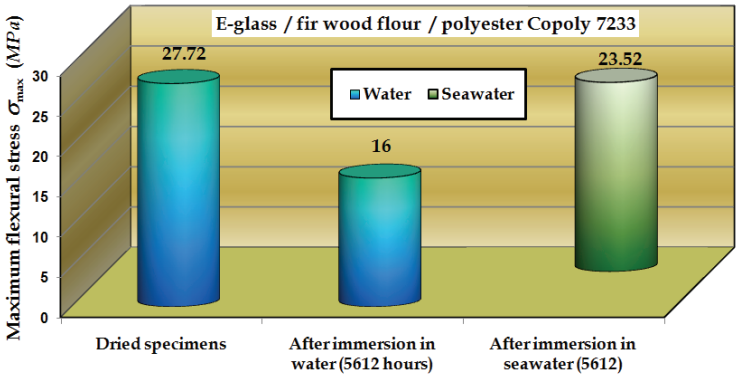

Fig. 29. The effects of water /seawater absorption on on the maximum flexural stress σ_{max} in case of E-glass EWR145 / fir wood flour / polyester Colpoly 7233

In case of the composite material filled with oak wood flour, it was also analysed the effect of the immersion time in water on the changing of the mechanical characteristics. Therefore, Young's modulus increased with 182.28 % after 861 hours of immersion in water while the increasing was only with 132.9%) after 5853 hours of immersion. With other words the increasing of the immersion time leads to a decreasing of the rigidity. The results concerning the changing of the maximum flexural stress σ_{max} show contrary that the maximum flexural stress σ_{max} increases with 7.14 % after 861 hours and it increases with 19.05% after 5853 hours of immersion.

But, the most important remark remains that concerning the values of the maximum deflection v_{max} of the midpoint of the specimens during and after the flexural test. The values recorded

for this quantity is shown in the Table 4 in case of the dried specimens made with oak wood flour. It may easily observe that the maximum residual deflection v_{max} after approximately 30 min. after flexural test had finished, was much smaller than the maximum deflection recorded at maximum load and also, than the one recorded at the final test.

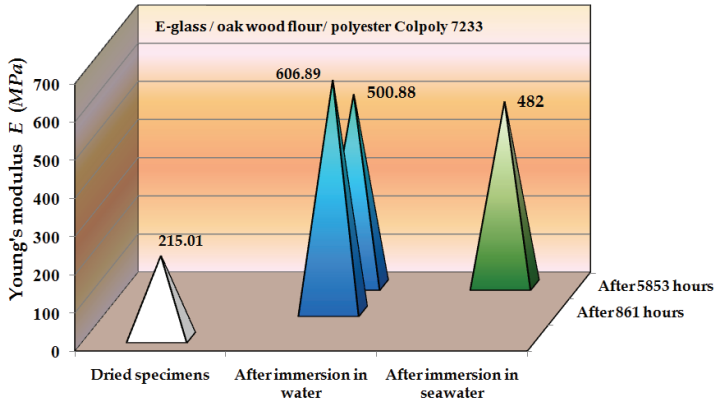

Fig. 30. The effects of water /seawater absorption on Young's modulus E in case of E-glass EWR145 / oak wood flour / polyester Colpoly 7233

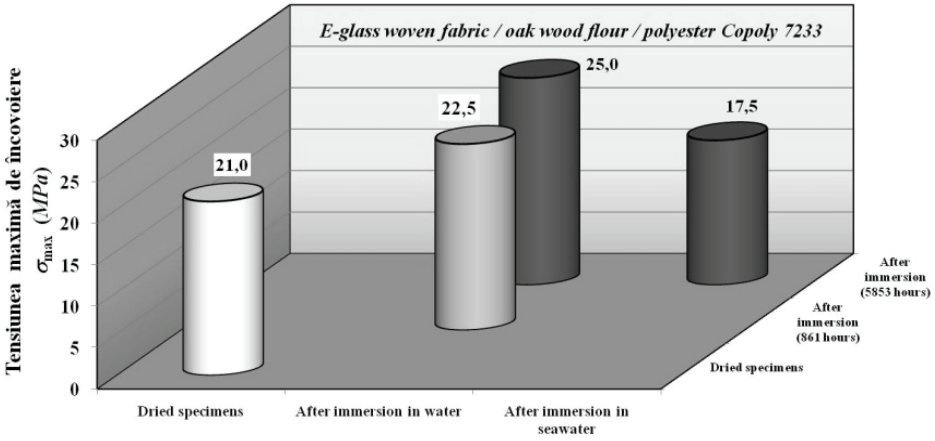

Fig. 31. The effects of water /seawater absorption on on the maximum flexural stress σ_{max} in case of E-glass EWR145 / oak wood flour / polyester Colpoly 7233

The reason of this mechanical behaviour could be assigned to the wood flour used to manufacture the composite specimen because no suchlike observation was recorded in case of E-glass / polyester composite materials tested within this work. Practically, this unexpected mechanical behaviour of the new hybrid composite after the flexural test could be owing to a good combination between the rheological behaviour of wood and the shape memory, property that is assigned to the E-glass fibres.

Specimen No.	1	2	3	4	5
vmax at max. load	22.143	29.513	19.984	39.387	31.504
vmax at final of the flexural test	58.674	54.592	59.396	59.400	59.396
vmax after ≈ 30 minutes after test	7.1	5.2	5.8	4.1	5.7

Table 4. Maximum values of deflection v_{max} in case of the dried specimens made of E-glass EWR145 / oak wood flour / polyester Colpoly 7233 composite material

3.4. Failure mode

Figure 32, a shows a specimen made of the E-glass EWR145 / fir wood flour / polyester Colpoly 7233 composite material, after it was subjected to the flexural test. On the other hand, figure 32, b is a photo of the failure area aquired in case of a flexural specimen made of E-glass EWR145 / oak wood flour / polyester Colpoly 7233 composite material.

It could be observed that only 1-2 layers was partially failured during the testing of the specimens filled with wood flour. Contrary, almost all plies was failured during the flexural test in case of the specimens made of composite materials reinforced only with glass fibres (Fig. 33).

a. b.

Fig. 32. Failure area occured during flexural tests in case of the specimens additionaly reinforced with wood flour: a. fir wood flour; b. oak wood flour

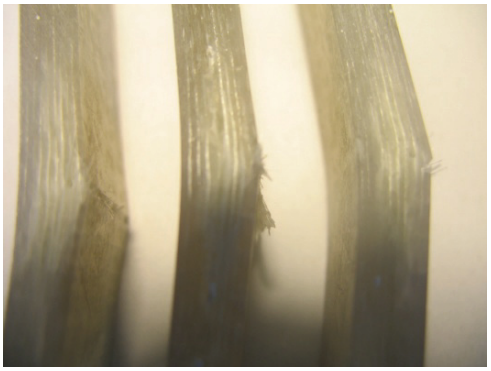

Fig. 33. Failure area of some specimens reinforced only with E-glass fibres, after flexural test

3.5. Degradation of the composite materials

The figure 34, a shows a photo of the two specimens made of composite material reinforced only with glass fibres, after immersion in water while the figure 34, b is a detailed photo of a damaged area located on the surface of the specimen. It was observed that more specimens analysed had similar brown spots located on the cut edge of the specimens. Since there was no spot before immersion in water, it may assume that the oxidation of the resin could be the cause of the spot appearance. The photos shown in figure 35, acquired by using a metallographic microscope, confirms this opinion.

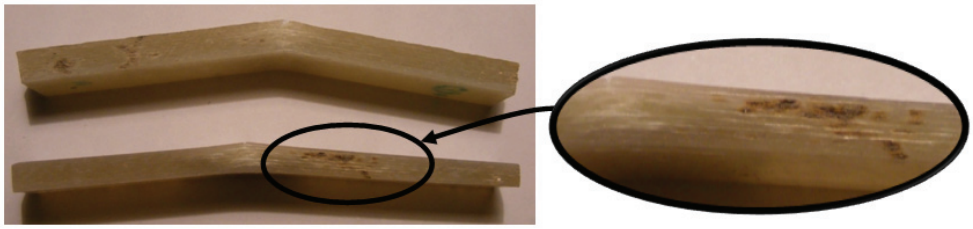

a. b.

Fig. 34. Photos of the damaged composite materials

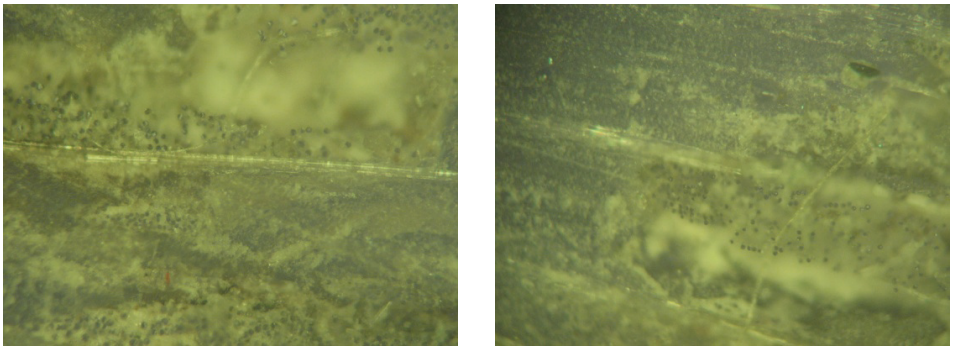

Fig. 35. Specimen photos (zoom 100x) acquired by using a metallographic microscope, after 7197 hours of immersion in water, in case of E-glass/polyester Heliopol 8431ATX composite

Fig. 36. Photo of the specimen surface made of E-glass EWR145 / fir wood flour / polyester Colpoly 7233 after immersion in water (5612 hours)

Concerning the degradation of the surfaces of the specimens made of E-glass EWR145 / fir wood flour / polyester Colpoly 7233, it was observed no spots or colour changes (Fig. 36).
The figure 37 shows two photos of some specimens made of E-glass / oak wood flour / polyester composite material after 5853 hours of immersion in water (Fig. 37,a) and seawater (Fig. 37, b), respectively. It may be easily observed that more specimens analysed had similar black spots located on the cut edges of the specimens, especially in case of the specimens immersed in seawater.

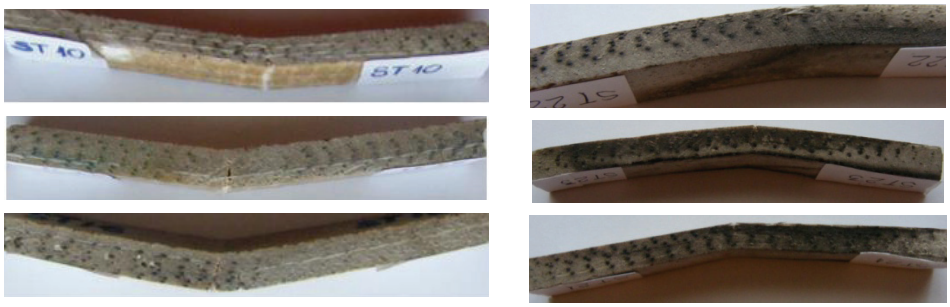

a. b.

Fig. 37. Photos of the edges of the specmens made of E-glass / oak wood flour / polyester after 5853 hours of immersion in: a) water; b) seawater

Since there was no spot before immersion in water, it may assume that the oxidation of the resin could be one of the causes of the spot appearance.
Moreover, it was remarked that in case of the specimens immersed in seawater, the damaged areas located on the specimen edge are larger in case of the composite material filled with oak wood flour than in case of the other one type of composite. The greater content of the tannin in case of oak wood than in case of the fir wood, could be the cause of the greater degradation of the specimens made of the E-glass / oak wood flour / polyester composite material.

4. Conclusions and discussions

We note that the moisture absorption into the composite materials reinforced only with glass fibres, leads to the decreasing of the tensile strength, flexural strength and Young's modulus E. It was observed that the flexural modulus E of these composite materials decreases with 10 - 20 %.
Decreasing of the tensile strength is about 40 % in case of E-glass / epoxy LY 554 composite after ≈ 7000 hours of immersion in water while the decreasing of the flexural strength is 30 % after 9200 hours.
In general, it was found that the E-glass / epoxy composite analysed absorbed more water than seawater or detergent solution. The sodium chloride molecules contained in seawater (as well as sulphate), appear to be limiting the diffusion of water into the matrix material. It was observed that the detergent effect was much more pronounced than the sodium chloride effect in case of E-glass / polyester composite.
The E-glass / polyester composites (E-glass / polyester Heliopol 8431 ATX and E-glass / polyester Polylite 440-M880) are recommended as composite materials in case of water or seawater environment.

Finally, it should remark that the absorption of water leads to the increasing of both Young's modulus E and maximum flexural normal stress σ_{max} in case of the hybrid composite material with oak wood flour. Contrary, the absorption of water leads to the decreasing of the mechanical characteristics (Young's modulus E and strength) in case of the other one composite with fir wood flour. It follows that wood oak flour should be recommended as filler for the parts that works in water environment and that made of the hybrid composite material involved. If the humid environment contains salts fir wood flour should be used as filler because the greater content of the tannins associated to the oak wood leads to the appearance of the large dark stains over the surface of the composite.

5. Acknowledgement

This work was supported by CNCSIS – UEFISCSU of Romania, project number PNII – IDEI 733 / 2008 (CNCSIS - National Council of Scientific Research in Higher Education; UEFISCSU - Executive Unit for Financing Higher Education and Research).

6. References

Adhikary, K. B.; PANG, S.; STAIGER, M. P. (2007). Long-term moisture absorption and thickness swelling behaviour of recycled thermoplastics reinforced with Pinus radiata sawdust. In: Chemical Engineering Journal, doi: 10.1016 /j.cej.2007.11.024.

Adhikary, K. B.; PANG, S.; STAIGER, M. P. (2008). Dimensional stability and mechanical behaviour of wood–plastic composites based on recycled and virgin high-density polyethylene - HDPE. In: Composites Journal (Part B) 39: 807–815.

Cerbu C. (2007). Aspects concerning the degradation of the elastic and mechanical characteristics in bending in case of th glass / polymer composite materials due to the moisture absorption, Materiale Plastice, ISSN 0025 / 5289, 44, nr. 2, 2007, pp.97-102;

Cerbu C. (2005) - *Researches concerning structural optimisation of some pieces made of composite materials, loaded in environmental aggressive conditions.* Doctoral thesis. Transilvania University of Brasov

Cerbu, C., Ciofoaia, V., Curtu I., Vişan, A. (2009). The effects of the immersion time on the mechanical behaviour in case of the composite materials reinforced with E-glass woven fabrics, Materiale Plastice, ISSN 0025 - 5289, 46, nr. 2, 2009, p.201;

Cerbu, C.; Teodorescu, H. (2009). Bending behaviour of the composite materials made by recycling of the CDs and DVDs, In: Proceedings of The World Congress on Engineering WCE 2009, vol. II: p.1753-1756.

Cerbu, C., Curtu, I. (2009). Particularities concerning the mechanical behaviour in wet environment in case of a hybrid composite material with wood flour, Rev. ProLigno, ISSN 1841-4737,vol. 5, Nr. 3, 2009, pp.37,

Cerbu, C., Motoc, D., Ciofoaia, V. (2009). Advantages of the using of the poliester resin to manufacturing of the composite materials based on wood flour, Annals of DAAAM for 2009 & Proceed. of the 20th International DAAAM Symposium "Intelligent Manufacturing & Automation: focus on Theory, Practice & Education", vol. 20, no. 1, 25-28th November 2009, Vienna, Austria, ISSN 1726-9679, ISBN 978-3-901509-70-4, Editor Branko Katalinic, pp.1417-1418.

Corum, J. M., Battiste, R. L., Ruggles, M. B., Ren, W. (2001). Durability – based design criteria for a chopped-glass-fibre automotive structural composite, Composite Science and Technology, no. 61;

Kamdem, D. P.; Jiang, H.; Cui, W.; Freed, J.; Matuana, L. M. (2004). Properties of wood plastic composites made of recycled HDPE and wood flour from CCA-treated wood removed from service. In: Composites Journal (Part A) 35: 347–355.

Klyosov, A. A. (2007). Wood-plastic composites, A John Wiley & Sons, Inc. Hoboken, New Jersey, USA.

Pomies, F., Carlson, L. A., Gillespie, J. W. (1995). Marine environmental effects on polymer matrix composites, Composite Materials: Fatigue and Fracture, Fifth Volume, ASTM STP 1230, R. H. Martin, Ed., American Society for Testing and Materials, Philadelphia;

Springer, G. S. (1984). Environmental Effects on Composite Materials, Vol. 2, Technomic Publishing Inc., Lancaster, PA, ,;

SR EN ISO 527 / 1,2,3. Glass fibre reinforced plastics, Determination of the tensile properties;

SR EN ISO 178 (2001). Glass fibre reinforced plastics, Determination of flexural properties, Three point method, CEN, Bruxelles, 2001;

SR EN ISO 62 (2008). Plastics. Determination of water absorption, European Committee for Standardization, Brussels.

Takeshige, F.; Kawakami, Y.; Hayashi, M.; Ebisu S. (2007). Fatigue behavior of resin composites in aqueous environments, In: Dental Materials 23: 893–899.

20

Simulations of Woven Composite Reinforcement Forming

Philippe Boisse
Université de Lyon, LaMCoS, INSA-Lyon, 69621
France

1. Introduction

Complex preforms can be obtained by forming an initially flat textile composite reinforcement. Then the resin is injected on the preform in LCM processes (Liquid Composite Moulding)(Advani, 1994, Rudd & Long, 1997, Parnas, 2000). These processes and especially the RTM process (Resin Transfert Moulding) can be used to manufacture highly loaded composite part for aeronautical application (e.g. the helicopter frame and the motor blade presented in figures 1 and 2).

Numerical optimization of products and production processes becomes increasingly important in the design phase of composite structures. Numerical simulations of the composite forming processes are an essential part of these optimization tools. They permit to determine the conditions of the feasibility of a process without defect (wrinkling, fracture of yarns, porosities…) but above all, they give the fibre orientations after shaping. This is mainly important because redistribution of the fibres is inevitable when double curved products are considered. The fibre orientations strongly influence the mechanical behaviour of the final part and the permeability of the reinforcement and thus the injection of the resin in the case of a liquid moulding process

The first method used for analysing composite forming processes, and especially draping in woven composite reinforcements, is "kinematic models". The fibre distribution of a woven cloth is predicted on a given geometry based on a pin jointed net assumption (fishnet algorithm). The yarns of the fabric are assumed to be inextensible and the rotation between warp and weft yarns is free. The woven reinforcement is placed progressively from initial lines. Several packages are commercially available. This method is briefly described in section 2. It is fairly efficient for hand draping in classical prepreg fabrics, but the models do not account for load boundary conditions, for possible sliding of the fabric in relation to the tools, and for the mechanical behaviour of the woven reinforcement

For a physical analysis of a composite forming process, the complete model must include all the equations for the mechanics, especially equilibrium, constitutive equations, and boundary conditions. These equations must be solved numerically, with some approximations. Finite Element Analysis of the composite forming process includes the tools modelling, the contact and friction between the different parts, and above all, the mechanical behaviour of the composite during forming. If these models can be numerically costly, problems of computation time are steadily reduced through improved processing

capabilities. The main problem for the FE approach therefore lies in the requirement for accurate models of all the significant aspects of the forming process.

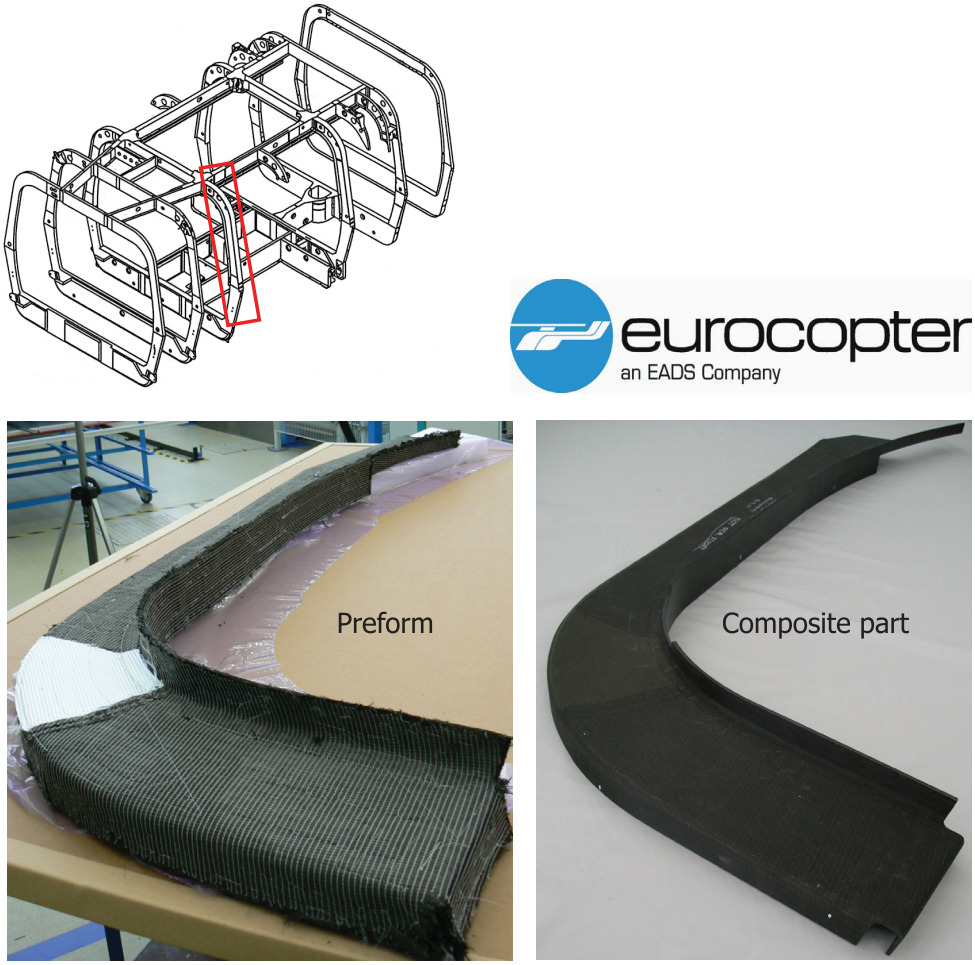

Fig. 1. Preform/RTM parts in NH90 (Dumont et al. 2008) (Courtesy of Eurocopter, EADS Group)

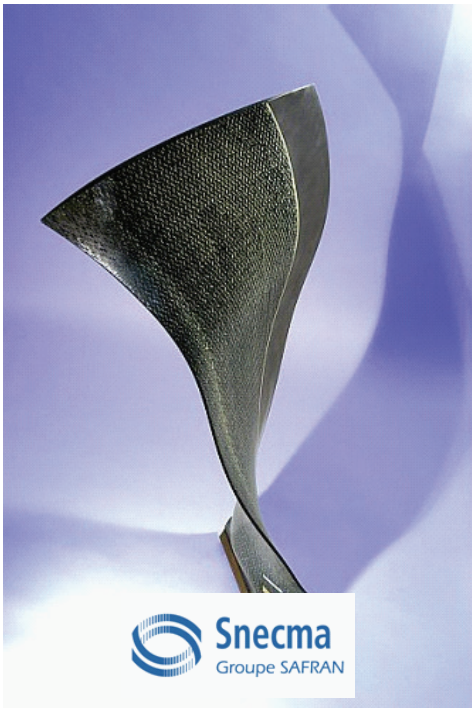

Fig. 2. Plane motor blade (Courtesy of Snecma, Groupe Safran) (De Luycker et al. 2009)

The mechanical behaviour of fabrics is complex due to the intricate interactions of the yarns and fibres. It is a multi-scale problem. The macroscopic behaviour is very dependent on the interactions of yarns at the meso-scale (scale of the woven unit cell) and at the micro-scale (level of the fibres constituting yarns). Despite the many works in the field, there is no widely accepted model that accurately describes all the main aspects of a composite woven reinforcement mechanical behaviour. The approaches to model the forming of textile composite reinforcements belong to two main families that are related to the scale at which the analysis is made. The textile reinforcement is a set of yarns (or fibres). The analysis of the forming can be made considering and modelling each of these yarns (or fibres) and their interactions (contact with friction). In this case the approach is called discrete or mesoscopic. Of course the number of yarns is high and the interactions are complex. On the opposite, the continuous approaches consider a continuous medium juxtaposed with the fabric and the mechanical behaviour of which is equivalent to those of the textile reinforcement. This mechanical behaviour is complex because it concerns large strains and strong anisotropy. Furthermore, it strongly changes during the forming.

The present chapter aims to present continuous and discrete approaches for composite reinforcements forming simulations. First two continuous approaches are described within a membrane assumption. The first one is based on a hyperelastic model and the second on a hypoelastic one. Then simulations of woven fabric forming based on a discrete approach are presented. Finally a semi-discrete approach which can be seen as an intermediate method between continuous and discrete ones is presented. This approach is extended to 3D interlock forming simulations. The advantages and drawback of the different approaches are discussed.

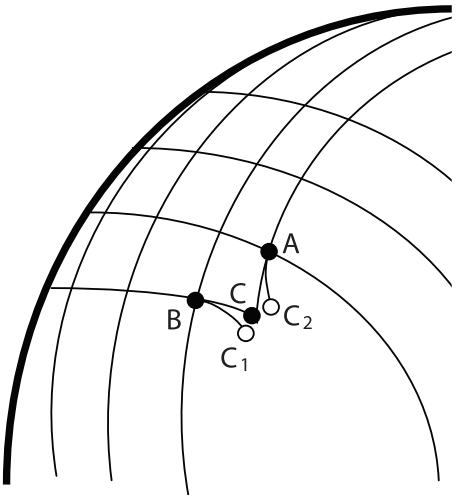

Fig. 3. Fishnet algorithm: Calculation of the position of point C knowing those of A and B

2. Kinematic models

"Kinematic models" also called fishnet algorithms are commonly used in industry for analysing composite forming processes, and especially draping in woven composite reinforcements (Mark, 1956, Van Der Ween, 1991, Long et al, 1994, Borouchaki et al, 2002). Several packages are commercially available. The method is based on the (strong) following assumptions : i/ The yarns are inextensible, ii/ there is no sliding at the intersection between warp and weft yarns, iii/ The rotations between warp and weft yarns are free, iv/ there is no sliding between the fabric and the tool.

As shown on figure 3, the position of the node C can be determined if those of its neighbours A and C are already known. AC and BC have prescribed length. C is defined as the intersection of two geodesics coming from A and B and that intersect in C. This constitutes a small scalar problem, generally non-linear that can be solved very fast. The surface of the tool must be defined analytically of by curved elements. In order to initiate the draping as shown figure 3, it is necessary to position a first node and to fixe two initial draping directions. These directions are the symmetry axes if they exist. The result of the draping depends on these directions.

This method is very fast and fairly efficient for hand draping in classical prepreg fabrics, but the models do not account for load boundary conditions, for possible sliding of the fabric in relation to the tools, and above all for the mechanical behaviour of the woven reinforcement.

3. Mechanical behaviour of textile composite reinforcement

The diameter of each fibre constituting the textile composite reinforcements is very small: 5 to 7 μm for carbon, 5 to 25 μm for glass, 10 to 20 μm for aramid. A yarn is made up of several thousands juxtaposed fibres (usually 3. 10^3 to 96. 10^3). These yarns are woven following standard weaves (plain, satin, twill) or more complex structures such as braiding or ply to ply interlock weaves (Figure 4c). An alternative consists in stitching a ply made of parallel

fibres. This leads to the so-called NCF reinforcement (Non Crimp fabric) in which the fibres are not undulated (Figure 4d). The material resulting from this assembly of continuous fibres exhibits a very specific mechanical behaviour since relative motions are possible between the yarns and the fibres. The textile reinforcement pre-forming stage takes advantage of these possible motions. The forming is made on dry reinforcement (i.e. without resin) since it is performed before the injection stage.

A woven fabric is intrinsically a multiscale material and, depending on the specific application of interest, one or more scales of the woven fabric have to be explored.

Three scales can be distinguished (Figure 5). The macroscopic scale refers to the whole component level, with dimensions in the order of some centimetres to several meters (Figure 5a). At the mesoscopic scale, the woven reinforcement is seen as a set of yarns, respectively the warp and the weft (or fill) yarns in case of a woven fabric (Figure 5b) . Consequently, the corresponding working scale is the one of the yarn dimension, typically one to several millimetres. For periodic materials, mesoscopic models consider the smallest elementary

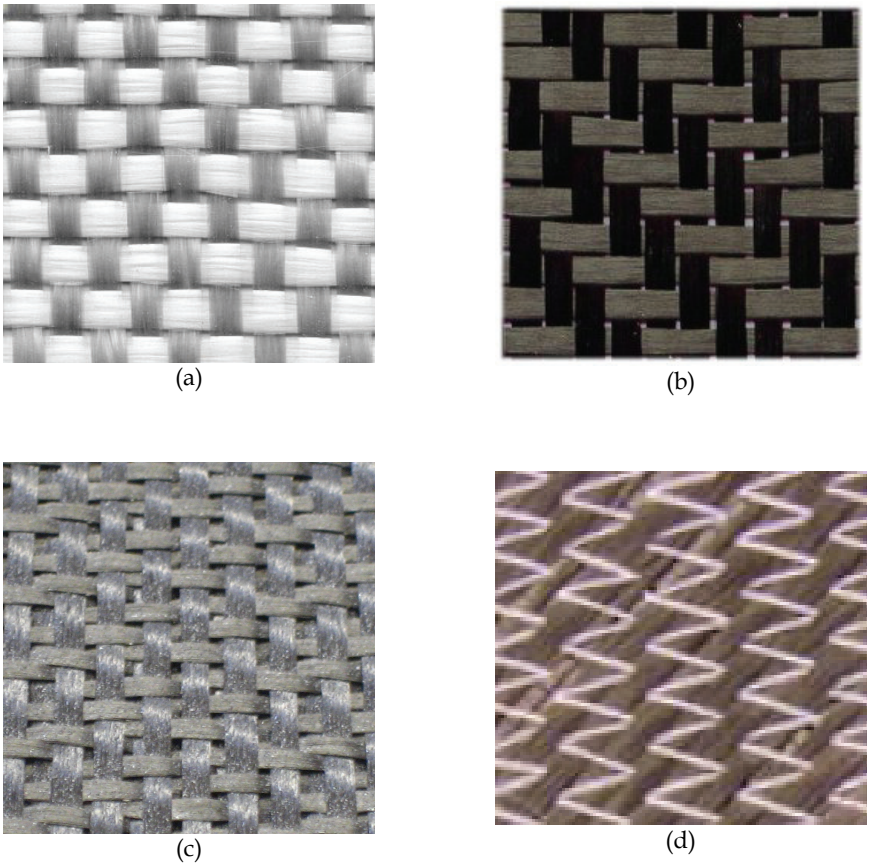

Fig. 4. Textile composite reinforcements (a) plain weave, (b) twill weave (c), interlock, (d) NCF

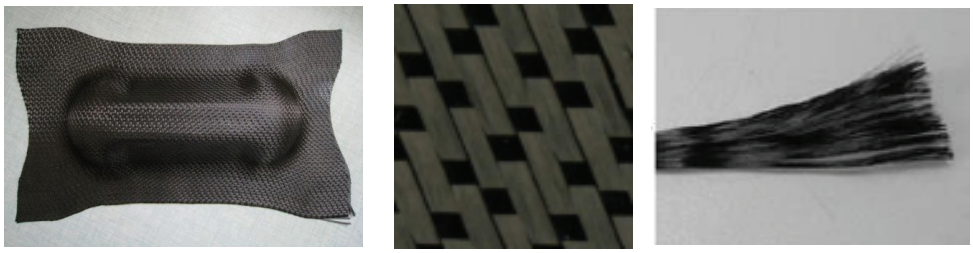

Macroscopique scale (a) Mesoscopic scale (b) Microscopic scale (c)

Fig. 5. The three scales of the fibre reinforcement

pattern which can represent the whole fabric by several translations. That domain is called the Representative Unit Cell (RUC). Each yarn is made up of thousands of continuous fibres which interact (Figure 5c), and thus the interactions of the reinforcement can be analyzed at the microscopic scale. At the microscopic level, the characteristic dimension is about one to several micrometers. This is the only scale at which the material is actually continuous.
Although the fibrous reinforcement is not strictly continuous because of possible relative sliding between fibres, several mechanical behaviour models have been proposed that consider the textile reinforcement as an anisotropic continuum (Spencer, 2000; Dong et al, 2001; Yu et al, 2002; King et al, 2005, Peng et al, 2005, Ten Thije et al, 2007, Badel et al, 2009)
Nevertheless there is no widely accepted model that describes accurately all of the main aspects of fabric mechanical behaviour. Actually, such a model must convey the specificities of the composition of the textile made of yarns and fibres and above all take into account the variation of the properties during the forming. These changes are very large because of the variations of fibre directions and of the local lateral compression of the yarns due to the forming.

4. Experimental texts

The specific mechanical behaviour of textile composite reinforcements has led to the development of specific experimental tests in order to quantify the tensile, in-plane shear and bending behaviour.

4.1 Biaxial tensile behaviour

The tensile behaviour of woven material is specific mainly because of the decrimping of tows when they are stretched. This leads to tensile behaviour non-linearities. The fabric is much softer than the tow for small axial strains. Because of the weaving, the decrimping phenomenon in warp and weft directions are interdependent and the tensile behaviour is biaxial. Some biaxial tests have been developed in order to measure these properties (Kawabata et al, 1973, Buet-Gautier & Boisse, 2001, Carvelli et al, 2008, Willems et al, 2008). Fig. 5. shows a biaxial tensile device using a cross shape specimen (Buet-Gautier & Boisse, 2001). The measurements of tensions in warp and weft directions $T_1(\varepsilon_{11}, \varepsilon_{22})$ and $T_2(\varepsilon_{11}, \varepsilon_{22})$ are shown Figure 5b for different ration between warp and weft strains. It has been experimentally shown that the influence of the shear angle on the tensile behaviour is usually weak and can be neglected (Buet-Gautier & Boisse, 2001).

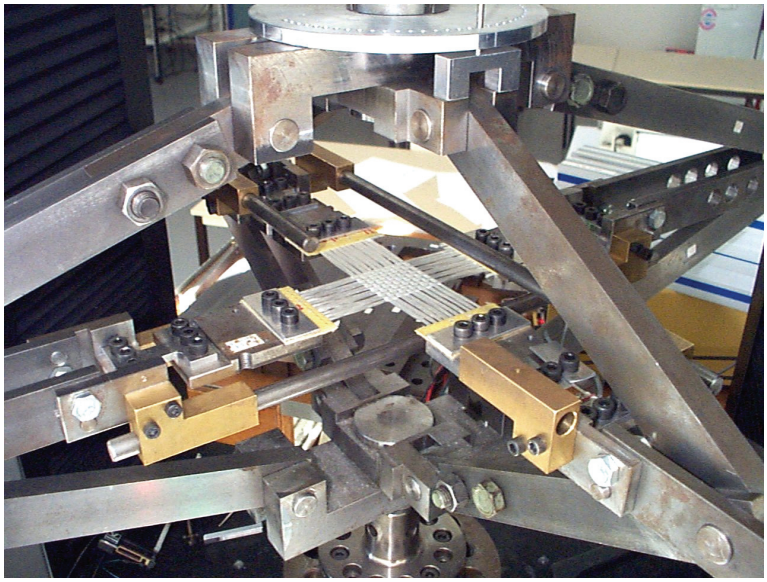

(a)

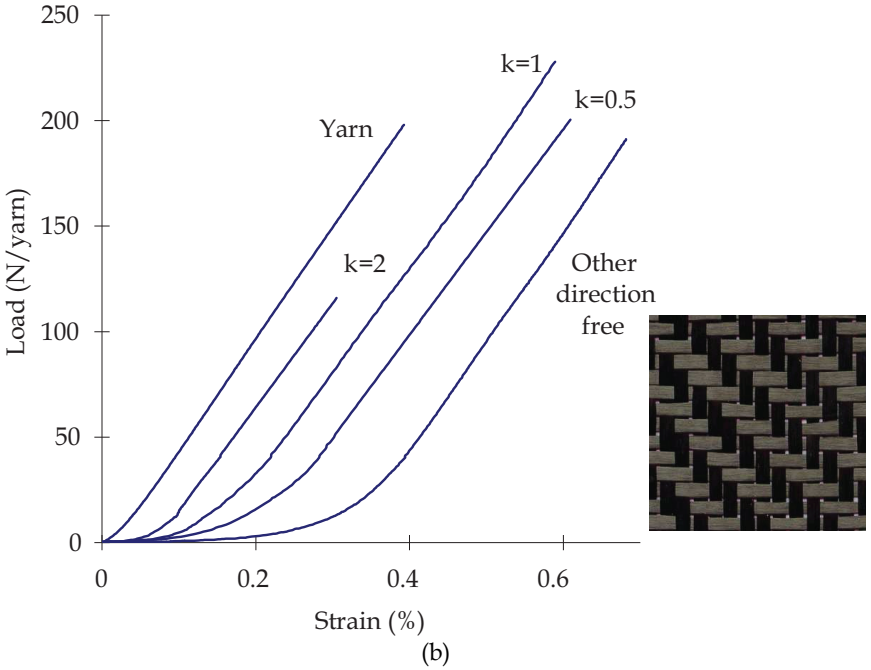

(b)

Fig. 6. (a) Biaxial tensile test on cross-shaped specimen (b) Load versus strain for carbon twill weave. $k = \varepsilon_{warp} / \varepsilon_{weft}$ (Buet-Gautier et al, 2001)

4.2 In-plane shear behaviour

Two experimental tests are used to determine the in-plane shear behaviour of textile composite reinforcements: the picture-frame (Figure 7) and the bias-extension tests (Figure 8). A great literature is dedicated to those tests (Prodromou & Chen, 1997, Rozant et al, 2000, Potter et al, 2002, Lebrun et al, 2003, Sharma et al, 2003, Peng et al, 2004, Harrison et al, 2004, Lomov et al, 2006, Launay et al, 2008, Lomov et al, 2008, Cao et al, 2008) mainly because the in-plane shear is the most dominant deformation mode in woven composite forming when

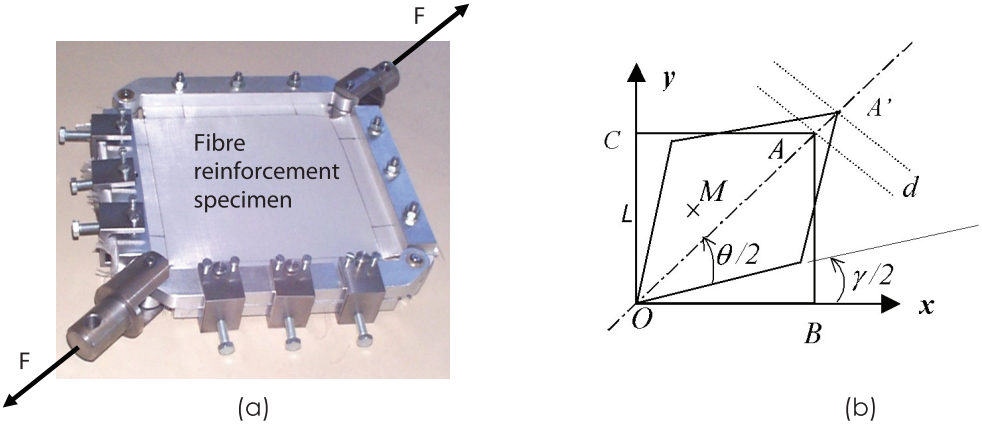

Fig. 7. Picture frame test. (a) Experimental device. (b) Kinematics of the test

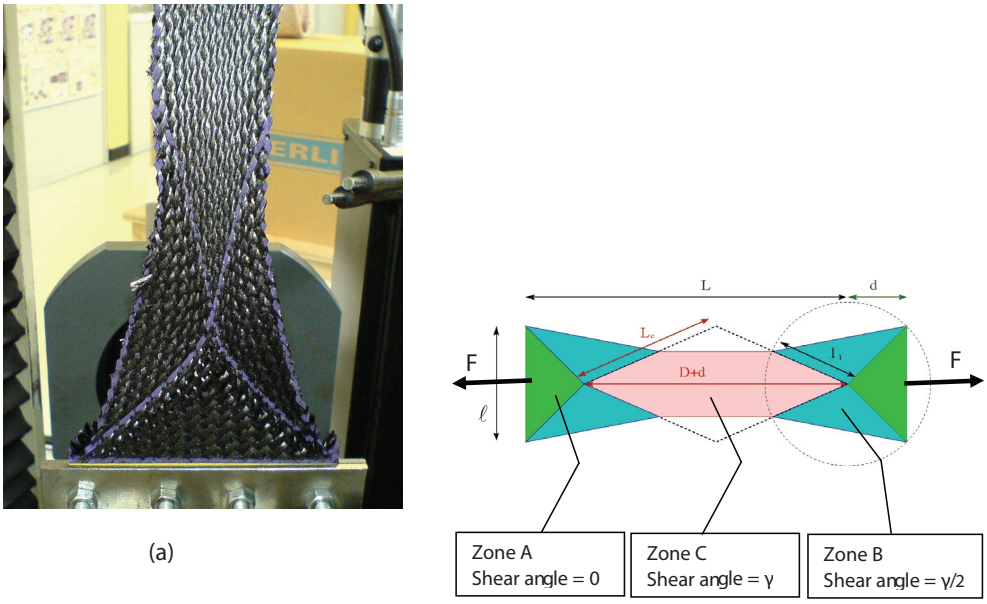

Fig. 8. The bias-extension test and the three zones

the manufactured part is doubly curved. The shear angle can reach 50° (and even more in some cases such as presented in section 5.6). For large values, wrinkling can occur depending on the process parameters and on the material properties. In addition, the two tests are difficult both from the experimental point of view and concerning the interpretation of the results. For these reasons an international benchmark has been launched recently. Eight laboratories of six different countries have performed picture frame and bias-extension tests on the same textile composite reinforcements (Cao et al, 2008).
The picture-frame (or trellis-frame) is made of four hinged bars. The fabric specimen is initially square and the tows are parallel to the bars. Consequently it is theoretically subjected to pure in-plane shear and the shear angle γ is function of the displacement d.

$$\gamma = \frac{\pi}{2} - 2\arccos\left(\frac{1}{\sqrt{2}} + \frac{d}{2L}\right) \tag{1}$$

Neglecting the dissipation due to friction in the hinged bars, the in-plane shear moment on a unit shell M_s is related to the force on the frame F using the equality of the power expressions. S_c is the surface of the unit woven cell in the initial state.

$$M_s(\gamma) = F\frac{S_c}{\sqrt{2}\,L}\left(\cos\frac{\gamma}{2} - \sin\frac{\gamma}{2}\right) \tag{2}$$

The bias-extension test is an alternative to the picture-frame test. It consists in clamping a rectangular specimen of woven fabric with warp and weft directions initially oriented at 45° with respect to the tensile load applied by a tensile machine (Figure 8). The initial length of the specimen L must be larger than twice the width ℓ. The zone C in the centre of the specimen is submitted to a pure shear γ if the yarns are assumed to be inextensible. That is a correct assumption for the type of yarns used as composite reinforcements. This inextensibility imposes that the shear angle in the zone B is half the value in the central region C. The shear angle γ is related to the specimen elongation d in equation (c). The in-plane shear moment is related to the force on the frame F in equation (d).

$$\gamma = \frac{\pi}{2} - 2\arccos\left(\frac{D+d}{\sqrt{2}D}\right) \tag{3}$$

$$M_S(\gamma) = \frac{FDS_c}{\ell(2D-\ell)}\left(\cos\frac{\gamma}{2} - \sin\frac{\gamma}{2}\right) - \frac{\ell}{2D-\ell}M_S\left(\frac{\gamma}{2}\right) \tag{4}$$

A shear curve $M_s(\gamma)$ measured in the case of glass plain weave is presented in Figure 9. In the first part of the curve (i.e. for small shear angles), the in-plane shear stiffness is small. For larger shear angles this rigidity increases and becomes significant. The optical field measurements performed within the tow show that during the first part of the loading, the tows rotate in a rigid body motion (Figure 9b). When the shear angle becomes larger lateral contacts between the yarns occur (Dumont et al, 2003). The tows are progressively compressed and the shear rigidity increases significantly. This increase of shear stiffness leads to wrinkling onset. The corresponding shear angle is called locking angle (in order of 40°- 45° for textile composite reinforcements (Prodromou & Chen, 1997, Cao et al, 2008).

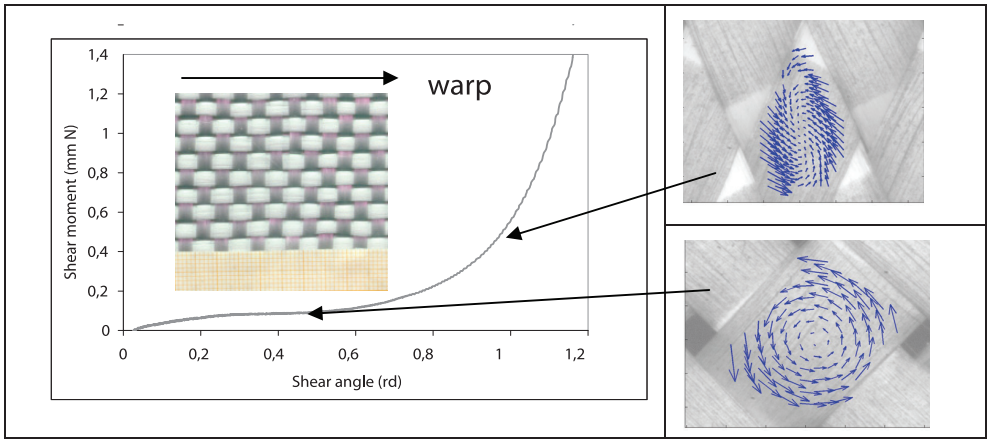

Fig. 9. (a) Shear curve of glass plain weave, (b) relative displacement field inside a yarn

4.3 Bending behaviour

The bending stiffness of the fibrous reinforcement is very low due to the possible motion between fibres. It is often neglected and membrane approaches are often used. Nevertheless this bending stiffness is important to obtain accurate wrinkle shape. Specific tests have been developed for these textile materials, the bending stiffness of which is much smaller than the one given by the plate theory (Kawabata, 1986, Lahey and Heppler 2004, de Bilbao et al, 2010). Figure 10 shows a cantilever bending test (de Bilbao et al, 2010). The own weight of the fabric defines the bending moments for a given length of the specimen. The curvatures are deduced from the measured geometry. These measurements, made for different length of a specimen give the bending moment in function of the curvature. They are made in warp and weft directions.

5. Continuous approach for the simulation of textile composite forming

In the continuous approaches, a woven fabric is seen as a continuous material with a specific mechanical behaviour, including high anisotropy and the ability to exhibit very large shearing and bending deformations. Investigation at the macroscopic level is the most popular for reinforcement forming simulations, as it allows using finite elements codes with standard shell or membrane elements and does not ask the description of the internal textile material structure. Despite the large amount of work in this field (Spencer, 2000; Dong et al, 2001; Yu et al, 2002; King et al, 2005, Peng et al, 2005, Ten Thije et al, 2007, Badel et al, 2009) there is no widely accepted model that accurately describes all aspects of the mechanical behaviour of fabrics. Two continuous approaches are described below.

5.1 Hyperelastic behaviour

The formulation of a hyperelastic behaviour law lies on the proposition of a potential energy from which derives the hyperelastic constitutive model. This potential aims to reproduce the non linear mechanical behaviour of textile composite reinforcements. The proposed potential is a function of the right Cauchy Green and structural tensor invariants defined

Fig. 10. Cantilever bending test

from the fibre directions. This potential is based on the assumption that tensile and shear strain energies are uncoupled. It is the sum of three terms.

$$W = \bar{W}_1(I_1) + \bar{W}_2(I_2) + \bar{W}_s(I_{12}) \tag{5}$$

This assumption (tensile and shear strain energies are uncoupled) are made for sake of simplicity. The independence of tensile behaviour relatively to in plane shear has been shown experimentally (Buet-Gauthier and Boisse, 2001). The other hypotheses are probably less true, but there are made for sake of simplicity and because there are few data available on some couplings.

The structural tensors $\underline{\underline{L}}_{\alpha\beta}$ are defined from the two unit vectors in the warp and weft directions $\underline{f}_{10}$ and $\underline{f}_{20}$ in the reference configuration C^0 (figure 11):

$$\underline{\underline{L}}_{\alpha\beta} = \underline{f}_{\alpha 0} \otimes \underline{f}_{\beta 0} \tag{6}$$

The two first terms $\overline{W_1}$ and $\overline{W_2}$ are the energies due to the tensions in the yarns. They are function of invariants I_1 and I_2 respectively, themselves depending on the right Cauchy Green strain tensor $\underline{\underline{C}} = \underline{\underline{F}}^T \cdot \underline{\underline{F}}$ and the structural tensors $\underline{\underline{L}}_{\alpha\alpha}$:

$$I_1 = \mathrm{Tr}(\underline{\underline{C}} \cdot \underline{\underline{L}}_{11}) = \lambda_1^2 \qquad I_2 = \mathrm{Tr}(\underline{\underline{C}} \cdot \underline{\underline{L}}_{22}) = \lambda_2^2 \tag{7}$$

λ_α is the deformed length of on initially unit fibre in the direction α.

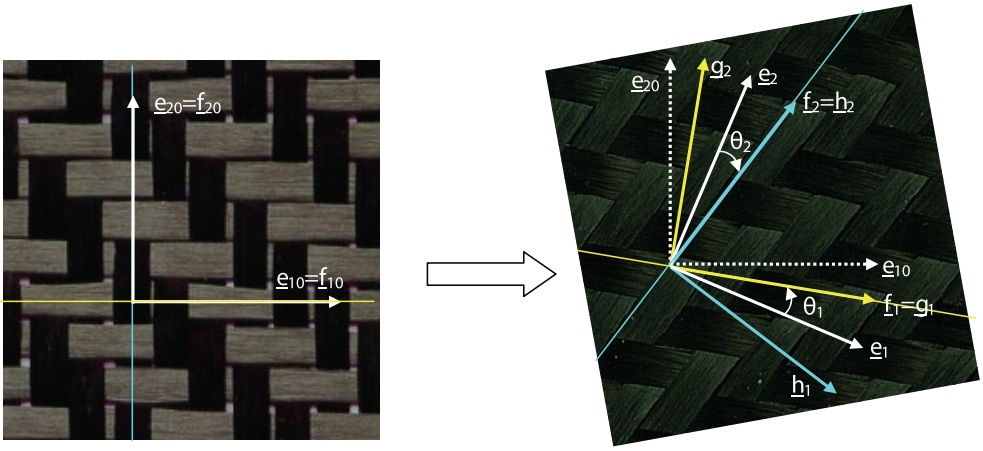

Fig. 11. Fibres axes and GN axes after deformation. Initially these axes are superimposed.

The third term $\overline{W}_s$ in equation (5) is a function of the second mixed invariants of $\underline{\underline{C}}$.

$$I_{12} = \frac{1}{I_1 I_2} \mathrm{Tr}(\underline{\underline{C}} \cdot \underline{\underline{L}}_{11} \cdot \underline{\underline{C}} \cdot \underline{\underline{L}}_{22}) = \cos^2 \theta \tag{8}$$

The second Piola Kirchhoff stress tensor is derived from this potential (Basar and Weichert, 2000):

$$\underline{\underline{S}} = 2\frac{\partial W}{\partial \underline{\underline{C}}} \tag{9}$$

And in the case of the present potential (5):

$$\begin{aligned} \underline{\underline{S}} = 2&\left[\frac{\partial \overline{W}}{\partial I_1} - \frac{I_{12}}{I_1}\frac{\partial \overline{W}}{\partial I_{12}}\right]\underline{\underline{L}}_{11} + 2\left[\frac{\partial \overline{W}}{\partial I_2} - \frac{I_{12}}{I_2}\frac{\partial \overline{W}}{\partial I_{12}}\right]\underline{\underline{L}}_{22} \\ &+2\left[\sqrt{\frac{I_{12}}{I_1 I_2}}\frac{\partial \overline{W}}{\partial I_{12}}\right]\left(\underline{\underline{L}}_{12} + \underline{\underline{L}}_{21}\right) \end{aligned} \tag{10}$$

In order to define the form of the potential two complementary assumptions are made taking into account the specific woven fabric behaviour and its deformation modes. As assumed above, i/ The tensions in the yarns and the in-plane shear are independent. ii/ The tensions in the warp and weft directions are uncoupled.

The potential has to vanish in a stress free configuration. Polynomial functions of the invariants are considered in the present work. The global form of the proposed potential energy is given by:

$$W\left(\underline{\underline{C}}\right) = \sum_{i=0}^{r} \frac{1}{i+1} A_i \left(I_1^{i+1} - 1\right) + \sum_{j=0}^{s} \frac{1}{j+1} B_j \left(I_2^{j+1} - 1\right) + \sum_{k=1}^{t} \frac{1}{k} C_k I_{12}^k \tag{11}$$

The resulting second Piola Kirchhoff tensor is:

$$\underline{\underline{S}} = 2\left(\sum_{i=0}^{r} A_i I_1^i - \frac{1}{I_1}\sum_{k=1}^{t} C_k I_{12}^k\right)\underline{\underline{L}}_{11} + 2\left(\sum_{j=0}^{s} B_j I_2^j - \frac{1}{I_2}\sum_{k=1}^{t} C_k I_{12}^k\right)\underline{\underline{L}}_{22} + 2\left(\frac{1}{\sqrt{I_1 I_2}}\sum_{k=1}^{t} C_k I_{12}^{k-1/2}\right)\left(\underline{\underline{L}}_{12} + \underline{\underline{L}}_{21}\right) \quad (12)$$

For strain-free configuration, stresses have to vanish. This condition imposes:

$$\sum_{i=0}^{r} A_i = 0 \quad ; \quad \sum_{j=0}^{s} B_j = 0 \quad (13)$$

To determine the constants A_i, B_j and C_k, three experimental tests are necessary: two tensile tests in the warp and weft directions and one in-plane pure shear test. The details of the calculations to obtain equations **???** to **???** are given in (Aimene et al, 2010). In this paper it is also shown that the form of the potential given above gives correct results concerning the direction of the loads on the boundary of a picture frame while other forms of the potential lead to boundary loads that are not correct for a woven fabric.
The proposed hyperelastic model is implemented in a user routine VUMAT of Abaqus/Explicit and it is applied to membrane elements. The simulation of a hemispherical punch forming process is performed in the case of strongly unbalanced twill (Daniel et al, 2003). The warp rigidity is 50 N/yarn and the weft rigidity is 0.2 N/yarn. The experimental deformed shape are shown figure 12 (a) together with the results of the simulation figure 12 (c). The computed deformed shape (made using the hyperelastic model proposed above) is in correct agreement with the experimental one. Especially the strong difference of the deformation in warp and weft directions is well verified.

5.2 Hypoelastic behaviour

Hypoelastic models have been proposed for material at large strain (Truesdell, 1955, Xiao et al, 1988)

$$\underline{\underline{\boldsymbol{\sigma}}}^{\nabla} = \underline{\underline{\underline{\underline{\mathbf{C}}}}} : \underline{\underline{\mathbf{D}}} \quad (14)$$

where $\underline{\underline{\mathbf{D}}}$ and $\underline{\underline{\underline{\underline{\mathbf{C}}}}}$ are the strain rate tensor and the constitutive tensor, respectively. $\underline{\underline{\boldsymbol{\sigma}}}^{\nabla}$, called the objective derivative of the stress tensor, is the time derivative for an observer who is fixed with respect to the material.

$$\underline{\underline{\boldsymbol{\sigma}}}^{\nabla} = \underline{\underline{\mathbf{Q}}} \cdot \left(\frac{\mathrm{d}}{\mathrm{d}t}\left(\underline{\underline{\mathbf{Q}}}^{\mathrm{T}} \cdot \underline{\underline{\boldsymbol{\sigma}}} \cdot \underline{\underline{\mathbf{Q}}}\right)\right) \cdot \underline{\underline{\mathbf{Q}}}^{\mathrm{T}} \quad (15)$$

$\underline{\underline{\mathbf{Q}}}$ is the rotation from the initial orthogonal frame to the so-called rotating frame where the objective derivative is made. The most common objective derivatives are those of Green-Naghdi and Jaumann. They use the rotation of the polar decomposition of the deformation gradient tensor $\underline{\underline{\mathbf{F}}} = \underline{\underline{\mathbf{R}}} \cdot \underline{\underline{\mathbf{U}}}$, (standard in Abaqus explicit), and the corotational frame, respectively. These are routinely used for analyses of metals at finite strains (Belytschko et al, 2000). It has been shown that, in the case of a material with one fibre direction the proper objective rotational derivative is based on the rotation of the fibre (Badel et al, 2009)

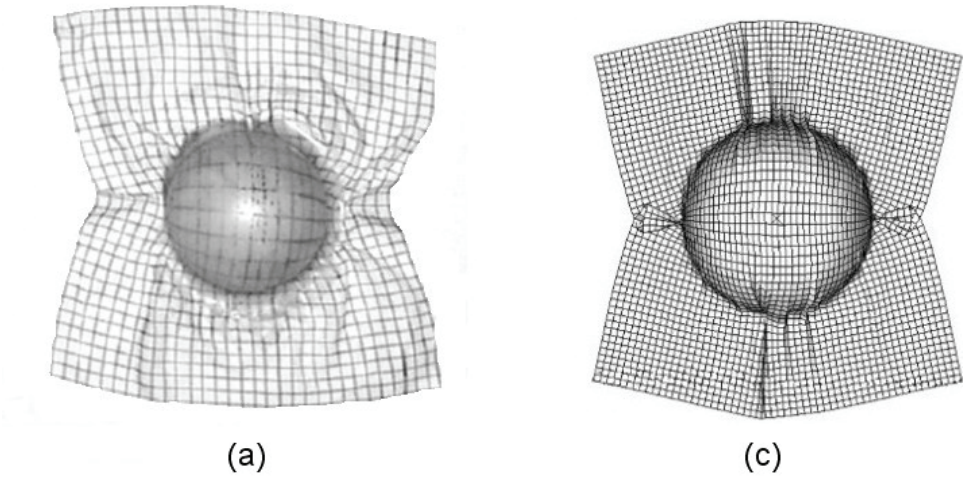

Fig. 12. Deformed shape in the case of an unbalanced fabric (experimental shape (a); Result of the simulation (c))

A membrane assumption is used. The Green-Naghdi's frame (GN) is the default work basis of ABAQUS/Explicit. Its unit vectors $(\underline{\mathbf{e}}_1, \underline{\mathbf{e}}_2)$ in the current configuration are updated from the initial orientation axes, $(\underline{\mathbf{e}}_1^0, \underline{\mathbf{e}}_2^0)$ using the proper rotation $\underline{\underline{\mathbf{R}}}$:

$$\underline{\mathbf{e}}_1 = \underline{\underline{\mathbf{R}}} \cdot \underline{\mathbf{e}}_1^0 \qquad \underline{\mathbf{e}}_2 = \underline{\underline{\mathbf{R}}} \cdot \underline{\mathbf{e}}_2^0 \tag{16}$$

In the current configuration, the unit vectors in the warp and weft fibre directions are respectively:

$$\underline{\mathbf{f}}_1 = \frac{\underline{\underline{\mathbf{F}}}.\underline{\mathbf{f}}_1^0}{\left\| \underline{\underline{\mathbf{F}}}.\underline{\mathbf{f}}_1^0 \right\|} \qquad \underline{\mathbf{f}}_2 = \frac{\underline{\underline{\mathbf{F}}}.\underline{\mathbf{f}}_2^0}{\left\| \underline{\underline{\mathbf{F}}}.\underline{\mathbf{f}}_2^0 \right\|} \tag{17}$$

Where $(\underline{\mathbf{e}}_1^0, \underline{\mathbf{e}}_2^0)$ and $(\underline{\mathbf{f}}_1^0, \underline{\mathbf{f}}_2^0)$ are assumed to coincide initially (Figure 3). Two orthonormal frames based on the two fibre directions are defined: $\mathrm{g}\left(\underline{\mathbf{g}}_1, \underline{\mathbf{g}}_2\right)$ with $\underline{\mathbf{g}}_1 = \underline{\mathbf{f}}_1$, and $\mathrm{h}\left(\underline{\mathbf{h}}_1, \underline{\mathbf{h}}_2\right)$ with $\underline{\mathbf{h}}_2 = \underline{\mathbf{f}}_2$ (Figure 11).

The strain increment $\underline{\underline{\mathbf{d\varepsilon}}}$ is given as a code's output in calculation loop from time t^n to time t^{n+1}. (The matrix of the components of this strain increment is given in the GN frame in the case of Abaqus explicit, but it could be any other frame). The components of the strain increment in the two frames g and h are considered (α and β are indexes taking value 1 or 2):

$$\underline{\underline{\mathbf{d\varepsilon}}} = \mathrm{d}\varepsilon_{\alpha\beta}^{\mathrm{g}}\ \underline{\mathbf{g}}_\alpha \otimes \underline{\mathbf{g}}_\beta = \mathrm{d}\varepsilon_{\alpha\beta}^{\mathrm{h}}\ \underline{\mathbf{h}}_\alpha \otimes \underline{\mathbf{h}}_\beta \tag{18}$$

The fibre stretching strain and the shear strain are calculated for the two frames g and h.

$$d\varepsilon_{11}^{g} = \underline{\mathbf{g}}_1 \cdot \underline{\underline{\mathbf{d\varepsilon}}} \cdot \underline{\mathbf{g}}_1 \qquad d\varepsilon_{12}^{g} = \underline{\mathbf{g}}_1 \cdot \underline{\underline{\mathbf{d\varepsilon}}} \cdot \underline{\mathbf{g}}_2 \tag{19}$$

$$d\varepsilon_{22}^{h} = \underline{\mathbf{h}}_2 \cdot \underline{\underline{\mathbf{d\varepsilon}}} \cdot \underline{\mathbf{h}}_2 \qquad d\varepsilon_{12}^{h} = \underline{\mathbf{h}}_1 \cdot \underline{\underline{\mathbf{d\varepsilon}}} \cdot \underline{\mathbf{h}}_2 \tag{20}$$

From these strain components the axial stress component and shear stress components are calculated in each frame g and h:

$$d\sigma_{11}^{g} = E^{g} d\varepsilon_{11}^{g} \qquad d\sigma_{12}^{g} = G d\varepsilon_{12}^{g} \tag{21}$$

$$d\sigma_{22}^{h} = E^{h} d\varepsilon_{22}^{h} \qquad d\sigma_{12}^{h} = G d\varepsilon_{12}^{h} \tag{22}$$

E^g and E^h are the stiffness in the warp and weft fibre directions respectively and G the in-plane shear stiffness of the fabric (They are not constant, especially G depends strongly on the in plane shear). Following the scheme of Hughes and Winget the stresses are then integrated on the time increment from time t^n to time t^{n+1} (Hughes & Winget, 1980):

$$\left(\sigma_{11}^{g}\right)^{n+1} = \left(\sigma_{11}^{g}\right)^{n} + d\sigma_{11}^{g^{n+1/2}} \qquad \left(\sigma_{12}^{g}\right)^{n+1} = \left(\sigma_{12}^{g}\right)^{n} + d\sigma_{12}^{g^{n+1/2}} \tag{23}$$

$$\left(\sigma_{11}^{h}\right)^{n+1} = \left(\sigma_{11}^{h}\right)^{n} + d\sigma_{11}^{h^{n+1/2}} \qquad \left(\sigma_{12}^{h}\right)^{n+1} = \left(\sigma_{12}^{h}\right)^{n} + d\sigma_{12}^{h^{n+1/2}} \tag{24}$$

The stress at time t^{n+1} in the fabric is the addition of the stresses in the two fibre frames:

$$\underline{\underline{\boldsymbol{\sigma}}}^{n+1} = \left(\underline{\underline{\boldsymbol{\sigma}}}^{g}\right)^{n+1} + \left(\underline{\underline{\boldsymbol{\sigma}}}^{h}\right)^{n+1} \tag{25}$$

For instance, denoting $\underline{\underline{\boldsymbol{\sigma}}} = \sigma_{\alpha\beta}^{e}\, \underline{\mathbf{e}}_\alpha \otimes \underline{\mathbf{e}}_\beta$ and omitting the superscript n+1 because all the quantities are at time t^{n+1}, the components of the Cauchy stress tensor in the GN frame (that are requested in the Abaqus Explicit code) are:

$$\begin{aligned}\sigma_{\alpha\beta}^{e} = {} & \sigma_{11}^{g}\left(\underline{\mathbf{e}}_\alpha.\underline{\mathbf{g}}_1\right)\left(\underline{\mathbf{e}}_\beta.\underline{\mathbf{g}}_1\right) + \sigma_{22}^{h}\left(\underline{\mathbf{e}}_\alpha.\underline{\mathbf{h}}_2\right)\left(\underline{\mathbf{e}}_\beta.\underline{\mathbf{h}}_2\right) + \sigma_{12}^{g}\left(\underline{\mathbf{e}}_\alpha.\underline{\mathbf{g}}_1\right)\left(\underline{\mathbf{e}}_\beta.\underline{\mathbf{g}}_2\right) \\ & + \sigma_{12}^{h}\left(\underline{\mathbf{e}}_\alpha.\underline{\mathbf{h}}_1\right)\left(\underline{\mathbf{e}}_\beta.\underline{\mathbf{h}}_2\right)\end{aligned} \tag{26}$$

More detail on this approach can be found in (Badel et al, 2009, Khan et al, 2010). This approach is used to simulate the forming double dome shape corresponding to an international benchmark (Khan et al, 2010). An experimental device has been realised in INSA Lyon in order to perform this forming (Figure 13). The woven fabric is a commingled glass/polypropylene plain weave that has been tested in the material benchmark study conducted recently (Cao et al, 2008). The computed and experimental geometries after forming are compared figure 14 and 15. The measured and numerical geometries and shear angles are in good agreement.

6. Discrete approach for the composite reinforcement forming

In discrete modelling (also called meso-modelling in the case of textile material), the modelling does not directly concern the textile material but each fibre bundle. This one is

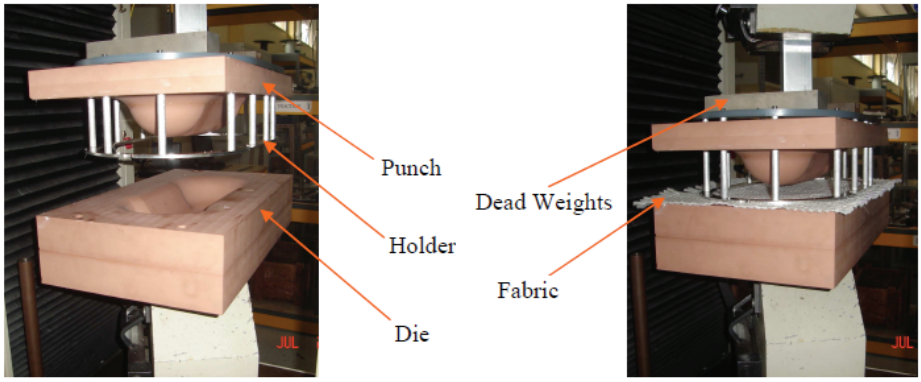

Fig. 13. Double dome forming: experimental device

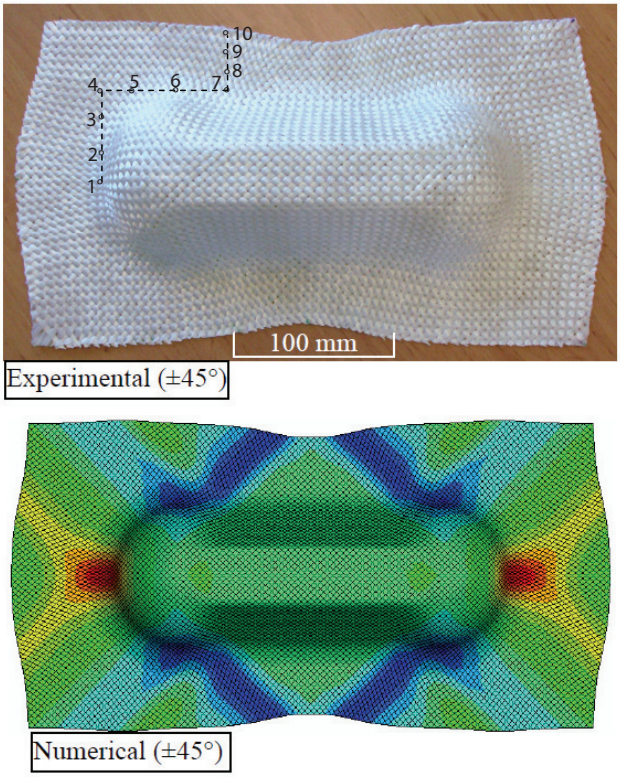

Fig. 14. Experimental and numerical outputs of double dome forming test

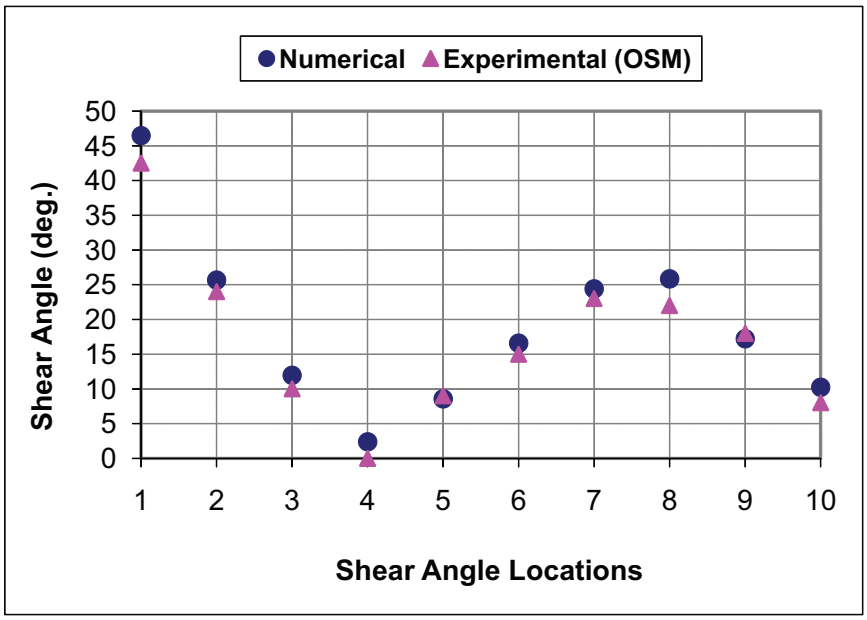

Fig. 15. Comparison of numerical and experimental shear angles at the locations shown in Figure 14.

modelled by elements simple enough to render the computation possible because it concerns the forming of the whole composite reinforcement and the number of yarns and contacts between these yarns is very large. The interactions between warp and weft directions are taken into account explicitly by considering contact behaviour and relative motions between the yarns are possible (Pickett et al, 2005, Duhovic et al, 2006, Ben Boukaber et al 2007).

At the microscopic level, each fibre is satisfactorily described as a beam but this approach is time consuming. The main difficulty is the great number of contacts with friction that have to be taken into account, especially for a woven fabric. For this reason, only very small elements of the fabric have been modelled to date (Durville, 2005, Miao et al, 2008). Nevertheless, this approach is promising because it does not necessitate any assumptions regarding the continuity of the material, the specific mechanical properties resulting at the macroscopic level naturally follow the displacements and deformations of the yarns and it provides an interesting way of taking the weaving operation into account. The fibres constituting the yarns can be modelled directly, but their very large number (3K to 48K per yarn) requires that the computations are made for a number of fibres per yarn significantly smaller than in reality. An alternative possibility is to use a continuous behaviour for each yarn (meso-modelling). This implies that the fibrous nature of the yarn is taken into account in this model especially in order to have rigidities in bending and transverse compression very small in comparison to the tensile stiffness. In any case, a compromise must be found between a fine description (which will be expensive from the computation time point of view) and a model simple enough to compute the entire forming process. Figure 16(b) show

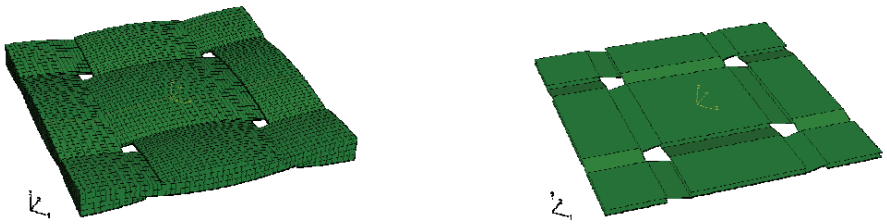

(a) (b)

Fig. 16. Meso-modelling of a unit cell of a plain weave. (a) FE model for the analysis of the behaviour of the unit cell. 47214 Dof. (b) FE model for simulations of the whole composite reinforcement forming. 216 Dof.

the finite element model used for discrete simulations of forming processes (216 dof (degrees of freedom)). It is compared to another FE model of the unit cell used in (Badel et al, 2009)(Figure 16(a)) to analyze the local in plane shear of a plain weave unit cell (47214 dof). It cannot be considered (at least today) to use this last FE model to simulate the forming of a composite reinforcement that is made of several thousands of woven cells. In the simplified unit cell (Figure 16(b)) each yarn is described by few shell elements and the contact friction and possible relative displacement of the yarns are considered. The in-plane mechanical behaviour is the same as the one defined in (Badel et al, 2009). The bending stiffness is independent of the tensile one and very much reduced in comparison to the one given by plate theories.

Two examples are presented in figures 17 and 18 based on a discrete modelling using the unit cell of figure 16(b) (Gatouillat et al, 2010) The first one is a picture frame test for which the wrinkles appear naturally in the simulation when the shear locking angle is reached. It must be noticed that the in-plane shear behaviour of the fabric is not an input data of the analysis and does not need to be known. It results at the macroscopic level of contact and friction between the yarns and lateral compression of the yarns. Figure 18 shows the results of a hemispherical forming simulation. It must be said that this study concerning forming simulation at the meso-scopic scale is beginning at INSA Lyon. If the discrete or mesoscopic modelling is a promising approach because a large part of the mechanical specificity of fabric behaviour is due to yarn and fibre interactions, and following fibre directions is simpler than for continuous models, it must be recognized that the forming simulations made with approaches that permits the relative sliding of the yarns in contact are not many.

7. The semi-discrete finite elements for the composite reinforcement forming

This approach can be seen as intermediate between the continuous and the discrete approaches. The textile composite reinforcement is seen as a set of a discrete number of unit woven cells submitted to membrane loadings (i.e. biaxial tension and in-plane shear) and bending (Figure 19)(Hamila et al, 2009)

In any virtual displacement field $\underline{\eta}$ such as $\underline{\eta} = 0$ on the boundary with prescribed loads, the virtual work theorem relates the internal, exterior and acceleration virtual works:

$$W_{ext}(\underline{\eta}) - W_{int}(\underline{\eta}) = W_{acc}(\underline{\eta}) \tag{27}$$

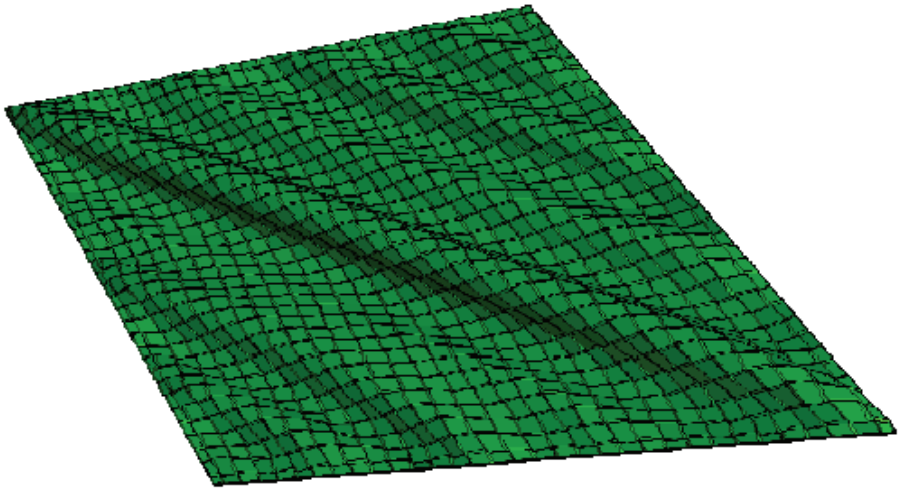

Fig. 17. Simulation of a picture frame test using the unit cell model of figure 16(b)

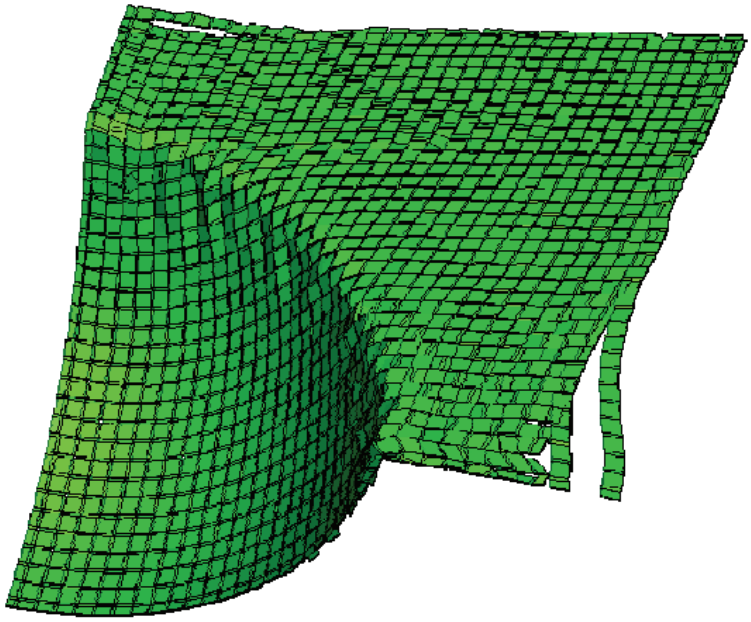

Fig. 18. Simulation of hemispherical forming test using the unit cell model of figure 16(b)

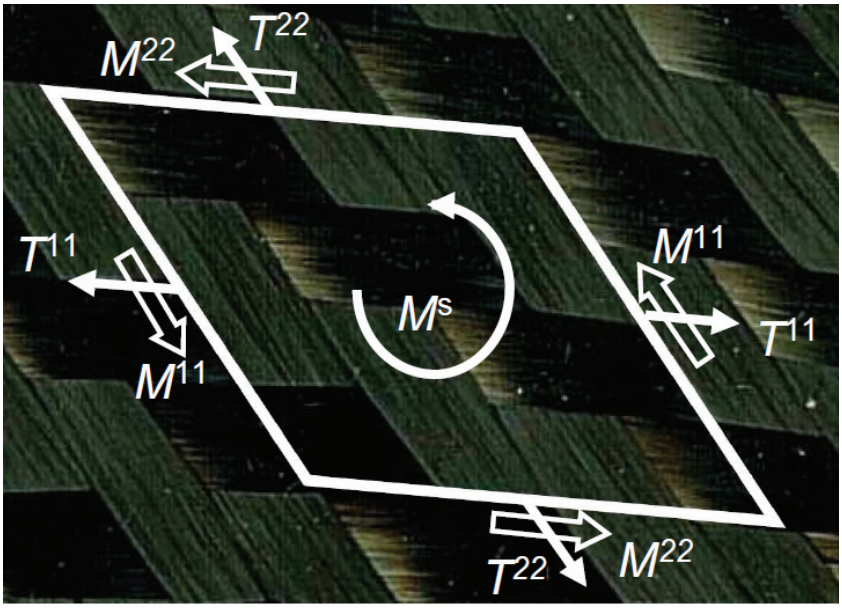

Fig. 19. Unit woven cell submitted to tension, in plane shear and bending

In the case of the woven fabric reinforcement, the internal virtual work is assumed to be separated into:

$$W_{int}(\underline{\eta}) = W^{t}_{int}(\underline{\eta}) + W^{s}_{int}(\underline{\eta}) + W^{b}_{int}(\underline{\eta}) \tag{28}$$

$W^{t}_{int}(\underline{\eta})$, $W^{s}_{int}(\underline{\eta})$, $W^{b}_{int}(\underline{\eta})$ are the internal virtual work of biaxial tension, in plane shear and bending respectively with :

$$W^{t}_{int}(\underline{\eta}) = \sum_{p=1}^{ncell} {}^{p}\varepsilon_{11}(\underline{\eta})\ {}^{p}T^{11}\ {}^{p}L_1 + {}^{p}\varepsilon_{22}(\underline{\eta})\ {}^{p}T^{22}\ {}^{p}L_2 \tag{29}$$

$$W^{s}_{int}(\underline{\eta}) = \sum_{p=1}^{ncell} {}^{p}\gamma(\underline{\eta})\ {}^{p}M^{s} \tag{30}$$

$$W^{b}_{int}(\underline{\eta}) = \sum_{p=1}^{ncell} {}^{p}\chi_{11}(\underline{\eta})\ {}^{p}M^{11}\ {}^{p}L_1 + {}^{p}\chi_{22}(\underline{\eta})\ {}^{p}M^{22}\ {}^{p}L_2 \tag{31}$$

where ncell is the number of woven cell. ${}^{p}A$ means that the quantity A is considered for the woven cell number p. L_1 and L_2 are the length of unit woven cell in warp and weft directions. $\varepsilon_{11}(\underline{\eta})$ and $\varepsilon_{22}(\underline{\eta})$ are the virtual axial strain in the warp and weft directions. $\gamma(\underline{\eta})$ is the virtual angle between warp and weft directions. $\chi_{11}(\underline{\eta})$ and $\chi_{22}(\underline{\eta})$ are the virtual curvatures of warp and weft directions. $\varepsilon_{11}(\underline{\eta})$, $\varepsilon_{22}(\underline{\eta})$, $\gamma(\underline{\eta})$, $\chi_{11}(\underline{\eta})$ and $\chi_{22}(\underline{\eta})$ are function of the gradient of the virtual displacement field. T^{11} and T^{22} are the tensions on the

unit woven cell in warp and weft directions. M^{11} and M^{22} are the bending moments on the woven cell respectively in warp and weft directions. M^s is the in-plane shear moment. The loads on an edge of the woven unit cell (presented Figure 19) result in the tensions T^{11} and T^{22} in one hand and shear forces in the other hand. This shear forces on a warp and weft sections have a moment at the centre of the woven unit cell in the direction normal to the unit cell. The component of this moment is called in-plane shear moment M^s. This quantity is conjugated to the in-plane shear angle γ . The internal virtual work of in plane shear is directly given from M^s and the virtual shear angle (Equation 30). In the case of a textile material, the shear angle γ is a significant and clearly defined quantity and it is interesting to express the internal virtual work of in plane shear in function of this quantity.
The mechanical behaviour of the textile reinforcement defines a relation between the loads $T^{\alpha\alpha}$, M^s, $M^{\alpha\alpha}$ and the strain field. The experimental tests specific to textile composite reinforcements that have been presented in Section 4 are used to obtain T^{11}, T^{22}, M^s, $M^{11}$and M^{22} in function of ε_{11}, ε_{22}, γ, χ_{11} and χ_{22}.
An alternative consists in virtual tests i.e. in 3D simulations of the deformation of a unit woven cell submitted to elementary loadings such as biaxial tensions or in plane shear (Badel et al, 2008, Badel et al, 2009)

7.1 Shell finite element made of woven cells

A three node shell finite element have been defined from the simplified form of the principle of virtual works given in equations 28 to 31. The details of its formulation are given in (Hamila et al, 2009). It is summarized below.
A finite element interpolation is introduced within the principle of virtual work. The displacement $\underline{u}$ and virtual displacement $\underline{\eta}$ of any point within an element are in the form:

$$\underline{u} = \mathbf{N}\mathbf{u}^e \quad \text{and} \quad \underline{\eta} = \mathbf{N}\boldsymbol{\eta}^e \tag{32}$$

$\mathbf{N}$ is the interpolation matrix of the element under consideration and $\mathbf{u}^e$ and $\boldsymbol{\eta}^e$ the single column matrices of its nodal displacements and virtual displacements respectively. Equation 28 leads to:

$$\mathbf{M}\ddot{\mathbf{u}} + \left(\mathbf{F}_{int}^t + \mathbf{F}_{int}^s + \mathbf{F}_{int}^b\right) - \mathbf{F}_{ext} = 0 \tag{33}$$

$\mathbf{M}$ is the mass matrix, $\mathbf{u}$ is the single column matrices of the nodal displacements. $\mathbf{F}_{int}^t$, $\mathbf{F}_{int}^s$, $\mathbf{F}_{int}^b$ are the single column matrices of the nodal internal forces respectively for tension, shear and bending.
This dynamic equation can be solved using an explicit scheme (central differences):

$$\ddot{\mathbf{u}}^{i+1} = \mathbf{M}_D^{i\ -1}\left(\mathbf{F}_{ext}^i - \mathbf{F}_{int}^{ti} - \mathbf{F}_{int}^{si} - \mathbf{F}_{int}^{bi}\right) \tag{34}$$

$$\dot{\mathbf{u}}^{i+1/2} = \dot{\mathbf{u}}^{i-1/2} + \frac{1}{2}\left(\Delta t^{i-1} + \Delta t^i\right)\ddot{\mathbf{u}}^{i+1} \tag{35}$$

$$\mathbf{u}^{i+1} = \mathbf{u}^i + \dot{\mathbf{u}}^{i+1/2}\Delta t^i \tag{36}$$

There is no system to solve since $\mathbf{M}_D$ is a diagonal matrix calculated from $\mathbf{M}$ (Zienkiewicz & Taylor, 2000). This explicit scheme requires the time step to be small enough to insure the

stability of the scheme (Belytschko, 1983). It is effective for many dynamic applications and also in material forming. For the sake of numerical efficiency, the speed can be larger than the real one under the condition that the dynamic effects do not modify the solution.
The 3 node shell finite element $M_1M_2M_3$ made up of ncelle woven cells is considered (Figure 20). The vectors $\underline{k}_1=\underline{AM}_2$ and $\underline{k}_2=\underline{BM}_3$ respectively in warp and weft directions are defined. The internal virtual work of tension on the element defines the element nodal tensile internal forces $\mathbf{F}_{int}^{te}$:

$$\sum_{p=1}^{ncelle} {}^{p}\varepsilon_{11}(\underline{\eta})\ {}^{p}T_1\ {}^{p}L_1 + {}^{p}\varepsilon_{22}(\underline{\eta})\ {}^{p}T_2\ {}^{p}L_2 = \boldsymbol{\eta}^{eT}\mathbf{F}_{int}^{te} \tag{37}$$

The internal tensile force components are calculated from the tensions T_1 and T_2:

$$\left(F_{int}^{te}\right)_{ij} = ncelle\left(B_{1ij}T_1\frac{L_1}{\left\|\underline{k}_1\right\|^2} + B_{2ij}T_2\frac{L_2}{\left\|\underline{k}_2\right\|^2}\right) \tag{38}$$

i is the index of the direction (i=1 to 3), j is the index of the node (j=1 to 3). B_{1ij} and B_{2ij} are strain interpolation components. They are constant over the element because the interpolation functions in equation 32 are linear in the case of the 3 node triangle.
The internal virtual work of in-plane shear on the element defines the element nodal tensile internal forces $\mathbf{F}_{int}^{se}$:

$$\sum_{p=1}^{ncelle} {}^{p}\gamma(\underline{\eta})\ {}^{p}M_s = \boldsymbol{\eta}^{eT}\mathbf{F}_{int}^{se} \tag{39}$$

The internal in-plane shear force components are calculated from the in-plane shear moment:

$$\left(F_{int}^{se}\right)_{ij} = ncelle\ B_{\gamma ij}M^s(\gamma) \tag{40}$$

In order to avoid supplementary degrees of freedom and consequently for numerical efficiency, the bending stiffness is taken into account within an approach without rotational degree of freedom (Onate & Zarate, 2000, Sabourin et Brunet, 2006). In theses approaches the curvatures of the element are computed from the positions and displacements of the nodes of the neighbouring elements (Figure 20). The internal virtual work of bending on the element defines the element nodal bending internal forces $\mathbf{F}_{int}^{be}$:

$$\sum_{p=1}^{ncelle} {}^{p}\chi_{11}(\underline{\eta})\ {}^{p}M_1\ {}^{p}L_1 + {}^{p}\chi_{22}(\underline{\eta})\ {}^{p}M_2\ {}^{p}L_2 = \boldsymbol{\eta}^{eT}\mathbf{F}_{int}^{be} \tag{41}$$

The internal bending force components are calculated from the bending moments M_1 and M_2:

$$\left(F_{int}^{be}\right)_{km} = n_{celle}\left(Bb_{1km}M_1\frac{L_1}{\left\|\underline{k}_1\right\|^2} + Bb_{2km}M_2\frac{L_2}{\left\|\underline{k}_2\right\|^2}\right) \tag{42}$$

The finite element presented above is used to simulate the hemispherical forming of the very unbalanced fabric presented in section 5.1. The experimental forming by a

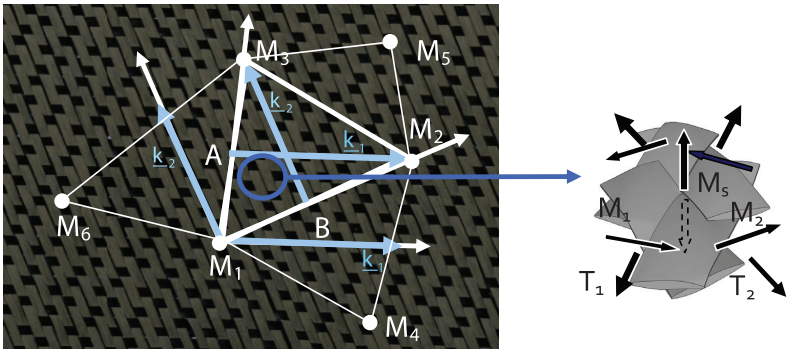

Fig. 20. Three node finite element made of unit woven cells,

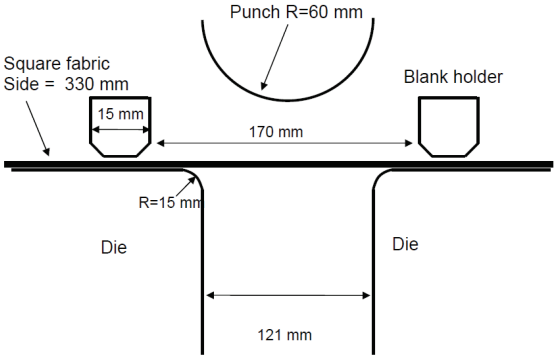

(a)

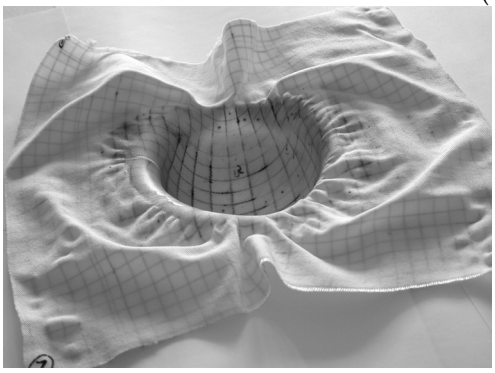

(b)

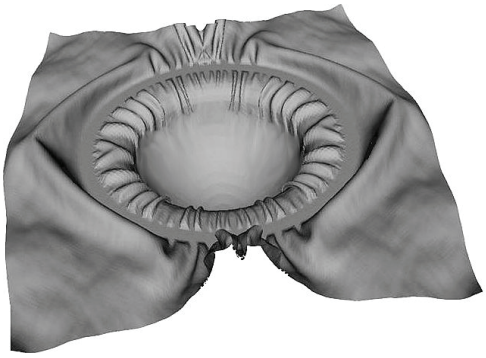

(c)

Fig. 21. Forming of an unbalanced textile reinforcement

hemispherical punch has been performed at the University of Nottingham (Daniel et al, 2003). A 6 kg ring was used as blank-holder avoiding reinforcement wrinkling in the hemispherical zone (Figure 21a). The experimental shape obtained after forming is shown in Figure 21b. In warp direction (with the strongest rigidity) large fabric sliding is observed relatively to the die. On the contrary, in the weft direction (weak direction) no edge

movement is depicted and the yarns are subjected to large stretch deformations. The computed shape after forming is shown in Figure 21c. It is in good agreement with experiments. Especially the extension ratio at the centre of the hemisphere (l_{weft}/l_{warp} = 1.8) is correctly computed. The shape of the many wrinkles in the flat part of the textile is also properly simulated.

7.2 Extension to 3D interlock textile reinforcements

When the thickness of a composite part is large, the use of these laminated composites is restricted by manufacturing problems and their low resistance to delamination cracking. To overcome these difficulties composites with 3D fibre architecture called ply to ply interlock fabric have been proposed (Tong et al, 2002). This material is not fully 3D since there is no third yarn set in the transverse direction but the properties through the thickness are much improved. Above all, the possible delaminations of the 2D laminated composites are overcome. (Figure 22). The semi-discrete approach has been extended to 3D hexahedral finite elements for interlock forming simulations; These elements are made of yarns as shown Figure 23. The simulation of a thick twisted plate made of interlock textile reinforcement is shown figure 24. The formulation of these finite elements for interlock forming simulations is given in (De Luycker et al, 2009).

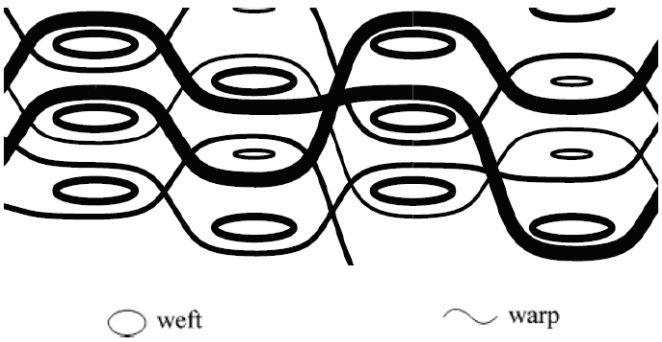

Fig. 22. Example of complex layer interlock weave

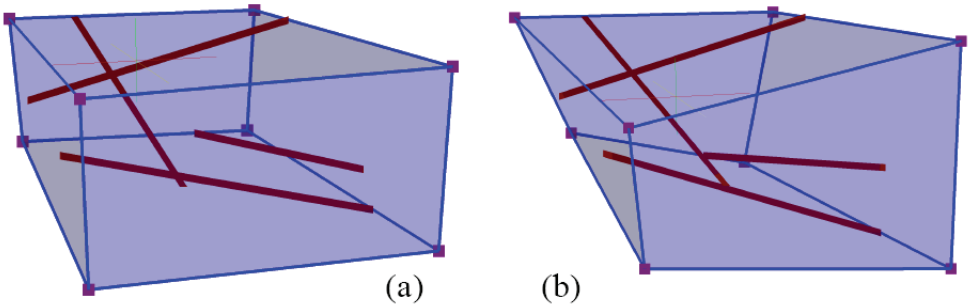

Fig. 23. Height node hexahedral finite element containing yarns – (a) Initial state– (b) Deformed state.

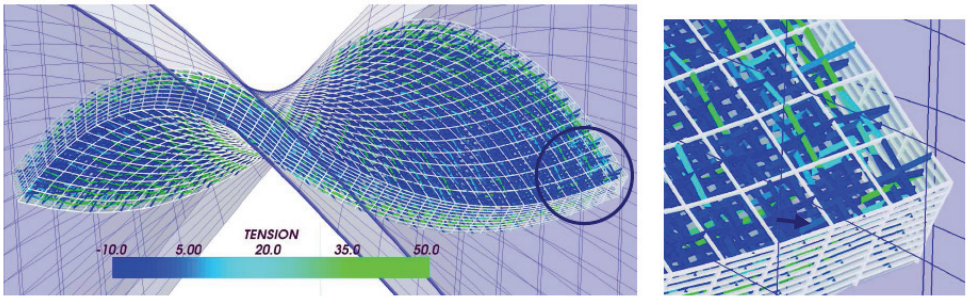

Fig. 24. Forming of a 3D interlock twisted plate

8. Conclusion

Different approaches for composite forming simulations have been presented in this chapter. They are continuous discrete or semi-discrete element. These different approaches are based on the strong multi-scale nature of the textile reinforcements.

The discrete approach is attractive and promising. The very specific mechanical behaviour of the textile material due to the contacts and friction between the yarns and to the change of direction is explicitly taken into account. If some sliding occurs between warp and weft yarns, they can be simulated. This is not possible by the continuous approaches that consider the textile material as a continuum. This is an important point because it can be necessary to prevent such a sliding in a process. Nevertheless, the main difficulty of the discrete approach is the necessary compromise that must be done between the accuracy of the model of the unit woven cell and the total number of degrees of freedom. The modelling of the unit cell must be accurate enough to obtain a correct macroscopic mechanical behaviour, but the number of degrees of freedom of each cell must remain small in order to compute a forming process for which there will be thousand of woven cells. There are a lot of improvements to achieve in the meso-modelling of different textile reinforcements. The continuous increase of the computer power is a strong argument in favour of this approach.

The continuous approach is the most commonly used in composite reinforcement forming today. The main advantage is to use standard shell or membrane finite element. The only mechanical behaviour has to be specified in order to take the very particular behaviour of textile materials into account. Many models exist, but none of them is clearly admitted. The semi-discrete approach aims to avoid the use of stress tensors and directly define the loading on a woven unit cell by the warp and weft tensions and by in-plane shear and bending moments. These quantities are simply defined on a woven unit cell and above all they are directly measured by standard tests on composite reinforcements (biaxial tension, picture frame, bias extension and bending tests).

9. References

Advani SG. Flow and rheology in polymeric composites manufacturing. Elsevier, 1994.

Aimène Y, Vidal-Sallé E, Hagège B, Sidoroff F, Boisse P, A hyperelastic approach for composite reinforcement large deformation analysis, Journal of Composite Materials Vol. 44, No. 1/2010, 5-26

Badel P, Vidal-Sallé E, Maire E, Boisse P (2009) Simulation and tomography analysis of textile composite reinforcement deformation at the mesoscopic scale. Composites Science and Technology 68:2433-2440

Badel P, Gauthier S, Vidal-Salle E, Boisse P. Rate constitutive equations for computational analyses of textile composite reinforcement mechanical behaviour during forming. Composites: Part A 40 (2009) 997–1007

Basar Y, Weichert D (2000) Nonlinear continuum mechanics of solids. Springer, Berlin

Belytschko T. An overview of semidiscretisation and time integration procedures. In: Belytschko T, Hughes TJR, editors, Computation Methods for Transient Analysis. Amsterdam: Elsevier, 1983.

Ben Boukaber B, Haussy G, Ganghoffer JF (2007) Discrete models of woven structures. Macroscopic approach. Composites: Part B 38:498-505

Borouchaki H, Cherouat A. Une nouvelle approche pour le drappage des structures composites. Rev Comp Mat Avanc 2002;32:407–22

Buet-Gautier K., Boisse P. Experimental analysis and modeling of biaxial mechanical behavior of woven composite reinforcements. Experimental Mechanics 2001; 41 (3): 260-269.

Cao J., Akkerman R., Boisse P., Chen J. et al. Characterization of Mechanical Behavior of Woven Fabrics: Experimental Methods and Benchmark Results. Composites Part A 2008; 39: 1037-1053.

Carvelli V., Corazza C., Poggi C. Mechanical modelling of monofilament technical textiles. Computational Materials Science 2008; 42: 679-691.

Dong L, Lekakou C, Bader MG. Processing of composites: simulations of the draping of fabrics with updated material behaviour law. Journal of Composite Materials 2001; 35: 38–163.

Daniel JL, Soulat D, Dumont F, Zouari B, Boisse P, Long AC, Forming simulation of very unbalanced woven composite reinforcements. International Journal of Forming Processes 2003, 6:465-480

de Bilbao E, Soulat D, Hivet G, Gasser A., Experimental Study of Bending Behaviour of Reinforcements, Experimental Mechanics (2010) 50:333–351

De Luycker E, F. Morestin, P. Boisse, D. Marsal, Simulation of 3D interlock composite preforming, Composite Structures, 88, Issue 4, May 2009, Pages 615-623

Duhovic M, Bhattacharyya D (2006) Simulating the deformation mechanisms of knitted fabric composites. Composites: Part A 37:1897-1915

Dumont F, Hivet G, Rotinat R, Launay J, Boisse P, Vacher P. Field measurements for shear tests on woven reinforcements. Mécanique et Industrie, 2003; 4:627–35.

Durville D, 2005, Numerical simulation of entangled materials mechanical properties. Journal of Materials Science 40:5941-5948

Gatouillat S, Vidal-Salle E, Boisse P, Advantages of the meso/macro approach for the simulation of fibre composite reinforcements, Proceedings of the ESAFORM 2010 Conference, Brescia, April 2010, Italy

Hamila N., Boisse P., Sabourin F., Brunet M. A semi-discrete shell finite element for textile composite reinforcement forming simulation. Int J Numerical Methods in Engineering 2009; 79: 1443-1466.

Harrison P., Clifford MJ., Long AC. Shear characterisation of viscous woven textile composites: a comparison between picture frame and bias extension experiments. Compos Sci Tech 2004; 64: 1453-1465.

Hughes TJR, Winget J (1980) Finite rotation effects in numerical integration of rate constitutive equations arising in large deformation analysis. International Journal for Numerical Methods in Engineering 15:1862-1867

Kawabata S., Niwa M., Kawai H. The Finite Deformation Theory of Plain Weave Fabrics Part I: The Biaxial Deformation Theory. Journal of the Textile Institute 1973; 64(1): 21-46.

King MJ, Jearanaisilawong P, Socrate S. A continuum constitutive model for the mechanical behavior of woven fabrics. International Journal of Solids and Structures 2005; 42: 3867–3896.

Kawabata S. The Standardization and Analysis of Hand Evaluation. Osaka: The Textile Machinery Society of Japan, 1986.

M.A. Khan, T. Mabrouki, E. Vidal-Sallé, P. Boisse, Numerical and experimental analyses of woven composite reinforcement forming using a hypoelastic behaviour. Application to the double dome benchmark, Journal of Materials Processing Technology 210 (2010) 378–388

Lahey TJ., Heppler GR. Mechanical Modeling of Fabrics in Bending. ASME Journal of Applied Mechanics 2004; 71: 32-40.

Launay J., Hivet G., Duong AV., Boisse P. Experimental analysis of the influence of tensions on in plane shear behaviour of woven composite reinforcements. Compos Sci Tech 2008; 68: 506-515.

Lebrun G., Bureau MN., Denault J. Evaluation of bias-extension and picture-frame test methods for the measurement of intraply shear properties of PP/glass commingled fabrics. Compos Struct 2003; 61: 341-52

Lomov S., Boisse P., Deluycker E., Morestin F., Vanclooster K., Vandepitte D., Verpoest I., Willems A. Full field strain measurements in textile deformability studies. Composites: Part A 2008; 39: 1232-1244.

Lomov SV., Willems A., Verpoest I., Zhu Y., Barburski M., Stoilova Tz. Picture frame test of woven composite reinforcements with a full-field strain registration. Textile Research Journal 2006; 76 (3): 243-252.

Long A.C., Rudd C.D. (1994), 'A simulation of reinforcement deformation during the production of preform for liquid moulding processes', *I. Mech. E. J. Eng. Manuf.*, 208, 269-278.

Mark C., Taylor H. M. (1956), 'The fitting of woven cloth to surfaces', *Journal of Textile Institute*, 47, 477-488

Miao Y, Zhou E, Wang Y, Cheeseman BA (2008) Mechanics of textile composites: Micro-geometry. Composites Science and Technology 68:1671-1678

Parnas RS. Liquid Composite Molding. Hanser Garner publications, 2000.

Onate E., Zarate F. Rotation-free triangular plate and shell elements. Int J for Num Meth in Eng 2000; 47: 557-603.

Peng XQ., Cao J., Chen J., Xue P., Lussier DS., Liu L. Experimental and numerical analysis on normalization of picture frame tests for composite materials. Compos Sci Tech 2004; 64: 11-21.

Peng X, Cao J. A continuum mechanics-based non-orthogonal constitutive model for woven composite fabrics. Composites Part A 2005; 36: 859–874.

Pickett AK, Creech G, de Luca P (2005) Simplified and Advanced Simulation Methods for Prediction of Fabric Draping. European Journal of Computational Mechanics 14:677-691

Potter K. Bias extension measurements on cross-plied unidirectional prepreg. Composites Part A 2002; 33: 63-73.

Potluri P., Perez Ciurezu DA., Ramgulam RB. Measurement of meso-scale shear deformations for modelling textile composites. Composites Part A 2006; 37: 303-314.

Prodromou AG., Chen J. On the relationship between shear angle and wrinkling of textile composite preforms. Composite Part A 1997; 28A:491-503.

Rozant O., Bourban PE., Manson JAE. Drapability of dry textile fabrics for stampable thermoplastic preforms. Composites: Part A 2000; 31: 1167-1177.

Rudd CD., Long AC. Liquid Molding Technologies. Cambridge: Woodhead Pub. Lim., 1997.

Spencer AJM. Theory of fabric-reinforced viscous fluid. Composites Part A 2000; 31: 1311–1321.

Sabourin F., Brunet M. Detailed formulation of the rotation-free triangular element "S3" for general purpose shell analysis. Engineering computations 2006; 23 (5): 469-502.

Sharma S.B., Sutcliffe M.P.F., Chang S.H. Characterisation of material properties for draping of dry woven composite material. Composites Part A, 2003; 34:1167–1175.

Spencer A.J.M. – Theory of fabric-reinforced viscous fluids – Composites: Part A 31 (2000) 1311–1321

Ten Thije RHW, Akkerman R, Huetink J. Large deformation simulation of anisotropic material using an updated Lagrangian finite element method. Computer methods in applied mechanics and engineering 2007; 196(33–34): 3141–3150.

Tong L, Mouritz AP, Bannister MK. 3D Fibre reinforced polymer composites. Elsevier Science, 2002.

Truesdell C (1955) Hypo-elasticity. J Ration Mech Anal 4:83-133

Van Der Ween F. (1991), 'Algorithms for draping fabrics on doubly curved surfaces', *International Journal of Numerical Method in Engineering*, 31, 1414-1426.

Willems A., Lomov SV., Verpoest I., Vandepitte D. Optical strain fields in shear and tensile testing of textile reinforcements. Composites Science and Technology 2008; 68: 807-819.

Xiao H, Bruhns OT, Meyers A (1998) On objective corotational rates and their defining spin tensors. International Journal of Solids and Structures 35:4001-4014

Yu W.R., Pourboghrata F., Chungb K., Zampalonia M., Kang T. J. – Non-orthogonal constitutive equation for woven fabric reinforced thermoplastic composites – Composites: Part A 33 (2002) 1095–1105

Zienkiewicz OC., Taylor RL. The finite element method, vol. 2: Solid Mechanics. Oxford: Butterworth, Heineman, 2000.